Politecnico di Milano

School of Industrial and Information Engineering
Master of Science in Energy Engineering
Power Production

Numerical modeling of PEM Fuel Cell through 3D and 1D approaches: an analysis of geometrical features and relative humidity effects

Advisor:
Dr. Riccardo MEREU

Co-Advisor:
Dr. Andrea BARICCI

Ing. Amedeo GRIMALDI

Candidate:
Filippo GIOVANAZZI
873695

Academic Year 2018/2019

Filippo Giovanazzi
Numerical modeling of PEM Fuel Cell through 3D and 1D approaches: an analysis of geometrical features and relative humidity effects
Advisor: Dr. Riccardo Mereu
Co-Advisor: Dr. Andrea Baricci
Co-Advisor: Dr. Amedeo Grimaldi

Politecnico di Milano
School of Industrial and Information Engineering
Department of Energy

Acknowledgement

Le prime persone che voglio ringraziare sono senz'altro il mio relatore, il prof. Riccardo Mereu e il mio correlatore, il prof. Andrea Baricci, che si sono sempre dimostrati disponibili ad aiutarmi durante tutte le fasi della tesi, in un percorso che si è rivelato stimolante, ma anche pieno di insidie.

Un grazie particolare ad Amedeo Grimaldi, vero e proprio punto di riferimento in questi mesi, che è sempre stato disponibile a consigliarmi ed aiutarmi per ogni problema che è sorto durante il lavoro. Forse queste poche righe non bastano per dimostrargli tutta la mia gratitudine, ma spero che possano almeno rendere l'idea.

Vorrei ringraziare la mia famiglia che non mi ha mai fatto mancare il suo sostegno durante questi anni.

Ringrazio anche tutti i miei amici più cari, impossibile elencarvi tutti, ma so per certo che sappiate di chi sto parlando. Grazie per avermi sostenuto nei momenti più difficili di questo periodo, per avermi strappato un sorriso, per le birre insieme, per le serate ignoranti, per le battute stupide, che non sono mai troppe, per i bei ricordi che abbiamo costruito in tutti questi anni.

Un ringraziamento speciale lo devo anche alla mia ragazza, Alessandra, che è sempre stata un punto fermo per me durante questi anni di università, e nella vita di tutti i giorni. Mi ha aiutato tutte le volte che ne avevo bisogno senza mai tirarsi indietro. Mi ha sempre supportato (ma soprattutto sopportato!). Se ho concluso questo percorso, lo devo anche a lei.

Abstract

Polymer Electrolyte Membrane Fuel Cell (PEMFC) represents a promising technology that has received a great attention in the last two decades, both in the automotive and micro-cogeneration sector. Indeed, they presents a lot of advantages, such as high efficiency and power density, low emissions, low operating temperature (< 100 °C), fast start-up, modularity. Nevertheless, it presents some important issues and water management is one of the most critical, since water transport through the cell has a significant impact on performance and durability. Flow field geometry and relative humidity of reactants play a key role in water management inside PEMFC and performance's optimization. In this view, the present work presents a 3D CFD analysis of PEMFC performance in different operating conditions and geometrical configuration, and a 1D model analysis in order to develope a methodology to include those effects in 1D configuration.

Key-words: PEMFC; CFD; dehydration; flooding; flow field.

Sommario

Le celle a combustibile a membrana polimerica (PEMFC) rappresentano una tecnologia promettente che ha ricevuto negli ultimi due decenni una grande attenzione, sia nel settore dell'automotive che della microcogenerazione. Infatti, presentano una serie di vantaggi, quali alta efficienza, densità di potenza elevata, basse emissioni, bassa temperatura operativa (< 100 °C), avviamento rapido, modularità. Ciò nonostante, questa teconologia presenta delle criticità importanti e la gestione dell'acqua rappresenta una delle più importanti, poichè il trasporto d'acqua all'interno della cella ha un impatto significativo sulle prestazioni della cella e sulla durabilità dei suoi componenti. La geometria del flow field e l'umidità relativa dei reagenti svolgono un ruolo chiave nella gestione dell'acqua all'interno delle PEMFC e nell'ottimizzazione delle prestazioni. In questa prospettiva, il presente lavoro presenta un'analisi CFD 3D delle prestazioni PEMFC in diverse condizioni operative e configurazioni geometriche, e un'analisi del modello 1D al fine di sviluppare una metodologia per includere tali effetti nella configurazione 1D.

Parole-chiave: PEMFC; modello multifase; CFD; idratazione; allagamento, flow field.

Extended Abstract

1. Introduction

Polymer Electrolyte Membrane Fuel Cell (PEMFC) represents one of the most recurrent topics in the field of energy systems. The interest in this technology is the result of the great advantages and its feasible application in automotive sector, as well as micro co-generation one. PEMFC, indeed, ensures high power density, low operating temperature, quiet operation, fast start-up, fast response to load changes, modularity and zero emissions, allowing to reduce greenhouse gases and air pollution. Moreover, PEMFC results to be fuel-efficient, converting energy from fuel with more efficiency than today automotive power systems. Nevertheless, there are still important issues that have prevented immediate commercialization on a large scale of PEMFC. The main disadvantages are the absence of distribution network for hydrogen, that hinders a capillary use of this technology, a high cost of technology, a low durability of components, and, last but not least, water management inside cell.

2. PEMFC technology

PEMFC technology is introduced. Its operating principle, structure and current challenges is reported. It is understood that water balance inside PEMFC represents a critical issue for its correct operation. Actually, water transport through membrane, catalyst layers and diffusion media of PEMFC affects strongly performance and durability of the cell. Indeed, water transport is responsible of technical problems inside cell, related to flooding of porous media and gas flow channels that prevents reactant to reach active sites in catalyst layer, worsening performance of the cell. From the other side, membrane protonic conductivity is strictly related to its hydration state; thus, it needs to absorb enough water to allow a good protonic transport and better performance of the cell. During years, several experimental techniques have been developed to visualize the motion of liquid water inside cell, as nuclear magnetic resonance, beam interrogation and direct optical photography. After all, by themselves, those experimental means have been demonstrated to be very limited and numerical

modelling of PEMFC has started during years to play an important role in understanding better electrochemical mechanism and transport phenomena.
Two factors which have a great impact on water management and, therefore, also on performance are introduced: flow field geometry and inlet relative humidity of reactants. The geometry of the flow field plays a crucial role, since it helps not only the delivery of the reactants and the removal of products, but also in evenly distributing reactants over the entire active areas, which results in uniform current distributions and high power density. Parameters of bipolar plate are greatly influencing the mass transfer in polymer electrolyte membrane fuel cells. To carve out the mass transport problems, the optimum design of flow channel is essential with profound understanding of water transport phenomena. In recent years, numerous studies and research on PEMFC have attempt to optimize the geometry of the flow field in order to ensure better performance. Three main different flow fields are typically used: interdigitated, parallel and serpentine flow fields and, in this context, the ratio of rib width to channel width, R/C ratio, is the most studied parameter even if also the channel's shape, new different configurations and materials have been studied with the aim of optimize performances. The relative humidity of the reactant impacts strongly on water management and water transport through the membrane inside PEMFC, and it is not possible to optimize performance without taking account of its contribution. Therefore, first objective of this thesis work is the investigation of the impact of geometrical parameters and relative humidity of reactants on transport phenomena related to water management, membrane hidratation and liquid water flooding in porous media, on a 3D configuration evaluating their impact on cell performance.

3. PEMFC Mathematical Models

To simulate PEMFC behavior the formulation of the mathematical PEM fuel cell model and details about the implementation are needed. The basic formulation of multiphase model is presented in terms of conservation of mass, momentum and species. For what concerns gas species transport, classical modelling is reported. Different laws for diffusion flux are presented, like Fick's law, Stefan-Maxwell law and Knudsen diffusion mechanism. In order to describe electrochemical reaction rate, the Tafel equation and the more complete Butler-Volmer equation are reported. Moreover, it is decided to take into account the effect of Tafel slope doubling by including formation of Platinum Oxides into Tafel law for Oxygen Reduction Reaction. Analysing water transport, firstly water production mechanism is clarified, and it is assumed, as done in preceding works present in literature, that water produced inside cell is in the polymer phase. Secondly, water transport mechanisms are modelled. The diffusive model approach for dissolved

phase transport inside electrolyte is used. It is assumed that from dissolved phase water can be transferred both in vapour and liquid phases, through a non-equilibrium mechanism, that is not only mathematically better posed but also physically more meaningful with respect to the equilibrium approach. Moreover, two-fluid model approach is used for modelling liquid phase transport both in porous media and channel and volume-averaged continuity equations are used. In the case of porous media, liquid phase is transported by capillary diffusion mechanism, described by Darcy's law, whereas, in the case of flow channel, it is assumed that liquid phase is mainly transported as result of drag force exercised by gas phase. Phase transfer between vapour and liquid phase is modelled using an evaporation / condensation law based on unidirectional diffusion theory. Moreover, it is assumed continuity in capillary pressure at interface between different porous media and a one way liquid flux is set as boundary condition at GDL-channel interface, instead of arbitrary saturation value, thus allowing a high liquid saturation level in case of low water outflow.

4. PEMFC 3D Numerical Modeling

Numerical implementation of multiphase mathematical model, described above, into a 3D model is reported. The software used for developing 3D model, is ANSYS Fluent®, where a module for governing equations of charge, dissolved phase and liquid water is already built in. Platinum Oxides coverage dependence of Oxygen Reduction Reaction has been included in a previous work, as well as tortuosity correction for binary diffusion coefficients. It has been also assumed that processes of adsorption and desorption from vapour and from liquid water to dissolved phase are symmetric. 3D meshes are then introduced. A straight single channel, 15 cm long, for 3D configuration to model real PEMFC operation is considered. The accuracy of a CFD solution is governed by a number of cells in the grid. In general, the larger number of cells, the better the solution accuracy. Both the accuracy of a solution and its cost in terms of necessary computer hardware and calculation time are dependent on the refinement of the grid. To assess the reliability of the results, an analysis of the mesh is necessary to ensure the independence of the solution from the mesh used. Three simulations have been performed: one with the mesh used in the simulations, a less refined mesh and a more refined mesh, doubling and halving the cell width, respectively. Solutions show very low sensitivity to a mesh refinement ensuring that are independent of grid size. Boundary conditions are specified for all the governing equations at each interface between different domain components. It is assumed continuity in capillary pressure at interface between different porous media and a one-way liquid flux is set as boundary condition at GDL-channel interface, instead of

arbitrary saturation value, thus allowing a high saturation level in case of low water outflow.

5. Results 3D model

The results regarding the analysis of the effects of 3D geometry on the mass transport of reactants in the cathode region are reported, with great care about water management and performance of a PEMFC. Firstly, preliminary analysis focused on the main instrument used to evaluate the performances, that is on the polarization curves, is performed. The trend of the curve is influenced by four main losses that determine its possible separation into distinct regions based on the dominant physical processes: fuel crossover and internal current losses, activation losses, charge transport or ohmic losses, and concentration losses. Water management has a great impact on polarization curve. Protonic conductivity locally varies, because of increasing in hydration state of electrolyte membrane as current increases, resulting in a non-linear trend of voltage losses related to membrane, instead of the linear trend predicted by simple single-phase models where protonic conductivity of membrane is constant. As current increases, increasing voltage losses are determined, from one side, by the effect of increasing transport resistance due to flooding of porous media and, from the other side, by an increase in membrane resistance because of dehydration of the anodic region caused by a higher electro-osmotic water transport from anode to cathode. Then, results of 3D simulations are reported. The aim of this analysis is to investigate the effects of geometrical features and operating conditions on water management inside the PEMFC and on performances. Two different geometrical parameters have been investigated: rib/channel ratio in order to simulate different flow field geometrical configurations and Gas Diffusion Layer (GDL) thickness. Three different geometrical configurations are investigated by varying the width of rib of current collector with respect to the channel one (R/C=1/3 - 1 - 3), without changing the sum of the two lengths. Increasing rib width, by keeping same operating conditions, it is observed a lower current density at same voltage, as is shown in Figure 1-a, because less liquid water is able to exit from GDL and oxygen availability in the region under the rib is more and more limited. Indeed, the greater decrease in the performances is found to be in the high density of current region, where the water, produced by the cathodic semireaction, tends to condense and to accumulate under the rib hindering even more the diffusion of the reactants towards the active area and, thus, a homogeneous exploitation of the active sites.

Three configurations with different GDL thickness value (150 μm - 225 μm - 300 μm) are also analysed. It is understood that the influence of a variation in GDL

thickness on the polarization curves shows is not as marked as that of the R/C parameter. Depending on the size of the rib, however, the optimization of the GDL thickness is crucial in order to prevent an excessive decrease of performances. For high values of rib/channel ratio, the behavior of the PEMFC is strongly affected by the three-dimensional effects related to the presence of a wider rib and thinner thickness disadvantages the performances because it associates to the diffusion problems related to the high value of R/C, also a lower average path for diffusion, resulting in an increase in the disomogeineity in the exploitation of the active area as well as in the diffusion of reactants. A greater thickness, instead, allows a more homogeneous diffusion and lower losses. At low values of rib/channel ratio, on the contrary, a finer thickness favours an increase in the mass transport through GDL and consequently a decrease of mass transport losses and better performaces. At the same time, also the breakthrough into the channel of the liquid water is favored, given the lower average path that the liquid water must permeate in order to reach the GDL-channel interface. 3D model is then validated on different operating condition. The effect of increasing inlet relative humidity values for gases fed at cathode side, as well as the effect of different inlet dry partial pressure of oxygen, are investigated deeper by analysing local profiles of selected variables along channel direction and in the region under the rib. Regarding cathode relative humidity, a dry case with RHc=30% and a wet case with RHc=80% were studied. The results, as reported in chapter 4, show the same trend, varying all the simulated geometric configurations. A shown in Figure 1-b, at high current densities, a lower cathode relative humidity value promotes an improvement in performance because a correct hydration state of the membrane, from which the protonic conductivity depends, is guaranteed by water that is formed in phase dissolved at the cathode catalyst layer. A higher cathode relative humidity results in an excessive increase in the molar fraction of water at the cathode side, thus increasing the risk of condensation and flooding. At low current density instead the amount of water that is formed by the cathodic reaction is minimal and therefore a high relative humidity value in cathode reactant flow is necessary to improve the hydration state of the membrane and, thus, the performance.

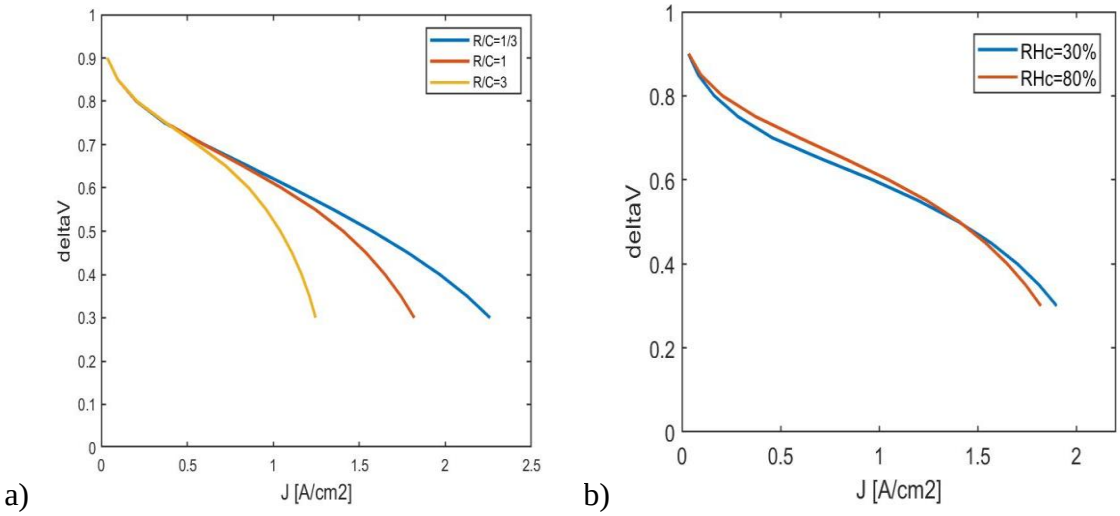

a) b)

Figure1 -a). Polarization curve with different flow field. RHc=30%, δGDL=150 µm.
- b). Polarization curve of R/C=1, δGDL=150µm.

A better insight of how presence of real geometrical elements play an important role on multiphase transport, thus on hydration and flooding phenomena, is obtained.

6. Comparison 1D-3D model

The second objective of this thesis work is finding a methodology that allows to make a comparison between a 1D model, that has the advantage of being much less time-consuming, and 3D model. Starting from the 3D analysis and from an investigation of the models, a selected parameter calibration among the two approaches is presented for a wide range of operating conditions. Investigation of parameters, and validation of coefficients are the key points. Firstly, a 1D model description is provided. The software used for developing a 1D multiphase steady state and AC model is MATLAB® and they describe the physical phenomena occurring along through-plane direction, across Membrane Electrode Assembly (MEA). Some simplifying assumptions are done, neglecting momentum transport along this direction, considering negligible pressure drop, and electron transport in GDLs and MPLs. 1D Stefan-Maxwell equation with constant pressure has been used to describe flux of species across porous media. Binary diffusivities, D_{ij}, are computed by means of the correlation by Chapman-Enkog. It has been decided to neglect the contribution of Knudsen diffusion to transport of gas species inside porous media. Electric charge transport is not solved along Anode and Cathode

GDLs and MPLs, thus determining that potential, ϕ_s is only defined in CLs and membrane. Another assumption is that the processes of adsorption and desorption from vapour and from liquid water to dissolved phase are symmetric. Another step is to evaluate whether 1D and 3D model are implemented in the right way. Both a local and a global comparison are performed, and a valid procedure is developed. The comparison between the two models starts with the identification of the 3D geometrical configuration that guarantee the most monodimensional characteristics. The 1D model does not resolve channels and does not consider the presence of the rib so the 3D configuration selected is the one where the impact of the rib is lower, and the reactants diffusion is homogeneous. Geometric configuration of R/C=1/3, δGDL=300 μm results to be the most suitable one. Profiles of variables as water content in membrane, liquid water saturation and species mole fraction, exported from lines placed at location of 50 % from inlet boundary along symmetry plane in 3D geometry, are compared with profiles of the same variables in 1D model at same voltage, after having set the same species mole concentrations at GDL-channel boundary for both the models. This analysis is performed for two different voltage values, the first one at 0.90V in which the amount of water produced in cathode catalyst layer is very limited and therefore also the presence of liquid water is minimal, and the second one at 0.30V in water which is present also in liquid phase. From preliminary results, at 0.90V trends and gradients of species molar fractions are consistent and follow the diffusion correction as declared in chapter 3. Thus, there is a good accordance between 1D and 3D model, and comparison method works well. At 0.30V instead discrepancies emerge in prediction of liquid water saturation and water content profiles. Indeed, this profiles in 3D simulation are strongly related to the flow field geometry and threedimensional effects. Global comparison, performed by simulating polarization curve, confirms even more the conclusions drawn from local comparison and it is understood the importance of the effects of real geometrical elements on performance of PEMFC and the necessity of developing a methodology to include those effects in 1D configuration. An important step is the identification of the requirements that need to be achieved by a 1D simulation to be able to confirm that the results obtained are consistent with the 3D simulation of reference. Three different requirements have been individuated: water content value inside membrane and catalyst layers, liquid saturation in cathode porous layers and polarization curve. In order to achieve the requirements at the same time, it is necessary to identify as few parameters as possible of the 1D model to be considered. The parameters do not belong to material characteristics nor to operating conditions in order to not distort the simulation itself. The parameters selected are: δ_{GDL} multiplier of GDL thickness, $k_{ads,l}$ adsorption/desorption rate constant from liquid phase and $k_{ads,g}$ adsorption/desorption rate constant from vapour phase. Before calibrating and validating 1D model selected parameters on 3D model results, is important to

understand what is the effect of these parameters on PEMFC performance thanks to sensitivity analysis. It is realized that the presence of a region not directly contacted by gas channel, that is the region under rib of current collector, determines an increase in the effective length of GDL. Therefore, an increase in the GDL thickness is introduced according to the geometry, whereas a variation of adsorption/desorption rate constant is introduced to modify the equilibrium condition between the gas and liquid phases to mimic the spatially non uniform relative humidity (RHc) from channel to rib. Then, a calibration of parameters is presented both at RHc=30% and 80%. The results show a good correspondence of the profiles analyzed in cases with more monodimensional characteristics. In figure 1.1 comparison between 1D and 3D models before and after the parameter calibration is shown.

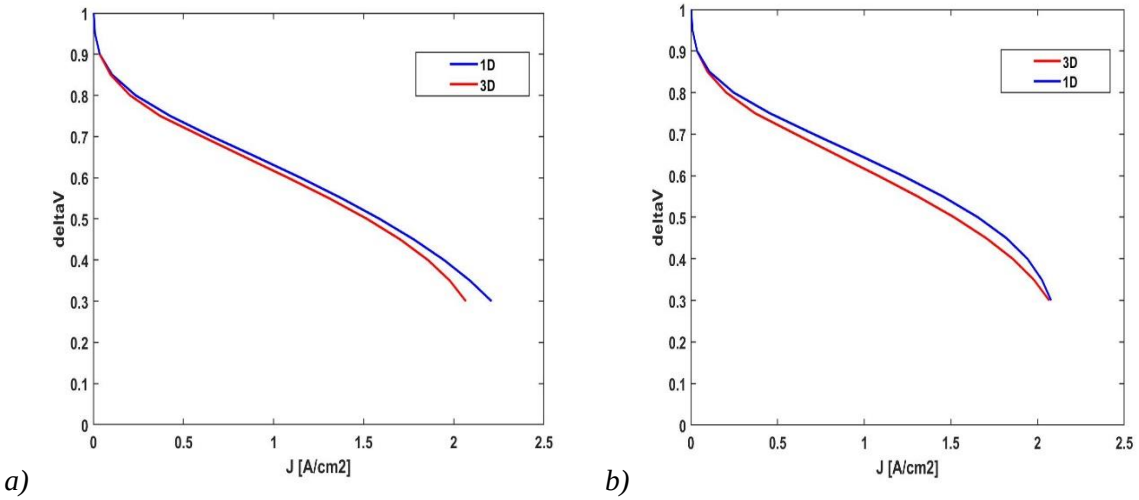

a) *b)*

Figure2 -a) -b). Polarization curve comparison before and after the introduction of coefficients.

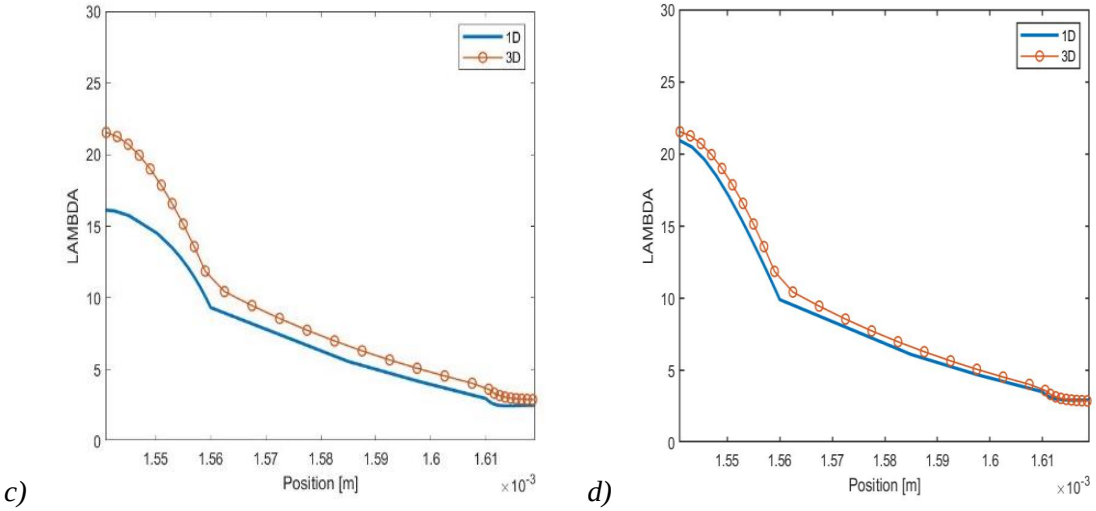

Figure2 -c) -d). Water content before and after the introduction of coefficients.

Even in the most critical cases, where the presence of rib causes a strong impact on the water management and on the diffusion path, the correspondence improves, and the 1D simulated profiles fall between the profiles collected in 3D model along lines drawn on the through plane in the middle of channel, at different locations, under the rib, under the rib-channel interface and under the channel. The last part of chapter is devoted to validation of coefficients changing another operating condition as oxygen partial pressure. Even under these conditions, the 1D model, thanks to selected parameters, is able to accurately predict 3D PEMFC behavior.

CONTENTS

1. Introduction 1

2. PEMFC technology 4

2.1. PEMFC working principles 4

2.2. PEMFC structure and components 5

2.3. Literature review of flow field geometry 9

2.4. Aim of the work 12

3. PEMFC Mathematical Models 15

3.1. Assumption 15

3.2. Governing Equations 16

3.2.1. Conservation of Mass and Momentum 16

3.2.2. Conservation of chemical species 17

3.2.2.1. Determination of species sources 19

3.2.3. Electtrochemical reactions and reactions rate 20

3.2.3.1. Effect of ptOx formation 21

3.2.4. Transport of Multi-Water Phases 22

3.2.4.1. Dissolved phase transport 23

3.2.4.2. Liquid water transport 26

3.2.5. Electric charge transport 30

4. PEMFC 3D Numerical Modeling 34

4.1. Geometry 34

4.2. Mesh and parameters 34

4.3. Boundary conditions 39

4.4. Numerical implementation of 3D model 42

5. Results 3D model 44
5.1. Validation: Polarization curve 44
5.2. Sensitivity Analysis 48
5.2.1. Effects of rib/channel ratio variation 49
5.2.2. Effects of GDL thickness variation 58
5.2.3. Effects of cathode relative humidity (RHc) 63
5.2.4. Effects of dry partial pressure of oxygen 72
5.3. Summary of 3D Analysis 75
6. Comparison 1D-3D model 78
6.1. 1D – Model 78
6.2. Introduction to local and global comparison 79
6.3. Calibration parameters 88
6.4. Sensitivity analysis on model parameters 89
6.4.1. Adsorption/desorption rate constant from vapour phase 90
6.4.2. Adsorption/desorption rate constant from liquid phase 91
6.4.3. Multiplication factor of GDL thickness 93
6.5. Methodology and calibration 94
6.6. Validation in the most critical case 97
6.7. Variation of oxygen partial pressure 101
6.8. Conclusions 102
7. Conclusions and final remarks 104
Bibliography 110
List of figures 115

1. Introduction

Polymer membrane fuel cell technology (PEMFC) is current topic in the field of energy conversion systems, as result of the advantages of this application and its real possibilities for use in the automotive and microcogeneration sectors. The interest received by PEMFC technology is due to several unique features: high efficiency and power density, low emissions, (<100 °C), quiet operation, fast start-up, fast response to load changes, modularity. Upon seeing the potential of this technology, the experimental activity has greatly increased in recent decades, with the aim of fully understanding physical phenomena and designing new configurations and new materials that guarantee an improvement in performance and lifetime. Indeed, in the last two decades relevant progress in the field of Polymer Electrolyte Membrane Fuel Cell (PEMFC) has been achieved. Due to the evolution of their structure and performance, polymeric membrane cells are playing a key role in programs that provide for their application on electric vehicles. In fact, among the different types of fuel cells, the PEMFCs assure the characteristics most required for applications in cars, such as the low operating temperature and the use of a chemically inert electrolyte. Several automotive manufacturers, such as Honda, Toyota, Hyundai, Chevrolet and Mercedes-Benz, are starting to bring proton-exchange membrane (PEM) fuel-cell electric vehicles (FCEVs) on the market. Nevertheless, there are still important issues related to the absence of distribution network for hydrogen, that hinders a capillary use of this technology, the high cost of technology, the low durability of components, and the water management inside the cell. A significant cost reduction has been obtained recently by decreasing loading of noble metals, mainly platinum, used as catalyst, and it is expected, by increasing number of produced cells, that the cost could benefit from economies of scale. In this view, durability of components is an additional impacting factor on the cost.

Water management inside PEMFC is responsible of technical problems inside cell, related to flooding of porous media and gas flow channels, that prevents reactant to reach active sites in catalyst layer, worsening performance of the cell. From the other side, membrane protonic conductivity is strictly related to its hydration state; thus, it needs to absorb enough water to allow a good protonic transport and better performance of the cell. Water management strongly depends on the geometry of the flow field obtained on the bipolar plates of the current collectors and on the state of hydration of the reactants. The aim of this work is therefore to analyse, through simulations using a 3D model, the effect of real geometrical elements in PEMFC on membrane hydration and porous media flooding phenomena. The main disadvantage of 3D simulations is the high

computational time required and, for this reason, another purpose of this thesis work is to demonstrate the possibility to implement the effects studied in the three-dimensional analysis by means of a calibration of several selected parameters, in a 1D model, already previously developed. Chapters content is briefly listed below.

- Chapter 2**.** State of art of PEMFC, with great attention on current challenges. Literature review about PEMFC flow field modelling and reactant relative humidity effects. Aims of the work.
- Chapter 3. Description of governing equations related to multiphase PEMFC modelling, boundary conditions and description of meshes used in 3D simulations.
- Chapter 4. Investigation and discussion of simulations performed with 3D model to investigate 3D geometrical effects. Validation of 3D model and analysis of results in different operating conditions and geometrical configurations.
- Chapter 5. Comparison between 1D and 3D model and introduction and development of methodology in order to include the effects of real geometrical elements and different reactants relative humidity in 1D configuration.

Chapter 2

This chapter gives a brief introduction to the technology and working principles of PEMFCs, followed by a review of the research in literature. Finally, the aims of this paper are presented.

2. PEMFC technology

Polymer electrolyte membrane fuel cells PEMFC are devices able to convert chemical energy of a fuel into electrical energy via electrochemical route. PEMFC are very promising for energy application mainly because no direct pollutants are produced during operation. Another distinct and unique features are quick start-up, high power density, fast response to load changes, low operating temperature, modularity and system robustness. For these reasons PEMFC represent a suitable candidate as the next generation power sources for transportation, stationary and portable applications. Conversion from chemical to electrical energy into a PEMFC is not due to a combustion process, exploiting thermodynamic cycles, meaning that there is no a theoretical maximum thermodynamic limit for the efficiency, that is the Carnot efficiency, but is possible to reach higher efficiencies without increase the temperature of the system. This chapter covers the following topics:

- PEMFC structure and working principles
- Actual state of art of PEMFC and literature review
- Aim and objectives of this work.

2.1. PEMFC working principles

A polymer electrolyte membrane is composed of two porous electrodes, a negative one named anode, where hydrogen is fed and a positive one, cathode, where air or oxygen is fed, separated by a polymer electrolyte membrane. In each of these a semireaction occurs, in particular at the anode side hydrogen oxydation reaction (HOR) while a oxygen reduction reaction at the cathode side (ORR). The membrane placed between the two electrodes allows proton transport and conduction, working as a ionic bridge, while it is impermeable to electrons transport, thus not allowing their conduction. Electrons like this are forced to pass through the external circuit, producing power output. Anodic and cathodic semireactions and complessive reaction are reported here.

$$H_2 \rightarrow 2H^+ + 2e^- \qquad (2.1)$$

$$\frac{1}{2}O_2 + 2H^+ + 2e^- \rightarrow H_2O \qquad (2.2)$$

$$\frac{1}{2}O_2 + H_2 \rightarrow H_2O \qquad (2.3)$$

From a thermodynamic point of view, the possibility of extracting work from this device is due to the difference in electrochemical potential between the two electrodes, which results in a difference in electrical potential capable of generating a motion of electric charges when the external circuit is closed.

2.2. PEMFC structure and components

A real Proton Exchange Membrane Fuel Cell (PEMFC) is composed of a cathode and anode electrodes and a protonic conducting membrane placed in between as shown in Figure 2.1. The set of electrodes and membranes (Membrane Electrode Assembly), mentioned above, is comprised between two graphite plates, called distributors, in which the supplying channels of the gaseous reactants are obtained. A detailed description of the components is given below.

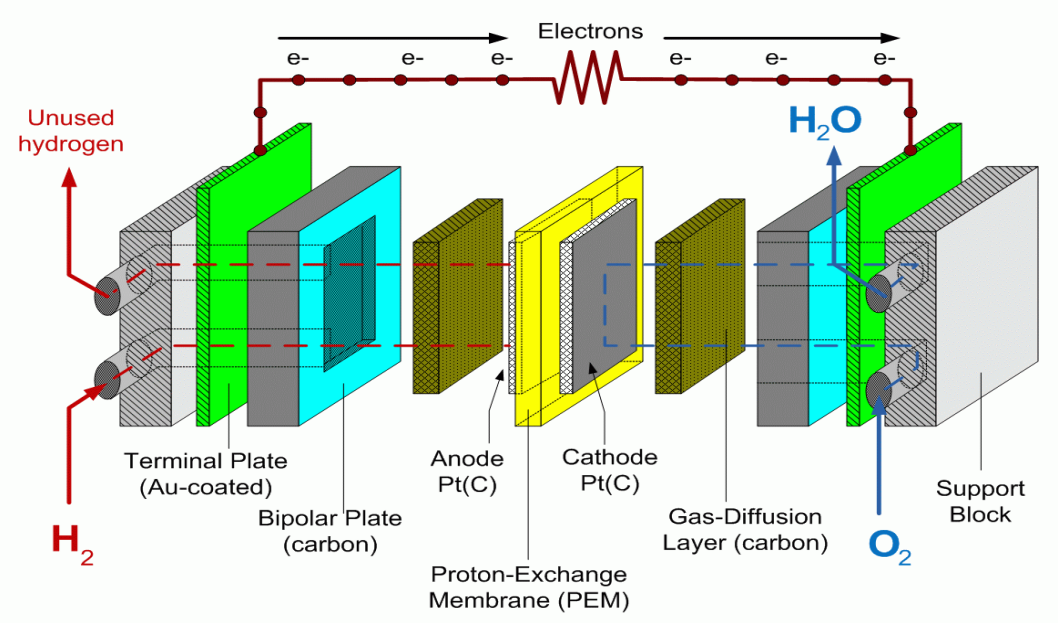

Figure 2.1. Schematic representation of fundamental PEM fuel cell components. From "Fuel cell. What is it and how does it work?". In Renewable Energy (2017).

Gas diffusion layer (GDL)

Gas diffusion layer is a porous medium, some hundred microns thick, which has the task of connecting the channel with the catalyst layer allowing reactants and products of electrochemical reactions to flow from the channel to the electrode and in the opposite direction. It also has the task of providing an electrical contact between the current collectors and the CL, ensuring the current produced here to flow to the external circuit connected to the load.

Micro porous layer (MPL)

Micro porous layer is a hydrophobic layer, often present between GDL and CL, characterized by lower porosity respect to GDL that has the task of improving the electrical connection between them and also improving the management of the water thanks to the fractures that form inside it and allow the water to leave the CL.

Catalyst layer (CL)

Catalyst layer is a porous medium, some tens of microns thick, located between the MPL and the membrane, in which the reactant flow and the electrochemical reactions necessary for operation occur. Catalyst layer is the most complex component of polymeric fuel cells. The current generated by the fuel cell is directly related to how fast the electrochemical reactions proceed. Fast electrochemical reactions result in a high current output from the fuel cell while sluggish reactions result in low current output. High current output is desirable. Therefore, catalysts are generally used to increase the speed and efficiency of the electrochemical reactions. In fact, electrochemical reactions occur in the presence of the so-called triple-phase-boundary, that is the interface where there is simultaneous availability of oxygen, H^+ ions and electrons, in the presence of the catalyst. Catalyst is the active phase on which the electrochemical reactions occur and is present composed of platinum nanoparticles dispersed on a carbon-based support; its role in the catalyst layers of a PEM fuel cell is to lower the activation energy barrier for the half-cell reaction and increase the overall rate of conversion of reactants to products thus enhancing the overall performance on a per m^2 geometric active area basis. Through the solid matrix electrons are conducted to or from the GDL, while through the ionomer fibres positive electrical charges are conducted from or to the membrane. Reactants flows through the void pore space that is very limited in this domain.

Membrane

A Polymeric membrane is located between anode and cathode catalyst layer and is generally composed of an acid and ionically conductive polymer, typically Nafion®. The polymer membrane is, in some ways, the heart of the PEMFC as it provides the primary function of transferring ions between the two electrode reactions allowing for them to be coupled. In particular it has the function of conducting protons efficiently and preventing direct electron and reactant transport between the two electrodes. Nafion® needs to be constantly hydrated to ensure proton transport in fact protonic conductivity depends on water activity. Actually, sufficient water needs to be absorbed into to have a good hydration state and therefore a high protonic conductivity. However, water is also transported between the two CLs, but excess water can determine flooding of cathode, hindering fuel cell performance. It is therefore a critical component.

Current collectors

The external parts, named bipolar plates or current collector, are generally made in graphite or in a corrosion resistant metal and are in contact with both GDL and the external circuit. They are a solid domain and have the task to collect electrons coming from anodic region and redistribute them in the cathode one, after having been transported through the external circuit. Over the two graphite plates, referred as flow fields, gas flow channels are obtained. The shape, size, and pattern of flow channels can significantly affect the performance of the fuel cell. The task of the channels is to supply the reactant gases, humidified and pressurized, and to transport the products of reactions while the presence of ribs, at the same time, allow the passage of current from the electrodes to the outside, thanks to their high electrical conductivity. In this context, the geometry of the flow field plays an important role, since it helps not only the delivery of the reactants and the removal of products, but also in evenly distributing reactants over the entire catalyst layer (CL), which results in uniform current distributions and high power density. The flow field could be of different shapes, indeed, there are three different typically used configurations: interdigitated, parallel and serpentine flow fields with one or more channels in parallel. Interdigitated flow field consists of ended channels, which forces the gases to flow into the gas diffusion layer (GDL), promoting water removal. Such a design shows a high performance at high current densities when water is produced significantly, but its pressure drop is also the highest among these three types of flow fields. Pressure drop within parallel flow field is low, but water is prone to accumulate in channels, resulting in water flooding. The serpentine flow field is considered as a compromised design, which has higher pressure drop than parallel flow field due to the long channel length and numerous turnings. However, for serpentine flow

field, water flooding can still occur at the outlet region and U-bend regions; in addition, membrane dehydration might occur at the inlet region. Therefore, some work has been done for the optimization of serpentine flow field to keep a balance between the water removal and pressure drop. A key factor, whose effects will be analysed in Chapter 4, is the ratio between the width of the rib and the width of the channel (R/C ratio).

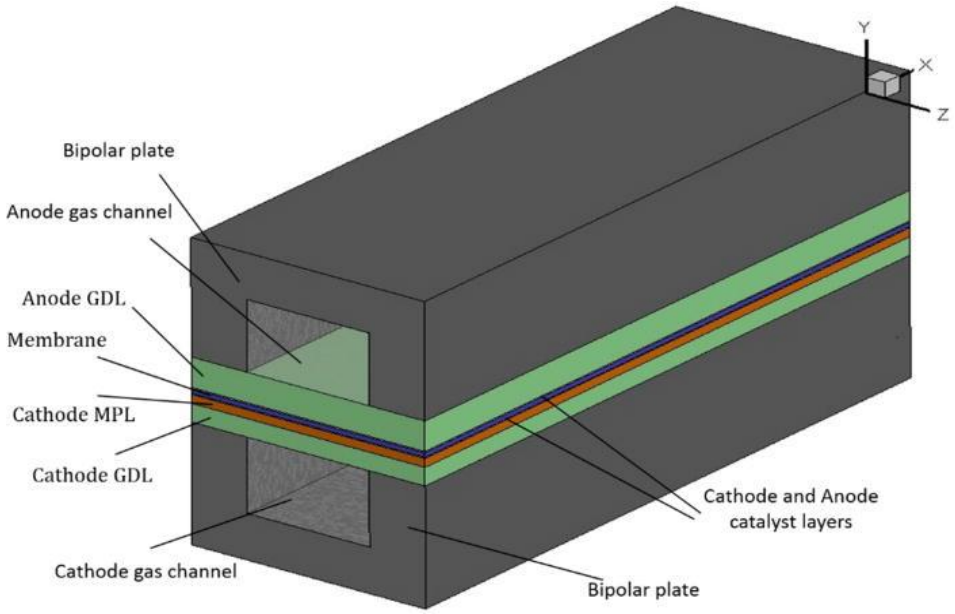

Figure 2.2 3D domain in the case of straight channel geometry.

In order to understand in which direction research has evolved, it is necessary to explain which are the main problems related to PEMFCs that limit their commercialization on a large scale. One of the biggest challenges related to the operation of PEMFC, in addition to the high cost of materials and the fragility of the membrane, is water management, as essential in the membrane and layers to ensure better performance. In fact, the membrane in the PEMFC must be hydrated enough to ensure good protonic conductivity, otherwise the duration of the component is strongly affected and also the performance of the cell decreases, increasing the internal resistance of the membrane itself. Water is also produced at the cathode through the electrochemical semireaction during operation and, if flooding occurs, hinders the diffusion of the gaseous reactants blocking pathway

in layers, resulting in a reduction in performance. For these reasons it is necessary to ensure a right balance of water inside cell.

2.3. Literature review of flow field geometry

In recent years many fuel cell studies have been carried out analyzing different characteristics and using different approaches. Different mathematical models have been developed to simulate as accurately as possible the behaviour of PEMFCs on CFD software packages, including ANSYS Fluent® and COMSOL Multyphysics® and also exsperimentally it has been attempted to study which geometric configuration of the flow field, channels and GDL is the best in terms of performance of the cell. In the literature review will be presented the main studies and experiments carried out to verify how the performance of PEMFC changes with the variation of the geometry of the flow field and of the relative humidity of the incoming reactant flows. In the first decade of the years 2000 several researchers studied channel and rib width ratio effect numerically [2][7] or experimentally [30]. Among them, Xuyang Zhang et al. [3] study a single serpentine flow fields with four different land widths used in PEM fuel cells. Three different inlet flow rates are studied for all the flow fields with four different land widths. The effects of land width and inlet flow rate on fuel cell performance are studied based on the polarization curves and power densities. Without considering the pumping power, cell performance always increases with the decrease in the land width and the increase in the inlet flow rates. However, when taking into consideration the pumping power, the net power density reaches the maximum at different combinations of land widths and reactant flow rates at different cell potentials. S. Shimpalee et al [5] numerically investigated how serpentine flow-fields with different channel/rib's cross section areas affect performance and species distributions for both automotive and stationary conditions. Their results revealed that for automotive condition, wider channel with narrower rib spacing gives higher performance but opposite results when stationary condition is applied.
Chao Wang et al [8] study the effects of under-rib convection and pressure drop on cell performance, investigating the channel/rib width and channel cross-sectional area of parallel-serpentine flow fields, both experimentally and numerically. The results show that the performance differences with various flow field configurations mainly derive from the oxygen transport resistance which is determined by the water accumulation degree, and the cell performance would benefit from the narrower channels and smaller cross sections. It reveals that at low current densities when water starts to accumulate in GDL at under-rib regions, the under-rib convection plays a more important role in water removal

than pressure drop does; in contrast, at high current densities when water starts to accumulate in channels, the pressure drop dominates the water removal to facilitate the oxygen transport to the catalyst layer. Dong Hyup Jeon [9] investigated the effect of channel-rib width on dynamic behavior of liquid water in a gas diffusion layer using the multiphase lattice Boltzmann method. He simulates various channel-rib width configurations ribs. The ratio of channel width to rib width is fixed at one and both widths are altered with same ratios. The results show that at the early stage the water distribution is uniform. On the other hand, the water distribution becomes different as the flow paths closely reach the channel and rib, indicating that the Channel-Rib width significantly affects the water transport behavior. The C-R width influences also the location of water breakthrough into the channel. In fact due to the higher pressure at the center of channel and rib area, the dominant path stretches toward the lower pressure region that is located at the point offset from the center of channel toward the rib.

In addition to investigating the effect of the Rib/Channel ratio many studies have focused on different possible channel configurations, shapes and materials. Nguyen Duy Vinh and Hyung-Man Kim [4] evaluated the effects of flow-field designs, including a serpentine flow field with sub channel and bypass and a conventional serpentine flow-field on single-cell performance. Both the experiment and computer simulation indicated that the serpentine flow field with sub channel and by pass configuration enables more effective utilization of the electrocatalysts since it improves reactant transformation rate from the channel to the catalyst layer, minimizes the pressure drop and facilitates the discharge of liquid water, thereby improving the fuel cell performance. Nima Ahmadi et al [1] focused their investigation on the improvement of the PEMFC performance by changing the geometrical configuration of the gas channels. In their work the cross section of gas channel inlet has changed from square to inverse trapezoidal shape, that is, the bottom width of the channel is kept fixed at 1 mm while the width of the top of the channel is increased with the discontinuity of 0.2 mm from 1 mm (square) to 1.6 mm. Results show that the best performance, in terms of higher membrane conductivity, lower ohmic losses, higher water activity, is obtained for the inverse trapezoid channel with the 1.2mm width in the top section of channel. In a similar study Hang Guo et al [16] developed a two-dimensional, two-phase, non isothermal, steady-state model to investigate the mass transfer and power loss in proton exchange membrane fuel cells with different baffled flow channels (rectangular, trapezoidal, waved, semicircular and triangular baffles). Chowdhury et al. [19] investigated the convergent and divergent serpentine flow fields. The numerical results revealed that the modified convergent serpentine flow fields yield a uniform current density. This is because of the lower mass fraction of water concentration over the reaction zone. It provides better oxygen mass transport and also higher channel pressure distribution along the flow field in comparison to the conventional serpentine flow fields. Ikechukwu S. Anyanwu

et al [18] study the dynamics of liquid water characteristics in the sinusoidal channel of a PEMFC using a 3D computational fluid dynamics model together with the VOF method. Water removal rate increases compared to the straight channel base case. This improvement is due to the strength of the induced secondary flow caused as a result of the curvy nature of the side walls. This characteristic will lead to reduced flow maldistribution and improved cell performance. The pressure drop and gas velocity magnitude across the sinusoidal channel increases with a corresponding increase in sinusoidal distance, and are always slightly higher than the conventional straight channels. Houssein Pourrahmani et al [17] have tried to understand if an applicable way to improve proton exchange membrane fuel cell's (PEMFC) performance at low current densities is to enhance the convective heat transfer in the gas flow channel. They devise a porous ribs in gas flow channel to change the velocity and temperature profiles with subsequent performance improvement.

In order to ensure an optimal water management is important to optimize the flow field geometry, but also to evaluate the effects of a relative humidity variation of the reactant flows entering the anode and cathode. A large number of experimental and numerical models have been used to investigate liquid water transport in flow channels and gas diffusion layers of PEMFCs. The experimental investigations can be classified into direct and indirect methods. Direct methods employ in-situ visualization techniques such as direct optical visualization, X-ray radiography, Nuclear Magnetic Resonance imaging NMR; neutron radiography to observe twophase flow behavior in gas flow channels. Instead indirect methods adopt experimental techniques which evaluates externally measured parameter such as pressure drop, resident time and HFR (high frequency resistance) to examine the two-phase flow of water.

Sajad Rezazadeh et al [12] studied how cell performance varies with relative humidity, simultaneously decreasing the relative humidity of anode and cathode from level RH=100% to RH=75%, RH=50%, RH=25%. Because by this process the water level in the membrane diminishes thus the membrane ionic conductivity, consequently also the performance reduces. The current density loss is higher in humidity level RH=25 % case and tense decline of ionic conductivity in this humidity. Maintaining the same relative humidity value between anode and cathode is proved to be a limiting condition and not the most suitable solution in fact researchers such as Balogun O. Emmanuel et al [15] using the electrochemical impedance spectroscopy and electrical circuit model to analyze the impact of relative humidity and back pressure on water management within the cell and in general on the overall cell performance for various conditions, at both the anode and cathode electrodes. They discovered that for optimized PEMFC performance, there is need for a relative humidity gradient between the anode and cathode with the anode being more humidified than the cathode. Elif Eker Kahveci and Imdat Taymaz [14] used a single-phase, steady-state, three-

dimensional model to investigate the performance of PEM fuel cell with serpentine flow fields, and they found that as the relative humidity of anode side increases, both the chemical reaction and mass transfer of hydrogen are enhanced due to the increase of water content in the membrane, which leads to a better cell performance. They also found that for lower operating voltages, as the cathode relative humidity decreases, the cell performance is enhanced because the cell performance is mainly dependent on the cathode mass transport limitations due to the liquid water blockage effect. As RHc decreases, the oxygen concentration in the reactants increases and the water vapour concentration on the cathode side decreases, this reduces cathode flooding and improves the cell performance. Zhuqian Zhang et Al [10] studied the role of cathode relative humidity on transient performances, in fact they developed a three-dimensional transient model to numerically explore the dynamic behaviors of the membrane water content and the fuel cell current density during the voltage jump and gradual change processes under different cathode inlet humidification levels. Their results show that the cathode inlet humidification has a visible effect on the stabilization time of the membrane water content and the output current density and an increase or RHc enhances the start-up performance of a PEMFC. The geometry of the flow field and the relative humidity of the reactants impact strongly on the water management in the cell. Woo-Joo Yang et Al [11] studied the effects of these two factors at the same time. In fact they developed a three-dimensional numerical model to simulate, using the commercial software COMSOL, 3D PEMFC unit cell with a serpentine-type channel. Three different land ratio models and three different inlet relative humidity variations are considered and studied to obtain better configuration and operating conditions in terms of PEMFC performance. They results show thar a narrower rib gives the best performance, whereas a wider rib produces poor performance given a specific inlet relative humidity level and a smaller inlet relative humidity facilitates better PEMFC performance for all land ratio variations.

2.4. Aim of the work

In the light of the preceding bibliographical analysis, is clear the importance of a deep knowledge in water transport phenomena, reaction mechanisms as well as in flow field optimization. A great effort has been done in this direction both by means of experimental and modelling tests. One of the major drawbacks of these methods of analysis is the time required to conduct experiments in the laboratory as well as the high computational cost required by the 3D models developed. In this thesis work, the method used for analysis is initially based on ANSYS fluent simulations using a 3D model in a developed software package. In the second part

of the thesis a parameterized 1D model based on experimental data derived from a previous work is introduced and used.

Therefore, this work has the following objectives:

- Investigation of the impact of geometrical parameters and operating conditions on transport phenomena related to water management, membrane hidratation and liquid water flooding in porous media, on a 3D configuration evaluating their impact on cell performance. This parametric analysis will be carried out in a wide range of geometrical parameters relevant for flow field geometry, including the GDL and land thickness.
- Finding a methodology that allows to make a comparison between a 1D model, that has the advantage of being much less time-consuming, and a 3D model thus, obtaining a set of parameters by means of which both 1D and 3D model could be validated on a wide range of operating conditions and geometrical configuration of flow field.

Chapter 3

In this chapter a review of the governing equations used in this work is provided, based on the models in the literature for the description of the operation of the polymeric membrane fuel cells.

3. PEMFC Mathematical Models

This chapter is devoted to describe the physical concepts and governing equations that are used for the formulation of the mathematical PEM fuel cell model and details about the implementation. They are presented in this order:

- All the assumptions at the basis of the mathematical and numerical model. (Section 3.1)
- All the governing equations describing transport phenomena in PEMFC. (Section 3.2)

3.1. Assumption

In order to have a mathematical description of physical and electrochemical phenomena in PEMFC, it is needed to consider multicomponent gas species transport, multiphase water transport, phase change processes, electrochemical reaction kinetic, charge transport and in the most complete description also energy transport. A complete modelling of all the phenomena involved would be not applicable in practical simulation, because of insufficient comprehension of phase interactions and multi-step reaction kinetics.
Without weakening the generality of this model, some assumptions have been made for mathematical model.

- Gravity is ignored due to small Bond number.
- Gas species behaves as ideal gases.
- Gas flow in channels is considered to be laminar due to small Reynolds numbers.
- Production of water in the catalyst layer occurs in the polymer phase.
- Diffusion media and catalyst layers are isotropic and homogeneous.
- Contact resistance between any layers is assumed to be negligible.
- Isothermal operating conditions.
- Steady-state conditions.

Even if it was known that temperature variations affect PEMFC operation and transport phenomena, this, however, would require a deeper investigation that

does not represent the objective of this study. Nevertheless, assuming isothermal operation does not invalidate the obtained results.

3.2. Governing Equations

In this section the main equations used in the literature for PEMFC modelling are reported.

3.2.1. Conservation of Mass and Momentum

Inside each domain region containing a fluid phase, both flow channel and porous media, global conservation of mass needs to be granted. Conservation of mass is the continuity equation

$$\varepsilon^{eff}\frac{\partial \rho_g}{\partial t} + \nabla \cdot \left(\rho_g \overrightarrow{u_g}\right) = S_m \qquad (3.1)$$

where ρ_g represents the density of ideal gas mixture, u_g is the physical velocity vector, ε^{eff} is the effective porosity of medium for gas phase transport, which is related to the bulk porosity and liquid saturation *s* as:

$$\varepsilon^{eff} = \varepsilon\,(1 - s) \qquad (3.2)$$

and the source term, Sm represents generation or consumption of mass related to electrochemical reactions occurring in the domain. Moreover, in each domain containing a fluid, conservation of momentum should be guaranteed, analytically described by Navier-Stokes equations, here reported in its general form for porous media

$$\frac{\partial}{\partial t}\left(\frac{1}{\varepsilon^{eff}} \cdot \rho_g \overrightarrow{u_g}\right) + \frac{1}{\left(\varepsilon^{eff}\right)^2}\nabla \cdot \left(\rho_g \overrightarrow{u_g}\,\overrightarrow{u_g}\right) = -\nabla P_g + \nabla \cdot \bar{\tau} + S_u \qquad (3.3)$$

where S_u is the source term, that is not zero only in porous media and $\bar{\tau}$ is the viscous stress tensor, dependent on fluid viscosity.

3.2.2. Conservation of chemical species

Alongside mass overall conservation, gas phases are composed of different gas species. The transport of each species can be described using a general form of convection-diffusion equation.

$$\frac{\partial}{\partial t}(\varepsilon^{eff} X_k) + \nabla \cdot (\rho_g \overrightarrow{u_g} X_k) = \nabla \cdot \overrightarrow{J_k} + S_k \qquad (3.4)$$

where X_k is the mass fraction of the species k, $\overrightarrow{J_k}$ is the mass diffusive flux vector of species k and S_k is the source term related to generation or consumption of a certain species. The mass diffusive flux vector takes into account species diffusion, due to creation of concentration gradients inside porous media and channel.
Analytical models to describe species diffusion are the Fick's law, Stefan-Maxwell law and Knudsen law. Fick's law describes species diffusion and it is the easiest model [20]. It is formulated as:

$$\overrightarrow{J_k} = -\rho_g D_{m,k} X_k \qquad (3.5)$$

where $D_{m,k}$ is the mass diffusion coefficient for species k in the mixture. This is a good approximation in dilute mixtures when X_k << 1. Stefan-Maxwell's law is more complex and describes multi-component diffusion in very concentrated solutions, taking into account collisions between molecules of diffusing species, that determine a resistance to mechanism of diffusion transport.
The formulation of diffusive flux is not direct as in the case of Fick's law and it is in molar terms

$$\frac{P_g}{RT}\nabla Y_k = \sum_{j=1,j\neq k}^{N}\frac{Y_k N_j - Y_j N_k}{D_{ij}} \qquad (3.6)$$

where N_k are the molar fluxes, Y_k are the molar fractions and D_{ij} are the binary diffusion coefficients. An assumption of this model is to consider only collisions between molecules and to neglect interactions of molecules with the physical media in which they are diffusing. For this reason the applicability of this model in a porous medium is subject to verifying that the pore diameter is much larger than the mean free path of a certain molecule such that collisions with medium walls are negligible. Mass diffusion coefficients are dependent on pressure and temperature and that can be computed by different relations, such as Fuller-Schettler-Giddins and the approximate one of Chapman-Enskog. The second one, used in this work, is reported.

$$D_{ij} = \frac{\sqrt{T^3\left(\frac{1}{M_i} - \frac{1}{M_j}\right)}}{p\sigma_{ij}^2\Omega_D} \qquad (3.7)$$

where σ is the collision diameter of the molecules and Ω is the integral of the collisions, a dimensionless coefficient derived from the gas kinetic theory, which depends on the Lennard-Jones parameters.
Moreover, mass diffusion coefficients needs to be corrected in the case of porous media, in order to obtain effective mass diffusion coefficients, that are then use to compute the mass diffusive flux.

$$D_{ij}^{eff} = \frac{\varepsilon}{\tau}(1-s)^{\delta s}\, D_{ij} \qquad (3.8)$$

where τ is the tortuosity of porous medium, that takes into account the complexity and irregularity of his porous structure, while the term $(1-s)^{\delta s}$ accounts for the presence of pore flooding on diffusion coefficients, since liquid water reduces the pore volume available for gas transport.
Knudsen's model describes diffusion into a porous medium with a pore diameter that is comparable to the mean free path of molecules; thus, this contribute becomes predominant with respect to resistance effect determined by collisions between molecules. The characteristic equation of this diffusion model is

$$\frac{P_g}{RT}\nabla Y_k = -\frac{\overrightarrow{N_k}}{D_k^{Kn}} \qquad (3.9)$$

where D_k^{Kn} is the Knudsen diffusion coefficient, that depends upon the mean radius of pores r^{Kn} according to the following equation

$$D_k^{Kn} = r^{Kn}\sqrt{\frac{8RT}{\pi M_k}} \qquad (3.10)$$

The right-hand side of Equation 3.9 needs to be summed to Stefan-Maxwell one, in Equation 3.6, thus, including interactions with physical medium inside which diffusion transport is occurring. Besides these diffusive phenomena, when there is a pressure difference over a porous medium, another contribution to mass transport is arising, described by Darcy's law. It is a relation between convective molar flux of species k in gas phase and pressure gradient inside porous medium.

$$F_k = \frac{Y_k K K_{rg,k} P_g}{\mu_k RT}\nabla P_g \qquad (3.11)$$

where K is the absolute permeability of porous medium, dependent upon pore shape and dimension, porosity and tortuosity, $K_{rg,k}$ is the relative permeability of species k in gas phase, and μ_k is the viscosity of species k.

3.2.2.1. Determination of species sources

The source terms, S_K, in species transport equation takes into account the production or consumption of species due to electrochemical reactions or mass exchange between phases. The phase change, among the three gas species involved in PEMFC operation, occurs only for water vapour and this will be analysed in Paragraph 3.2.4.2. The rate of hydrogen and oxygen consumption are related directly to electrochemical reaction kinetics. From reactions 2.1 and 2.2, it is visible that for producing one mole of electrons, ½ mole of hydrogen and 1/4 mole of oxygen are consumed. Therefore, once volumetric current density is

known, source terms S_k in Equation 3.4 for oxygen and hydrogen species can be determined as

$$S_{H_2} = -\frac{1}{2F} i_a \qquad (3.12)$$

$$S_{O_2} = -\frac{1}{4F} i_c \qquad (3.13)$$

Where i_a and i_c are volumetric current generated from reactions and they will be introduced in the next paragraph. These equations are valid only in catalyst layer since electrochemical reactions occur there. For all other domain components, there is no hydrogen and oxygen consumption.

3.2.3. Electtrochemical reactions and reactions rate

Electrochemical reactions occurring inside the CL of a PEMFC are, as said above. the reaction of hydrogen oxidation (HOR) 2.1, occurring at anode side, and oxygen reduction (ORR) 2.2, ideally occurring at cathode side.
The anodic reaction frees electrons and protons, that, through GDL and external circuit and through membrane respectively, reach cathode side where they are involved in cathodic reaction. The rate according to which these reactions occur, can be expressed with different phenomenological expressions. The most general one is the so called Butler-Volmer equation, according to which the volumetric current generated from reactions is given as

$$i_a = n_e F K_o ECSA \left(\frac{C_{H_2}}{C_{ref}}\right)^{\gamma_{HOR}} \left[exp\left(\frac{\alpha_o F \Delta\phi_a}{RT}\right) - exp\left(-\frac{\alpha_r F \Delta\phi_a}{RT}\right)\right] \qquad (3.14)$$

$$i_c = n_e F K_r ECSA \left(\frac{C_{O2}}{C_{ref}}\right)^{\gamma_{ORR}} \left[exp\left(\frac{\alpha_r F \Delta\phi_c}{RT}\right) - exp\left(-\frac{\alpha_o F \Delta\phi_c}{RT}\right)\right] \qquad (3.15)$$

where C_{H2} and C_{O2} represent the local concentration of hydrogen and oxygen while C_{ref} is a reference value for concentration, HOR and ORR are the reaction

orders, o and r are the symmetry factors of reactions and they represents position and profile of energetic barrier related to reaction.

F is the Faraday constant equal to 96485 $\left[\frac{A\,s}{mol}\right]$, indicating the charge of one mole of electrons, while $\Delta\phi_a$ and $\Delta\phi_c$ are the difference between potential in solid phase, ϕ_c, and potential in ionomer phase, ϕ_m, evaluated in anode and cathode side respectively. n_e is the number of electrons and ECSA, standing for Electrochemically Catalytic Surface Area, represents the ratio between Pt surface area and volume of Catalyst layer. K_r and K_o are the specific catalyst activity per unit area of Platinum. The first exponential term in 3.14 is referring to the hydrogen oxidation while the second exponential term is related to the backward reaction of hydrogen, as well as the first exponential term in 3.15 is related to oxygen reduction while the second term indicates the rate of the backward reaction.

This equation could be further simplified when some particular conditions are present, that is, if reaction is sluggish, the second term, indicating the backward reaction, could be neglected because of its slow rate of reaction, obtaining the so-called Tafel equation.

$$i_c = n_e F K_r ECSA \left(\frac{C_{O2}}{C_{ref}}\right)^{\gamma_{ORR}} exp\left(\frac{\alpha_r F \Delta\phi_c}{RT}\right) \qquad (3.16)$$

3.2.3.1. Effect of ptOx formation

ORR rates are conventionally modelled using Tafel law, as indicated in Equation 3.16. Experiments for ORR have shown a transition in Tafel slope, i.e. the slope of plot of cell potential vs. the logarithm of kinetic current density, from low values, at high potentials (> 0.85V), where α_r is found to be equal to about 1, to high values at low potentials, where α_r is equal to about 0.5. In literature, this phenomenon is usually called as Tafel slope doubling. Several researchers have tried to understand the reason of divergence in Tafel slope. ORR is hindered by formation of surface oxides such that the apparent Tafel slope is resulting from a combination of the intrinsic Tafel slope and surface coverage determined by Pt-oxide formation that decreases as potential value decreases. PtOx forms in presence of water or oxygen. Here a simplified model has been employed to simulate PtOx formation, assuming a single electrochemical reaction governed by a Butler-Volmer equation.

$$\frac{d\Theta_{PtOx}}{dt} = k_{PtOx}\left[(1-\Theta_{PtOx})exp\left(\frac{\alpha_{o,PtOx}F\eta_{PtOx}}{RT}\right) - \Theta_{PtOx}exp\left(-\frac{\alpha_{r,PtOx}F\eta_{PtOx}}{RT}\right)\right] \quad (3.17)$$

Where $$\eta_{PtOx} = \phi_s - \phi_m - E_{PtOx} \quad (3.18)$$

k_{PtOx} is the reaction rate for $PtOx$, $\alpha_{o,PtOx}$ and $\alpha_{r,PtOx}$ are the forward and backward symmetry factors of reaction, E_{PtOx} is the equilibrium potential for PtOx formation and Θ_{PtOx} is the ratio between PtOx Pt active surface area covered by PtOx and the total one. Under steady state condition, the PtOx coverage ratio can be determined as

$$\Theta_{PtOx} = \frac{exp\left(\frac{\alpha_{o,PtOx}F\eta_{PtOx}}{RT}\right)}{exp\left(\frac{\alpha_{o,PtOx}F\eta_{PtOx}}{RT}\right)+exp\left(-\frac{\alpha_{r,PtOx}F\eta_{PtOx}}{RT}\right)} \quad (3.19)$$

The effect of surface coverage is included in Tafel law by reducing the area available for the occurrence of ORR, thus, the current produced by ORR.

$$i_c = n_e F K_r ECSA(1-\Theta_{PtOx})(1-s)\left(\frac{C_{O2}}{C_{ref}}\right)^{\gamma_{ORR}} exp\left(-\frac{\alpha_r F\Delta\phi_c}{RT}\right) \quad (3.20)$$

Moreover, water flooding in Cathode CL determines the blockage of active area, as indicated by Weber et al. [21], and to account for this effect, a factor of (1 – s) is considered in the expression as visible in Equation 3.20.

3.2.4. Transport of Multi-Water Phases

As said above, one of main research topic in PEMFC area is water transport inside cell and the corresponding loss mechanisms. One main challenge is the liquid water management inside porous media and, mainly, flow channels and how this affects cell performance. Moreover, there is still low consensus about the mechanism of water transport in the proton-conducting membrane. Actually, it is

still not completely understood the phase in which water is present inside ionomer. Some researchers assumes that water in membrane is in liquid phase whereas others think about it as a dissolved phase where water molecules are closely attached to a proton and appear as a clustered block. In this work, water in membrane is assumed to be in a dissolved phase. Another great challenge is related to understand how the three phases of water, that is water vapour, liquid water and dissolved phase, coexist, in which phase water is produced inside CL and what are the transfer mechanisms between them. To clarify the state in which water is produced from ORR, one needs to examine ORR process from a microscopic point of view. Oxygen reduction reaction can occur in the simultaneous presence of Pt catalyst, oxygen molecule, proton and electron, thus it can happen only in a particular zone, the so-called triple-phase zone (TPZ) where all the three species have access. Oxygen travels through the void space and can also dissolve in ionomer; protons travels only through ionomer and electrons through electrically conductive solids, that is carbon support of Pt particles. The ionic group $SO_3^-H^+$ can chemically bond at least one water molecules. Also the protons can attract water molecules, at lest three, and these cannot be assumed to be in vapour phase since are strictly bonded. Therefore, it has been assumed that water is produced in the form of dissolved phase and source term is defined as

$$S_{ORR} = \frac{i_c}{2F} \qquad (3.21)$$

since 1/2 mole of water is produced for each mole of electrons.

3.2.4.1. Dissolved phase transport

Water in electrolyte is usually assumed to be in the form of dissolved phase, as result of chemical interaction with the ionic groups and protons travelling through membrane. Water content inside membrane is modelled with the use of a quantity, called λ, that is defined as the ratio of the number of water molecules to the number of ionic groups SO_3^- , present in anode and cathode catalyst layer ionomer and in the membrane. There are two main mechanisms of transport across a polymer membrane. As mentioned above, water molecule can be affected by interactions with protons that are moving from anode side to cathode side, thus they tend to move with protons towards cathode because of the presence of the

electro-osmotic drag. The molar water flux associated with this phenomenon is given by the following equation:

$$\vec{N}_{drag} = \eta_d \frac{\vec{j}}{F} \qquad (3.22)$$

where j is the ionic current density and η_d is the electro-osmotic drag coefficient that gives the number of water molecules per proton. It depends upon the water hydration of ionomer, thus water content λ, and it has been found experimentally. In this thesis, a linear function developed by Springer et al. [28] is employed:

$$\eta_d = \frac{2.5\,\lambda}{22} \qquad (3.23)$$

A second transport mechanism is related to diffusion. At cathode catalyst layer, water production by ORR and electro-osmotic drag would create a large concentration of water, thus some water molecules could diffuse back to anode side and this phenomenon is called back-diffusion. The molar water flux is computed as:

$$\vec{N}_{d,diff} = -\frac{\rho_I}{EW} D_d \nabla\lambda \qquad (3.24)$$

where $\rho_I$is the dry membrane density and EW is the equivalent molecular weight of dry membrane, usually assumed to be 1.1 kg/mol for Nafion membrane. Summing both the two contributions to dissolved phase transport, the dissolved phase molar flux can be obtained

$$\vec{N}_d = -\frac{\rho_I}{EW} D_d \nabla\lambda + \eta_d \frac{\vec{J}}{F} \qquad (3.25)$$

Diffusivity of dissolved water D_d is determined on the basis of curve fitting of experimental data. Kulikovsky proposed a relation based on λ and it is used in this study [22].

$$D_d = \epsilon_I^{1.5} 4.1 \cdot 10^{-10} \left(\frac{\lambda}{25}\right)^{0.15} \left[1 + tanh\left(\frac{\lambda - 2.5}{14}\right)\right] \qquad (3.26)$$

Where ϵ_I is the volume fraction of ionomer inside catalyst layers and membrane. A Bruggeman correction $\epsilon_I^{1.5}$ is considered to account fro the reduction of the pathways for protons inside catalyst layers where ionomer volume fraction is less than 1. Mass conservation equation in molar terms for dissolved phase is

$$\frac{\partial}{\partial t}\left(\frac{\rho_I \epsilon_I}{EW}\lambda\right) + \nabla \cdot \left(N_{d.diff}\right) + \nabla \cdot \left(N_{d.drag}\right) = S_d \qquad (3.27)$$

where S_d is the source term for dissolved phase and it accounts for phase transfer of water between the three phases and water production from ORR. For what concerns the adsorption/desorption mechanism, that is phase transfer of water into membrane from water vapour and liquid or vice-versa, the model used in this work is the non-equilibrium membrane water sorption, initially proposed by Berg et al. [29] and now quite accepted in literature, as said above in Chapter 1. In this model, adsorbed water inside ionomer is proportional to the difference between the local water content λ and its value at equilibrium, λ_{eq}, that is found to be a function of water vapour activity, a_w . This last quantity is defined as

$$a_w = \frac{P_g Y_{H2O}}{P_{sat}} \qquad (3.28)$$

Different correlations are present in literature for λ_{eq} as a function of a_w. Here, it is decided to take the expression suggested by Weber and Newmann [23] that takes into account the Schroeder's paradox.

$$\lambda_{eq} = 0.3 + 6a_w(1 - \tanh(a_w - 0.5)) + 3.9\sqrt{a_w}\left[1 + tanh\left(\frac{a_w - 0.89}{0.23}\right)\right] + s(\lambda_{s=1} - \lambda_{a=1}) \quad (3.29)$$

where $\lambda_{s=1}$ is the water content when ionomer is completely contacted by liquid water and it is assumed to be 16.8, whereas $\lambda_{a=1}$ is the value obtained from Equation 3.29 when s = 0 and a_w = 1, that corresponds to the configuration where ionomer is completely surrounded by water vapour. Thus, the rate of mass change between water vapour and dissolved phase is given by

$$S_{vd} = \begin{cases} (1-s)k_{ads,g}\dfrac{\rho_I \epsilon_I}{EW}\left(\lambda_{eq}-\lambda\right) & \lambda_{eq} \geq \lambda \\ (1-s)k_{des,g}\dfrac{\rho_I \epsilon_I}{EW}\left(\lambda_{eq}-\lambda\right) & \lambda_{eq} < \lambda \end{cases} \quad (3.30)$$

whereas, the rate of mass change between liquid water and dissolved phase is given by

$$S_{ld} = \begin{cases} s\ k_{ads,l}\dfrac{\rho_I \epsilon_I}{EW}\left(\lambda_{eq}-\lambda\right) & \lambda_{eq} \geq \lambda \\ s\ k_{des,l}\dfrac{\rho_I \epsilon_I}{EW}\left(\lambda_{eq}-\lambda\right) & \lambda_{eq} < \lambda \end{cases} \quad (3.31)$$

where $k_{ads,g}$ and $k_{ads,l}$ are the water vapour and liquid water respectively mass exchange rate constants for adsorption process and $k_{des,g}$ and $k_{des,l}$ are the ones for desorption process and they have the dimension of the inverse of time. Indeed, it could occur that the rate of desorption is not equal to rate of adsorption, determining, thus, an asymmetry in the two processes.
The term s and $(1-s)$ accounts for the reduction in water vapour exchange surface and increase in liquid water one as s increases. In the end, the source term S_d present in Equation 3.27 is indicated in Equation 3.32. As it can be seen, it is confined in catalyst layer regions, whereas it vanishes into membrane since no other water phase is present and no production or consumption of water occurs.

$$S_d = \begin{cases} S_{vd} + S_{ld} & AnodeCL \\ S_{vd} + S_{ld} + S_{ORR} & CathodeCL \end{cases} \quad (3.32)$$

3.2.4.2. Liquid water transport

Liquid water is present inside porous electrodes and gas flow channels but they have to be treated separately because in channels physics of liquid water is assumed to be quite differently.

Liquid transport in porous media

Liquid saturation is defined in porous media as the ratio between the volume of liquid water and the volume of pore region. The mass conservation equation for liquid phase in
molar terms is given by

$$\frac{\partial}{\partial t}\left(\frac{\epsilon\rho_l}{M_{H2O}}s\right) + \nabla\cdot\left(\frac{\rho_l}{M_{H2O}}\,\overrightarrow{u_l}\right) = S_l \qquad (3.33)$$

where ρ_l is density of liquid water, M_{H2O} is the molecular weight of water, $\overrightarrow{u_l}$ is the superficial velocity of liquid water and S_l is the source term that takes into account phase change between water phases to liquid one. In porous media, $\overrightarrow{u_l}$ can be approximated using Darcy's law, that is the liquid counterpart of Equation 3.11,

$$\overrightarrow{u_l} = -\frac{K_{rl}K}{\mu_l}\nabla P_l \qquad (3.34)$$

where K is the absolute permeability of the porous media, function of pore structure, porosity and tortuosity, and K_{rl} is the relative permeability of liquid phase and depends upon the fluid. It will be clarified shortly. Liquid phase can be computed from capillary pressure, defined as the difference of non-wetting phase, generally the liquid one, and wetting phase, generally the gas one, by the following relation

$$P_l = P_c + P_g \qquad (3.35)$$

Substituting Equation 3.35 into Equation 3.34, it is obtained that

$$\overrightarrow{u_l} = -\frac{K_{rl}K}{\mu_l}\nabla\left(P_c + P_g\right) \qquad (3.36)$$

Capillary pressure can be expressed as a function of liquid saturation, *s*. The relation

$P_c(s)$ will be analysed shortly. Thus, the term ∇P_c could be expressed as

$$\nabla P_c = \frac{dP_c}{ds}\nabla s \qquad (3.37)$$

Finally, conservation of liquid phase can be expressed as a function of saturation.

$$\frac{\partial}{\partial t}\left(\frac{\epsilon\rho_l}{M_{H2O}}s\right) + \nabla\cdot\left[\left(-\frac{\rho_l K_{rl} K}{M_{H2O}\mu_l}\frac{dP_c}{ds}\right)\nabla s - \frac{\rho_l K_{rl} K}{M_{H2O}\mu_l}\nabla P_g\right] = S_l \qquad (3.38)$$

Source Term

In this section, source of liquid water are analysed, with main focus on evaporation/ condensation mechanism, that determine mass transfer between liquid and vapour phases.
In this work, mass transfer rate due to evaporation, S_{vl} is computed based on unidirectional diffusion theory [27]

$$S_{vl} = \begin{cases} \gamma_e \epsilon s D_{gl}\frac{M_{H2O}}{RT}P_g \ln\left(\frac{P_g - P_{sat}}{P_g - P_{H2O}}\right) & P_{H2O} \le P_{sat} \\ \gamma_e \epsilon (1-s) D_{gl}\frac{M_{H2O}}{RT}P_g \ln\left(\frac{P_g - P_{sat}}{P_g - P_{H2O}}\right) & P_{H2O} \ge P_{sat} \end{cases} \qquad (3.39)$$

where P_{H2O} is the partial pressure of water and *e* is a geometrical droplet factor that, together with quantity D_{gl}, determines the evaporation and condensation rate. D_{gl} has the following form:

$$D_{gl} = \begin{cases} 0.365\cdot 10^{-4}\left(\frac{T}{343}\right)^{2.334}\left(\frac{10^{-5}}{P_g}\right) & Cathode \\ 1.79\cdot 10^{-4}\left(\frac{T}{343}\right)^{2.334}\left(\frac{10^{-5}}{P_g}\right) & Anode \end{cases} \qquad (3.40)$$

In Equation 3.39, condensation and evaporation processes are differentiated considering partial pressure of water vapour. Thus, when P_{H2O} is lower than saturation pressure, liquid water starts evaporating and the rate of evaporation depends on liquid water surface, that is considered in the term *s*, whereas, if P_{H2O} is greater than saturation pressure, water vapour starts condensing and its rate is proportional to $(1 - s)$, that represents a correlation of water vapour exchange surface. In CLs, as seen above, it is not only present the phase transfer between vapour and liquid phase, but also between liquid and dissolved one in ionomer, while in all other regions of porous electrodes, phase change occurs only between liquid and vapour phase, thus

$$S_l = \begin{cases} -S_{ld} + S_{vl} & CL \\ S_{vl} & GDLs\ and\ MPLs \end{cases} \qquad (3.41)$$

Capillary Pressure and Relative Permeability

A correlation between capillary pressure, P_c and saturation is required to solve liquid water conservation equation, 3.38. For the two-phase flow in a porous medium, P_c can be modelled according to this empirical correlation, developed by Leverett et Al. [24]

$$P_c = -\sigma \cos(\vartheta_c) \sqrt{\frac{\epsilon}{K}} \left(1.417s - 2.120s^2 + 1.263s^3\right) \qquad (3.42)$$

where σ is the surface tension between water and air, and ϑ_c is the uniform contact angle of the porous materials. Actually, in GDL and MPL porous matrix, wettability could change locally because there is the simultaneous presence of hydrophilic material like the carbon substrate and of hydrophobic one as polytetrafluoroethylene (PTFE) coating. In this work, it has been decided to adopt Leverett approach, since it has been used widely in PEMFC modelling. Several relative permeability models are present in literature and they differ each other. It has been decided for K_{rl}, as well, to adopt a model widely used for PEMFC, that is the cubic power law function [25].

$$K_{rl} = s^3 \qquad (3.43)$$

Liquid water transport inside channels

Once liquid water emerges at Anode and Cathode GDL-channel interfaces, its transport is not capillary pressure driven since flow channel volume are not porous and capillary pressure is not defined. Water transport is, instead, mostly determined by drag created by
gas flow. A general diffusion-convection equation, 3.44, is used here to describe transport
of saturation *s*, defined, as previously done, as the ratio between volume of liquid phase and void volume.

$$\frac{\partial}{\partial t}(\rho_l s) + \nabla \cdot (\rho_l s \overrightarrow{u_l}) = \nabla \cdot (D_s \nabla s) \qquad (3.44)$$

where D_s is the liquid water diffusion coefficient in gas channel, $\overrightarrow{u_l}$ is the liquid phase velocity inside channel and it is assumed to be a fraction of the gas velocity $\overrightarrow{u_g}$, accordingly to Equation 3.45.

$$\overrightarrow{u_l} = \chi \overrightarrow{u_g} \qquad (3.45)$$

where χ is liquid to gas velocity ratio and it is assumed to be constant. Since it is reasonably to assume that flow is dominated by convection, no phase transfer is allowed
between vapour and liquid phase.

3.2.5. Electric charge transport

Transport of charge species occurs through the solid phase or through the electrolyte thanks to presence of a potential field, electric and protonic respectively. Electrons, with a negative charge, are taken off from hydrogen molecules that become protons as result of HOR. Then, electrons are expelled from Anode CL and have to travel through solid material of diffusion media, current collector and external circuit to enter again on the other side of the cell, reaching Cathode CL, where, together with protons and oxygen molecule, produce

water according to ORR. Protons reach Cathode side by travelling, instead, through electrolyte membrane. Governing equations of charge transport are reported for electron and proton transport respectively in Equations 3.46 and 3.47.

$$-C_{DL}\frac{\partial \eta}{\partial t} + \nabla \cdot (\overrightarrow{J_s}) = S_{\phi_s} \qquad (3.46)$$

$$-C_{DL}\frac{\partial \eta}{\partial t} + \nabla \cdot (\overrightarrow{J_m}) = S_{\phi_m} \qquad (3.47)$$

where C_{DL} is the capacity of double layer, that describes the capacitive effect determined by interface between electrolyte and electrode inside pore volume of CLs and η is the local overpotential, defined in Equation 3.47.

$$\eta = \phi_s - \phi_m - E \qquad (3.48)$$

where E indicate the equilibrium electrode potential and it is indicated with E^+ for Cathode and E^- for Anode. $\overrightarrow{J_s}$ and $\overrightarrow{J_m}$ are the electronic current density trough solid phase and protonic current density through the electrolyte membrane. S_{ϕ_s} and S_{ϕ_m} is the source terms indicated by HOR and ORR reaction rates. According to Ohm's law, the electronic and protonic current density can be written as follows.

$$\overrightarrow{J_s} = \sigma_s \nabla \phi_s \qquad (3.49)$$

$$\overrightarrow{J_m} = \sigma_m \nabla \phi_m \qquad (3.50)$$

where ϕ_s and ϕ_m are electric and protonic potentials and σ_s and σ_m are the electric conductivities of solid material and the protonic conductivity of electrolyte respectively. σ_m depends on local water content inside membrane and the following formula is used [26].

$$\sigma_m = \epsilon_i^{1.5}(0.005139\lambda - 0.00326)\exp\left(1268\left(\frac{1}{303} - \frac{1}{T}\right)\right) \qquad (3.51)$$

$S_{\phi_s}$and S_{ϕ_m} are defined as follows.

$$S_{\phi_s} = \begin{cases} i_a & Anode\ CL \\ -i_c & Cathode\ CL \end{cases} \quad (3.52)$$

$$S_{\phi_m} = \begin{cases} -i_a & Anode\ CL \\ i_c & Cathode\ CL \end{cases} \quad (3.53)$$

In all other regions, no electrochemical reactions occur; thus, both S_{ϕ_s} and S_{ϕ_m} are equal to 0.

Chapter 4

A description of the meshes needed for 3D model simulations and analysis of the independence of the results from the mesh is given. Finally, a description of numerical schemes is provided.

4. PEMFC 3D Numerical Modeling

In this chapter a 3D model introduction is provided and how mathematical model can be implemented on a three-dimensional geometry, is described. Structure and methodology of Chapter are listed below.

- Description of the meshes used, analysis of the result independence from the mesh, and presentation of operating and geometrical parameters used in the simulations.
- Description of boundary conditions in each domain.
- Introduction of the 3D model used to focus on the implemented equations and discretization schemes used in the iterative resolution of the equations.

4.1. Geometry

The flow field, as introduced in the first chapter, can be presented in three configurations: serpentine, interdigitated and single straight channel. In this work, in order to reduce the computational time therefore it has been decided to carry out the simulations on a 150mm straight single channel. These assumptions do not affect negatively the aims and the results obtained and described in this work, taking into account that feeding flow rates have been scaled up with respect to the active area. Nine different configurations are considered, necessary to study the effect on the performance of three different GDL thickness values (150 μm – 225 μm – 300 μm) and three different rib/Channel ratio values (1/3 – 1 – 3).

4.2. Mesh and parameters

The solution to a flow problem is defined at nodes inside each cell. The accuracy of a CFD solution is governed by a number of cells in the grid. In general, the larger number of cells, the better the solution accuracy. Both the accuracy of a solution and its cost in terms of necessary computer hardware and calculation time are dependent on the refinement of the grid. Optimal meshes are often non-

uniform: finer in areas where large variations occur from point to point and coaser in regions with relatively little change. Is important to find a suitable compromise between desired accuracy and solution cost. In this case, only half of the cell needs to be modelled since the cell is symmetric with respect to the y-z plane, as shown in Figure (4.2). To assess the reliability of the results, an analysis of the mesh is necessary to ensure the independence of the solution from the mesh used. Three simulations have been performed: one with the mesh used in the simulations of this work, a less refined mesh and a more refined mesh, doubling and halving the cell width, respectively. The Figure (4.1) shows the trend of some physical quantities as a function of the cell in y-direction: it is possible to observe how the selected mesh falls into the asymptotic zone of the curves, symptom that the solution obtained ensures a reduced error compared to the ideal exact solution.

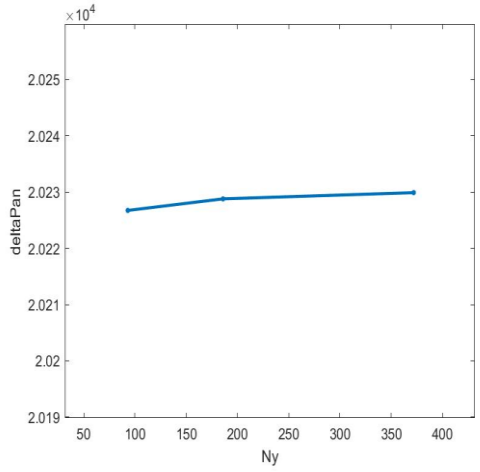

a)

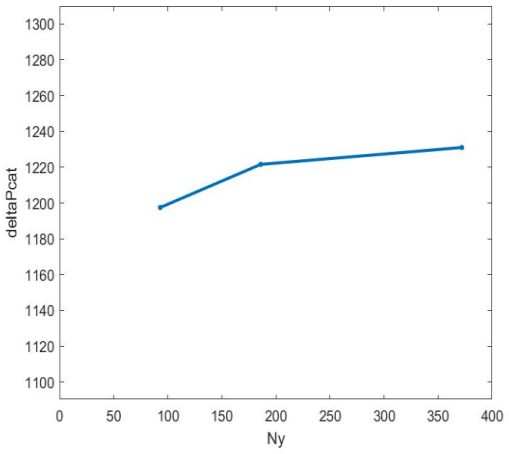

b)

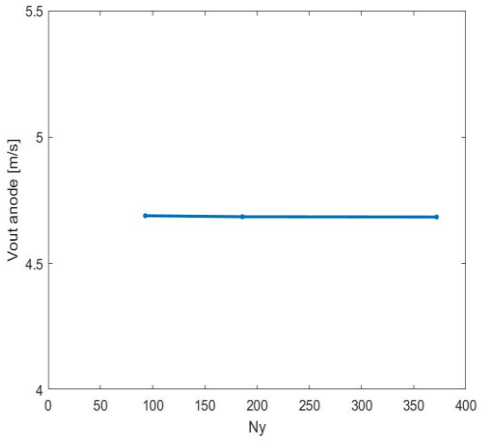

c)

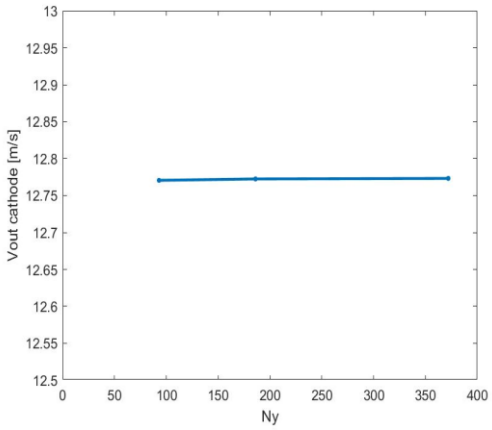

d)

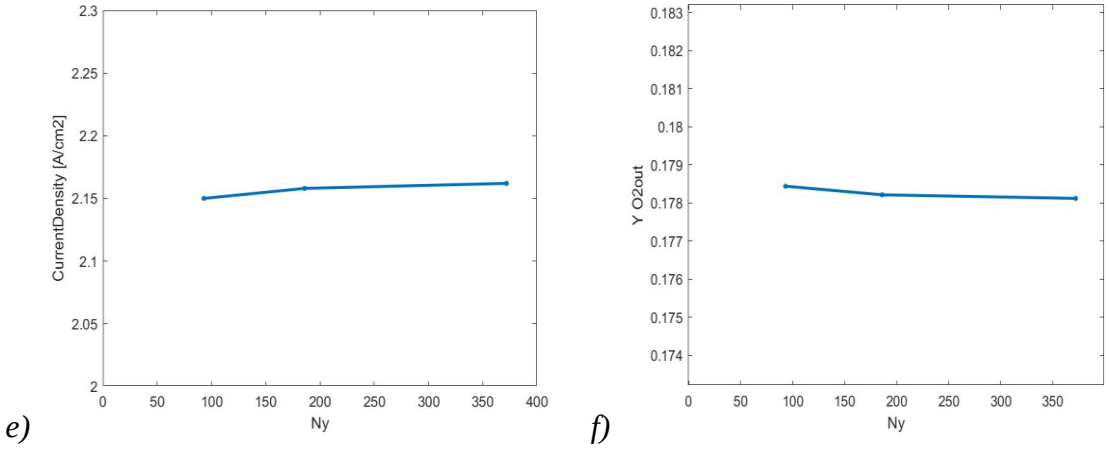

e) *f)*

Figure 4.1 Profile of solution variables as function of number of elements in y-direction Ny: a) ΔP anode b) ΔP cathode c) Velocity anode outlet d) Velocity cathode outlet e) Current density d) Oxygen mole fraction at cathode outlet.

To make an estimate of this error the calculation of the GCI (Grid Convergence Index) has been performed. Given in a percentage manner, the GCI can be considered as a relative error bound showing how the solution calculated for the finest mesh is far from the asymptotic value. It gives a prediction on how much the solution would change with a further refinement of the mesh. The smaller the value of the GCI, the better. This indicates that the computed solution is within the asymptotic range.

$$GCI_{12} = \frac{F_s \left| \frac{f_2 - f_1}{f_2} \right|}{(r^p - 1)}$$

$$GCI_{23} = \frac{F_s \left| \frac{f_3 - f_2}{f_3} \right|}{(r^p - 1)}$$

$$p = \frac{\ln \frac{(f_3 - f_2)}{(f_2 - f_1)}}{\ln r}$$

where 1,2,3 are the indices referring to the different meshes in increasing refinement order, f is the size considered, r the refinement ratio, p is the order of convergence and Fs is the safety factor, which using Roache's approach is equal to 1.25. The safety factor Fs should be thought of as representing a 95%

confidence bound on the estimate relative error. The theoretically correct value f * is obtained by extrapolation according to Richardson ().

$$f^* = f_2 + \frac{(f_3 - f_2)r^p}{(r^p - 1)}$$

The cathode and anode inlet pressure has been taken into account to evaluate the GCI.

Grandezza	Valore esatto f^*	GCI_{23} (Pa)
P_{in} anodo	250238.5	3.358 (0.0013%)
P_{in} catodo	231279	25.6 (0.011%)

Table. 4.1. Results of GCI for cathode and anode pressure inlet.

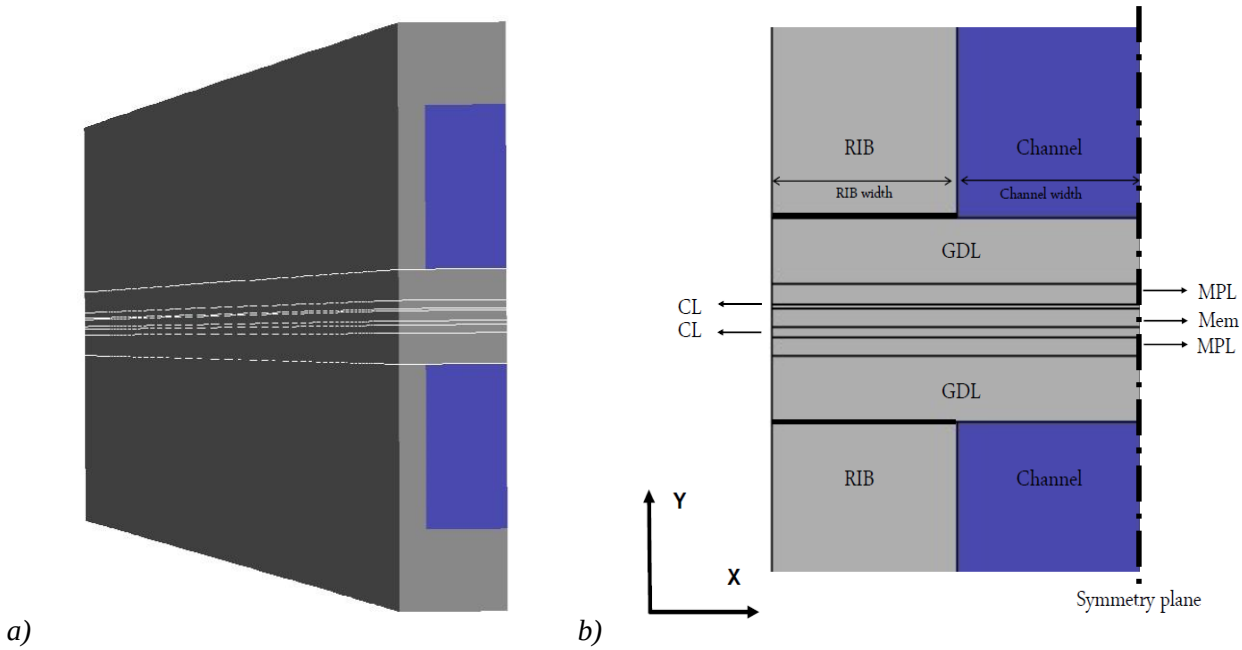

a) *b)*

Figure 4.2 Detail of mesh to show a) tridimensional development b) in x-y plane to show symmetry plane position in the middle of the channel and region of MEA under the rib of current collector.

The values of geometrical features of the PEMFC, parameters and properties used for 3D simulations are summarized in Table 4.2.

Parameter	Value	
Geometry		
Active area	1.275	cm^2
Channel lenght	15	cm
Channel + Rib width	85	µm
Anode GDL thickness	150-225-300	µm
Anode MPL thickness	40	µm
Anode CCL thickness	20	µm
Membrane thickness	50	µm
Cathode GDL thickness	150-225-300	µm
Cathode MPL thickness	40	µm
Cathode CCL thickness	10	µm
Mass transport and liquid phase		
GDL porosity ϵ_{GDL}	0.7	
MPL porosity ϵ_{MPL}	0.5	
CCL porosity ϵ_{CCL}	0.3	
GDL tortuosity τ_{GDL}	3	
MPL tortuosity τ_{MPL}	6	
CCL tortuosity τ_{CCL}	7	
GDL absolute permeability	3e-12	m^2
MPL absolute permeability	1e-12	m^2
CL absolute permeability	2e-13	m^2
Exponent of power law for flooding on D_{ij}^{eff}, δ_s	2.5	
Exponent of power law for flooding on ORR, γ_s	1	
Geometric factor of droplet size, γ_e	1e8	s^{-1}
Contact angle for GDL ϑ_{GDL}	110°	
Contact angle for MPL ϑ_{MPL}	130°	
Contact angle for CL ϑ_{CL}	95°	
Water removal coefficient, Θ	5e-5	
HOR Kinetics		
Reaction order of hydrogen, γ_{HOR}	0.5	
HOR transfer coefficient for forward reaction, α_0	0.5	
HOR transfer coefficient for backward reaction, α_r	0.5	
Equilibrium potential, E_0	0	V
ORR Kinetics		
Reaction order of oxygen, γ_{ORR}	0.7	

ORR transfer coefficient for forward reaction, α_r	0.5	
Cathodic transf. coefficient for PtOx formation, α_{PtOx}	0.25	
PtOx equilibrium potential, U_{PtOx}	0.8	V
Equilibrium potential, E_0	1.23– 9·10−4 T	V
Dissolved phase		
Volume fraction of ionomer inside CL, ϵ_I	0.3	
Adsorption/desorption rate from vapour phase, $k_{ads,g}$	0.2	s^{-1}
Adsorption/desorption rate from liquid phase $k_{ads,l}$	0.8	s^{-1}

Table. 4.2. Simulated PEM fuel cell geometry and parameters.

4.3. Boundary conditions

Boundary conditions at different locations in domain regions, are needed in order to have a complete model formulation, assuming that each one represents a single computational domain. Therefore, boundary conditions are needed to be set at each interface between regions. In figure 4.3 a schematic representation is provided.

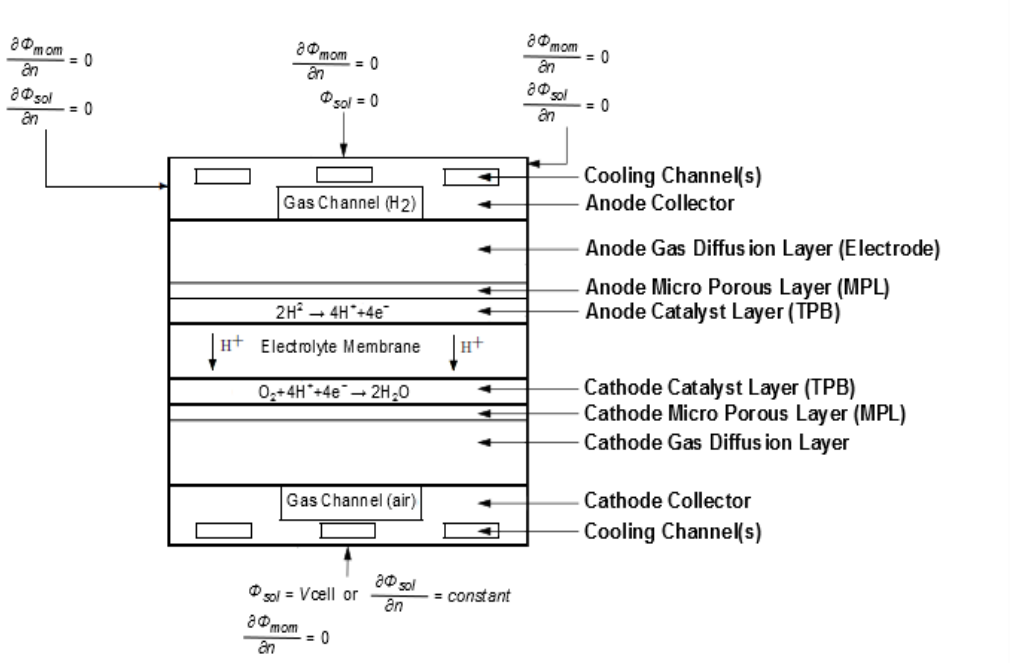

Figure 4.3. Schematic representation of domain and boundary conditions. From Fluent User's Guide release 19.1.

At Anode and Cathode CL - membrane interface, considering that membrane domain is assumed to be impermeable to gas species, liquid water and electrons, it is needed to set:

- Mass flux equal to zero (3.1).
- Species flux equal to 0, $\vec{J}_k = 0$.
- No slip boundary conditions, $\vec{u}_g = 0$.
- Electronic current density, $\vec{j}_s = 0$.
- Protonic potential, ϕ_m, and protonic current density, σ_m, continuity.
- Water content, λ, as well as dissolved phase flux, N_d, continuity across this interface.
- Liquid water flux equal to zero, $\vec{u}_l$ = 0.

At the interface between CLs and MPLs, and also between GDLa and GDLc and MPLs the following boundary conditions needs to be set:

- Mass flux continuity for 3.1.
- Pressure continuity, 3.3.
- Electric potential and electronic current density continuity.
- Protonic current density equal to zero, since no protons flow towards MPLs and GDLs.
- Capillary pressure and liquid water flux continuity 3.33.

No conditions are needed for protonic potential and dissolved phase since they are not defined either in GDL or in MPL or in channel or current collector region. At Anode and Cathode GDL interface contacting current collector, the following condition needs to be set, taking into account that it is a solid component

- Mass flux equal to zero (3.1).
- Species flux equal to 0, $\vec{J}_k = 0$.
- No slip boundary conditions, $\vec{u}_g = 0$.
- Electronic current density continuity.
- Liquid water flux equal to zero, $\vec{u}_l$ = 0.

At GDL-channel interface, the following boundary conditions needs to be set.

- Mass flux continuity for 3.1
- Mass fraction, Y_k as well as single species flux, $\vec{J}_k$ continuity for 3.4
- Pressure continuity, 3.3.
- Electronic current density equal to zero, $\vec{j}_s$ = 0.

In channel volume, no charge transport occurs, thus no electric potential is defined and equation of charge conservation is not resolved. Governing equation for liquid transport is different in those volumes. Liquid water transport is driven by gas transport, as described in Paragraph 3.2.4.2 Therefore, the flux continuity exiting the GDL needs to be guaranteed. As done by Scholz [27] the flux is driven by capillary pressure as reported in equation 3.54.

$$N_l iq = \Theta \epsilon s P_c \qquad (3.54)$$

Where Θ is the coefficient of liquid water removal and it has the dimensions of a time over length, *s/m*. The the boundary condition at GDL-channel interface for Equation 3.38 is the flux reported in 3.54. At Anode and Cathode channel inlets, conditions related to operation of PEMFC, need to be set

- Mass flow rate of reactants, m_{in}.
- Mass fraction of each species, Y_k
- No saturation present at inlets, $s = 0$.

At Anode and Cathode channel outlets, instead static pressure, $P_{out,g}$ needs to be set. At the interfaces of channels with current collectors, it needs to be guaranteed

- Mass flux equal to 0 for 3.1.
- Single species flux equal to zero, $\vec{J}_k = 0$.
- No slip boundary condition, $\vec{u}_g = 0$.
- Liquid water flux equal to zero, $\vec{u}_l = 0$.

Current collector is a solid component in which only electric potential ϕ_s is defined. For the external surfaces of current collectors that are linked with the electric circuit, conditions for electric charge transport needs to be set. On the anodic side, ground potential is set for ϕ_s while on the cathodic side, the operating voltage is imposed for ϕ_s, if the fuel cell is operated in Potentiostatic mode, whereas, the current flux density, $\vec{J}_s$ is imposed if operated in Galvanostatic mode. For what concerns the external surfaces of each domain component, the following conditions are imposed.

- Mass flux equal to 0 for 3.1.
- Single species flux equal to zero for 3.4, $\vec{J}_k = 0$.
- No slip boundary condition, $\vec{u}_g = 0$.
- Electronic and protonic current density equal to zero, $\vec{J}_s = 0$ and $\vec{J}_m = 0$.

- Dissolved phase flux equal to zero, N_d = 0;
- Liquid water flux, 2.35, equal to zero, $\vec{u}_l$ = 0;

4.4. Numerical implementation of 3D model

The simulations for the 3D model have been performed using ANSYS®Fluent, a finite volume-based software in which a basic module, called PEMFC module, is already implemented, where the load transport equations are already present, transport of dissolved water and liquid water. For the simulations in question, however, a PEMFC module has been used with modifications which will now be briefly listed:

- The parameter of tortuosity has been introduced taking into account the correction of Bruggeman for the diffusion coefficient in the porous media.
- Stefan Maxwell's law was used for diffusive flow.
- There is an improvement in both anode and cathode kinetic reactions, implementing the dependence of PtOx coverage on oxygen reduction reaction (ORR).
- Changes have been made to the diffusion of dissolved phase, Dw, and dependence on ionic potential σm has been introduced. Also in this case the contribution of Knudsen to diffusive transport has not been taken into account since its implementation in the mass transport equation is complicated in a software like fluent. Its contribution was considered by increasing tortuosity.
- It has been assumed that processes of adsorption and desorption from vapour and from liquid water to dissolved phase are symmetric, therefore kads,g = kdes,g and kads,l = kdes,g.

As discretization schemes, SIMPLE algorithm has been used for pressure-velocity coupling, while second order upwind schemes is chosen for the convective terms in all the governing equations to reduce diffusion errors, since flow in porous medium is not aligned with structured grid, used for simulations. PRESTO! scheme has been used for pressure discretization. The stiffness difficulties of PEMFC model equations, especially for multiphase water transport, has been already undertaken in PEMFC module by providing under-relaxation factors also for source terms S_{vl}, S_{vd} and S_{ld},, assumed to be 0.2.

Chapter 5

The results of the 3D simulations on the nine geometric configurations described above are reported, using the polarization curve as a validation tool.

5. Results 3D model

In this chapter, results regarding the analysis of the effects of 3D geometry on the mass transport of reactants in the cathode region are reported, with great care about water management and more generally performance of a PEMFC. Moreover, validation of 3D model is performed varying geometrical parameters and operating conditions and also, investigating the heterogeneous effects visible in a three-dimensional geometry.
Structure and methodology of the Chapter are listed below.

- Preliminary analysis focused on the main instrument used to evaluate the performances, that is on the polarization curves explaining its characteristics and the phenomena of loss related to its trend.
- Investigation of geometrical effects related to a variation of the rib/channel width ratio, focusing on the problems of mass transport that arise in porous layers especially in the areas under the current collector where there is no direct contact between the supply channel and gas diffusion layer.
- Description of the effects resulting from a change in the thickness of the gas diffusion layer, thus increasing or decreasing the average path needed for the reactant gases to reach the active area.
- Finally, the effects resulting from a variation of relative humidity in the inlet in the reactant gases at the cathode are investigated, maintaining the operating condition at the anode. The relative humidity of the reactants strongly affects the dry rather than wet conditions of the membrane, to the point of contributing to the possible problem of flooding in the porous layers. These effects are evaluated by simultaneously changing the geometric parameters described above to have a deeper understanding of water management.

5.1. Validation: Polarization curve

Polarization curve is a graph that relates the current density to the difference in potential applied to the cell heads. The trend of the curve is influenced by four main losses that determine its possible separation into distinct regions based on the dominant physical processes: fuel crossover and internal current losses,

kinetics (activation losses), charge transport (ohmic losses), and mass transport (concentration losses). They are briefly explained below.

Fuel crossover and internal current losses - The polymer electrolyte is a material which in ideality should only transport cations (in the case of a PEM, H^+) across the cell. However, in reality a small amount of hydrogen and oxygen will pass across the electrolyte, reach the adjacent electrode, and react according to the global reaction (2.3) resulting in an unwanted variation on the local reactant concentrations. OCV is a theoretical value which establishes the "no-loss" voltage and is the starting point in a voltage-loss equation for the unit cell. (5.1)

$$V_{cell} = E_{OCV} - \eta_{total} \qquad (5.1)$$

where η_{total} is the total voltage loss for the unit cell at a given operating set point.

Even at OCV there is an electrochemical conversion of reactants occurring on each electrode (though the net rate of reaction on the electrode is near zero), small numbers of electrons short across the non-conductive polymeric electrolyte effectively decreasing the number of electrons available to pass through the external circuit thus lowering the OCV. The dramatic effect of these processes in lowering the OCV is a function of the exponential current-potential relationship for the electrode reactions. The effects of fuel cross-over and internal current can be minimized through the use of thicker polymeric materials; however, thicker materials typically involve increasing ohmic losses.

Activation losses - Activation losses arise due to the sluggishness of the kinetics for both processes. The activation energy barrier for the electrode reactions is a sequence of energy barriers as a result of the multi-step nature of both the ORR and HOR reaction. The rate of the reaction on the anode and cathode electrodes is typically increased through the use of catalysts whose task is to effectively lower energy barriers in the reaction pathway; however, the use of catalysts alone is not enough to significantly enhance the rate of conversion and as such a potential bias, in the form of an activation overpotential, is applied to the cell as a driving force. It can be seen form the equation (5.2)

$$\Delta V = (E^+ + \eta^+) - \eta_{ele} - (E^- + \eta^-) \qquad (5.2)$$

Where $\eta^+$and η^- are the local overpotential respectively for cathode and anode side whereas η_{ele} is the voltage drop in protonic potential φm across membrane. The activation overpotentials reflect the amount of voltage produced by the cell

that is re-directed towards driving the electrochemical reaction and subsequently lost.

Ohmic losses - The movement of charge carriers within the cell is necessary in order to complete the electrochemical reactions at the anode and cathode electrodes. In both cases, there is a resistance to the charge movement through the conducting materials and this resistance will result in the development of a voltage or potential loss. These voltage losses can generally be expressed using the relationship of Ohm's law in which the voltage or potential loss is proportional to the material's resistivity and the overall flow of current across it. Ohmic losses due to the transport of electrons typically occur in the flow field plates, porous transport layers, catalyst layers, and other cell hardware whereas losses arising due to the transport of protons occur in the catalyst layers and polymeric electrolyte. An important observation of the behaviour of ohmic related voltage losses is that they tend to increase linearly with produced current. Usually, the minimization of a cell's ohmic losses can be done through the selection of highly conductive materials, the reduction of contact resistances, and, either, the selection of low equivalent weight polymers for the membrane and catalyst ionomers or adequate cell humidification, or both.

Concentration losses - One of the most debated and discussed voltage loss categories are of those arising due to concentration or mass transport related phenomena. The attention dedicated to this category is due in part to the sheer difficulty in quantifying the relevant physics and the overall understanding of various aspects of both the cell materials and the dynamics of phenomena such as liquid water transport. Overall, concentration losses are the result of a lowered concentration of reactants or increased concentration of products at the electrode surface such that a higher amount of driving force (activation over-potential) is required in order to produce the desired current. Within the cell there are several mechanisms by which reactants are delivered and products are removed from the electrode surface and the concentration losses of a PEMFC are typically further categorized based on the contribution of these individual transport processes. One of the primary observable manifestations of concentration losses is the limiting current; limiting current is the point at which the rate of delivery of the reactants to the electrode surface is insufficient to match the rate of electrochemical conversion at the catalyst sites and as a result increasingly more activation overpotential is required to achieve progressively smaller increases in overall current production.

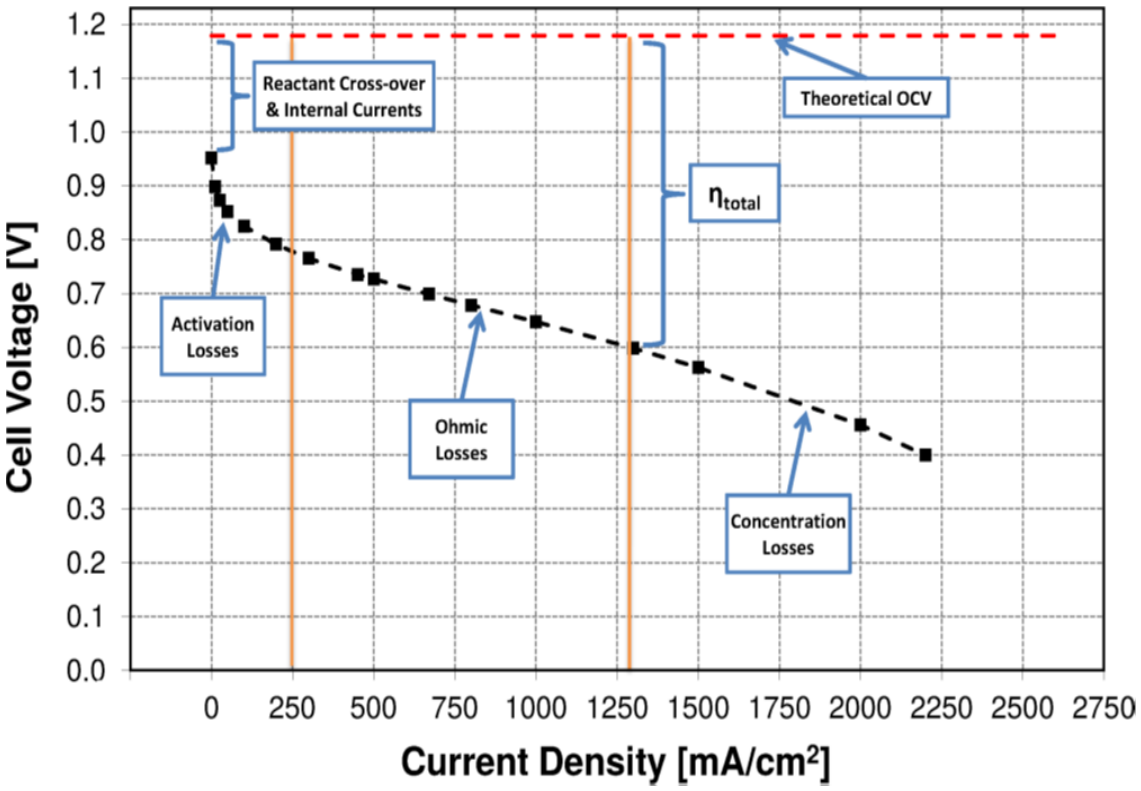

Figure 5.1 Contribution of major losses on the trend of the polarization curve

In the light of the above, from the figure (5.1), representing the global polarization curve, it is possible to recognize three different regions: low current density one that has a very high slope with a peculiar logarithmic trend in which activation losses dominate, a central region with a quasi-linear trend indicating a strong influence of ohmic losses and, finally, a high current density region with a typical sharp potential drop that determines the curve tend towards the limiting current value, that is, as mentioned before, the maximum current that PEMFC is able to provide, because of transport phenomena. In the low current density region, the predominant voltage loss is due to activation of cathodic reaction occurring in Cathode catalyst layer, that is ORR activation overpotential, η^+. As known from literature, the ORR kinetics dominates in this region because of its sluggishness that leads to a strong decrease in voltage, as it can be seen from the first part of cathodic overpotential curve. These losses have a logarithmic trend with respect to current density and can be described by Tafel law, according to the far-field approximation that holds for $|\eta^+| \geq 100$ mV.

In central region, ohmic losses are added and become predominant in polarization losses (η_{ele}), due to resistance opposed by carbon materials to the passage of electric current but, mainly, to ionic resistance opposed by electrolyte to protons.

If a single-phase model is taken into account with no resolution of water transport in membrane, the relationship between η_{ele} and current density is linear, since protonic conductivity, ϕ_m would be constant. Nevertheless, in multiphase models, as the one implemented in this work, the relation is non-linear due to the dependence of ϕ_m upon water content of membrane that varies locally across ionomer. When current density reaches very high values, polarization losses related to mass transport prevail. In this region, reactant flux to active sites is hindered. In case of multiphase models, as in this work, in addition to oxygen diffusivity there are contributions to transport resistance in porous media to take into account. Indeed, mass transport description becomes very complex because of flooding phenomenon. Water is condensing inside pores and determines their occlusion, that has a negative impact on the diffusivity of oxygen, according to Equation 3.8. At the same time, also η_{ele} increases more than linearly. In this case, indeed, it can be seen that, at higher current densities, the part of membrane near the Anode CL is getting more dehydrated, thus a greater ionic resistance to proton flux.

5.2. Sensitivity Analysis

In this paragraph the diagram of the 3D simulations performed is presented. The sensitivity analysis was applied to two geometric parameters and two operating conditions, as shown in Figure 5.2.

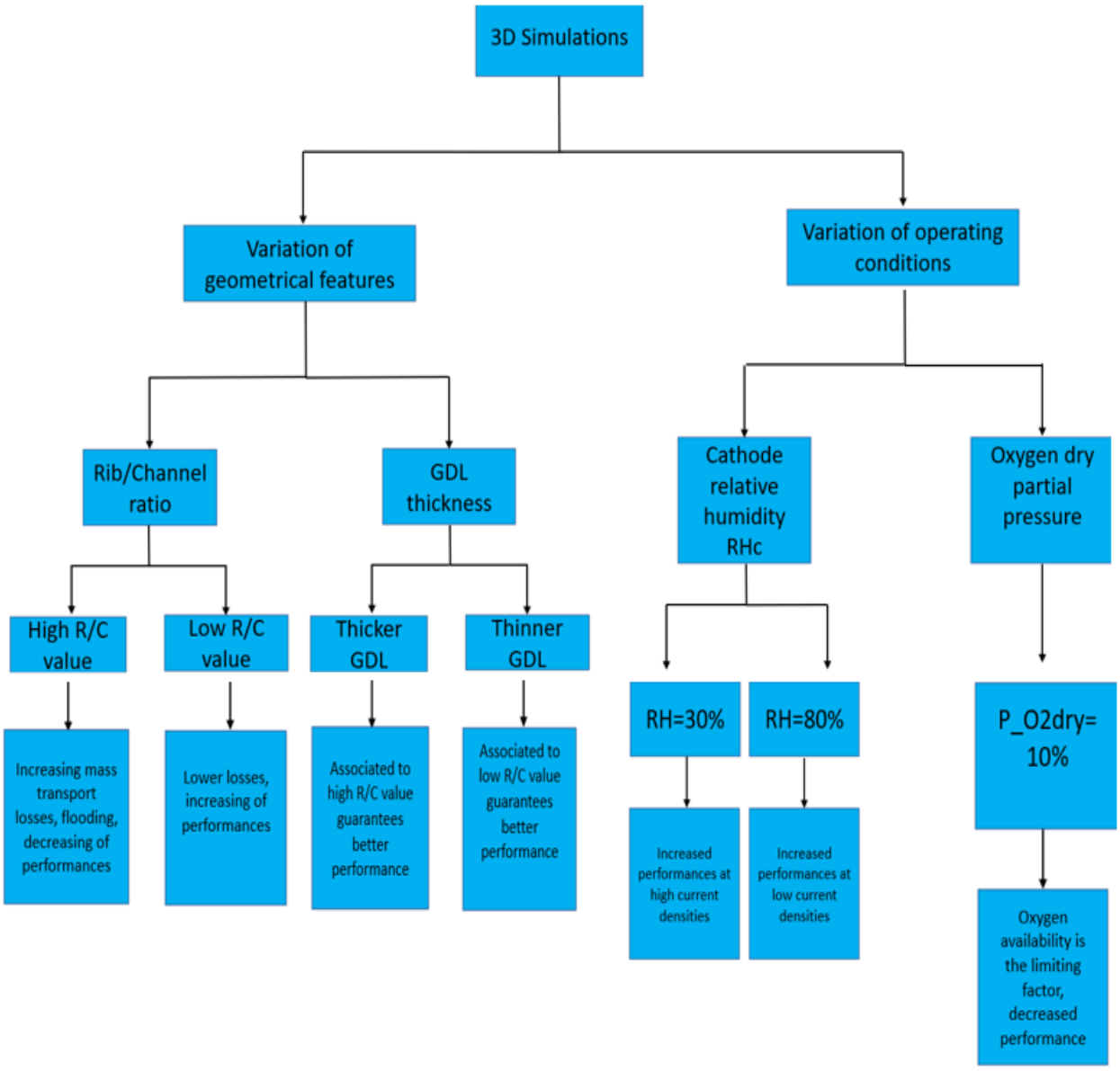

Figure 5.2. Summary of simulations

5.2.1. Effects of rib/channel ratio variation

Parameters of bipolar plate are greatly influencing the mass transfer in polymer electrolyte membrane fuel cells. Water accumulation in the catalyst layer and gas diffusion layer causes the mass transport limitation, resulting in an inhibition of gaseous reactant transport to the reaction sites. To minimize the mass transport

problems, the optimum design of flow channel is essential with profound understanding of water transport phenomena.
In this paragraph the analysis is performed on a single channel with a length of 15 cm for simplicity and, as described in paragraph (3.3.1), three different values of rib/Channel ratio (1/3-1-3) are taken into account, maintaining the sum of the two constant amplitudes equal to 0.85mm, to evaluate the effect of this ratio on the performance of the PEMFC going to investigate the transport of the reactants inside the channels, their diffusion to the active area through the GDL and the water content inside the different layers. Figure 5.3 shows the three configurations considered.

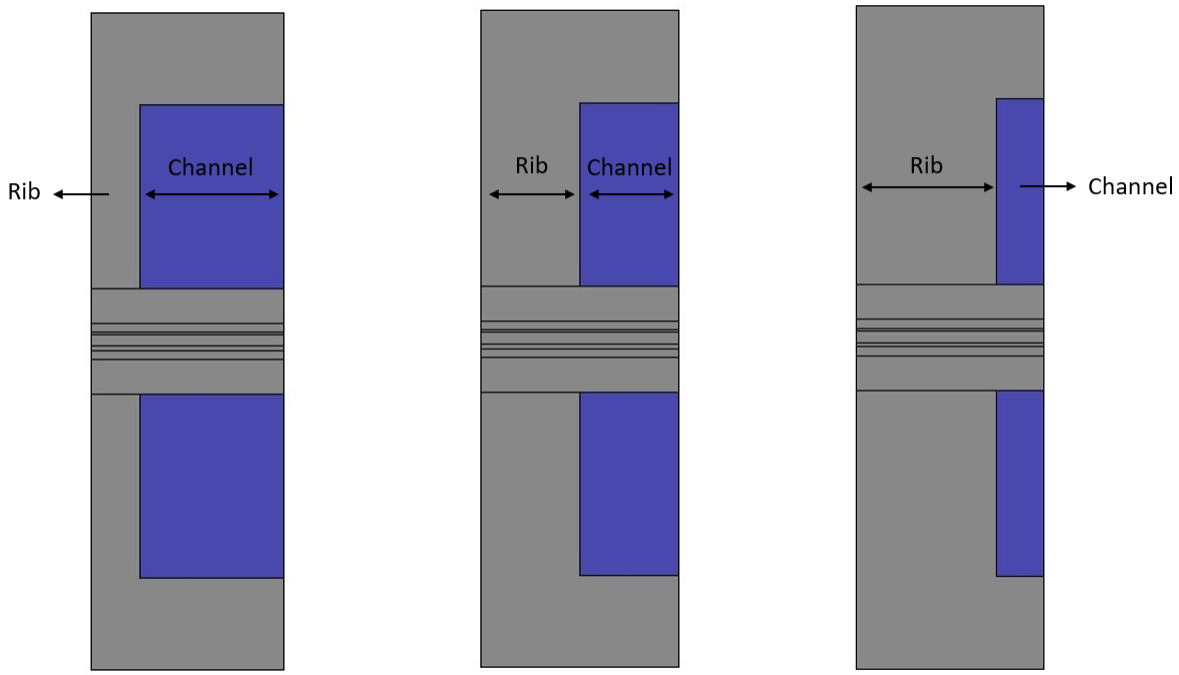

a) R/C=1/3 *b) R/C=1* *c) R/C=3*

Figure 5.3 Three different configuration.

The geometry of the flow field has as main function that to distribute the reactants towards the active area and to favor the expulsion of the accumulated water to the inside of the layers. As the ratio of rib/Channel varies, with the same active area, the portion of the channel in direct contact with the gas diffusion layer and consequently also the width of the rib varies. Two effects must be evaluated: on the one hand the rib guarantees a good electrical conductivity, necessary to the electrons to flow through the external circuit producing current, on the other hand also the diffusion gas in the different layers has the key role in the functioning of

the cell, to maintain the electrochemical reaction, removing and distributing the products and the reactants to and from the cell. The two effects are contrasting to the variation of the rib/Channel ratio because if the amplitude of the rib increases the electronic conductivity but at the same time the amplitude of the channel decreases favouring the diffusion of the reactants towards the active area of the cell and viceversa. For this reason there must be a tradeoff between electrical conductivity and diffusion gas.
In simulations a constant flow condition was used with a constant jref reference current. The stoichiometry used to calculate costant mass flow rate, for a constant value of current 3 A/cm2 as evidenced by the table (5.1) has been chosen and kept very high: the value is 10 both anode and cathode. This mainly to have homogeneous conditions along the whole channel. The main operating conditions are:

•	Operating temperature	T =353.15 K
•	Reference current density	$j_{ref} = 1 \left[\frac{A}{cm^2}\right]$
•	Gaseous pressure anode	P = 2.5 bar
•	Gaseous pressure cathode	P = 2.3 bar
•	Relative humidity at anode	RHa = 50%
•	Relative humidity at cathode	RHc = 30% - 80%
•	Stoichiometry ratio at anode	$\lambda_{an} = 10$
•	Stoichiometry ratio at cathode	$\lambda_{cat} = 10$

Tab 5.1 Operating conditions used in the study.

Analysis of species transport under the region of GDL directly contacting a portion of current collector, the rib, to ensure electrical contact, has been performed by varying the relative ratio between rib widht and channel width R/C ratio.

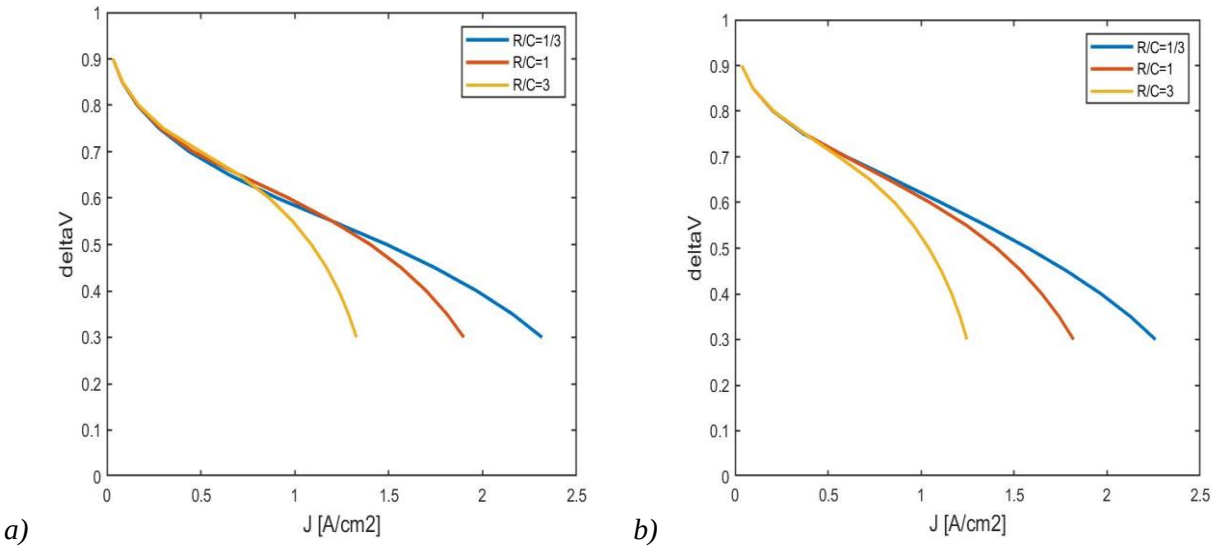

Figure 5.4 Polarization curve with different flow field. a) RHc=30%, δGDL=150μm b) RHc=80%, δGDL=150μm, varying Rib/Channel ratio

As shown in Figure 5.4, the variation in the rib/channel ratio has a strong impact on polarization curves. The three different trends are clearly distinguished because by varying the geometry of the flow field the average path that must be made by a particle of reactants to diffuse through the GDL and the MPL to reach the catalyst layer. The curve relative to a ratio R/C=3 turns out to be the curve more penalized because to parity of difference of potential set, the density of generated current is considerably smaller regarding the other two cases. Increasing the size of the rib in fact increases the difficulty of the reactants in reaching the active area especially at the centre of the rib itself, this results in a decrease in the current density generated and an increase in the unevenness of both the reactants and the current density in the active area. On the contrary by decreasing R/C ratio, more oxygen is able to reach the region under rib and, for these reason an increase in current densities is visible at same voltage value. The same conclusion can be drawn by analysing same current density at decreasing R/C ratio, a higher cathodic overpotential is obtained as a consequence of the mass resistance opposed by a higher diffusion path and by less availability of void pore volume.
The difference between the three curves becomes perceptible from low current density values while acquiring a significant value as the potential difference decreases. At low differences in potential imposed, in addition to the above mentioned difficulty, there is another problem related to the management of water that is formed in the cathode catalyst layer due to electrochemical reactions. The water thus formed occludes the pores of the porous medium further hindering the diffusion of the reactants towards the catalyst layer, resulting in the flooding phenomenon. The accumulation of an excessive amount of water produced is

therefore a limiting factor for the high current density performance of PEMFC. The only way to dispose of excess water in the porous layers is through the channels. In the case of a high rib/channel value also this operation is difficult because the area available of the liquid water to escape from the cell is inversely proportional to this ratio.
In order to have a more in-depth analysis of the phenomenon described, further charts of comparison of the polarizations are brought back varying the ratio rib/channel, but changing the conditions of RH and of thickness of the GDL. The final results confirm the trend already highlighted above: the polarization curve referring to the ratio rib/channel greater (in studied case, value R/C=3) is always the most penalized, achieving lower current density values than in the other two cases.

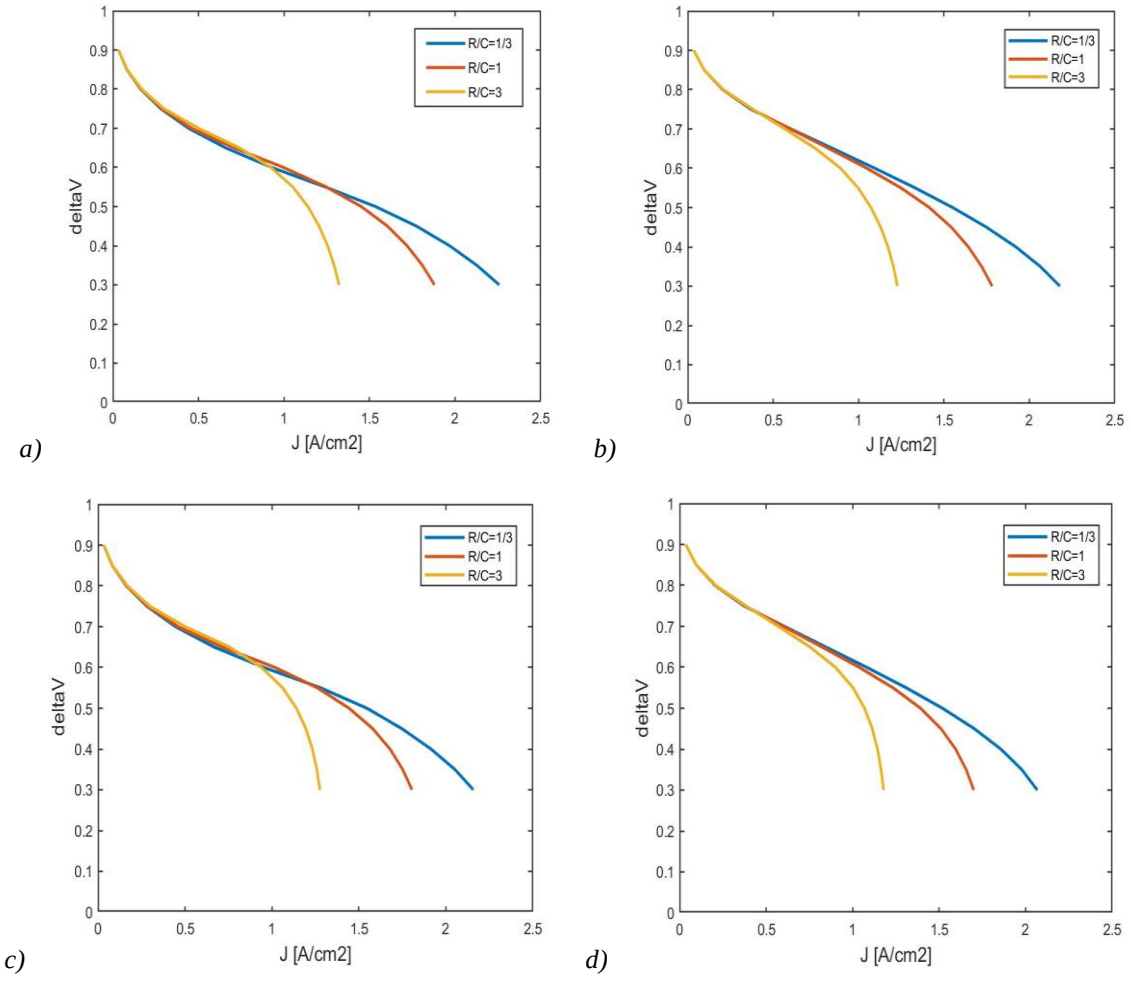

Figure 5.5 Polarization curves: a) RH=30% GDL=225 µm, b) RH=80% GDL=225 µm, c) RH=30% GDL=300 µm, d) RH=80% GDL=300 µm.

Comparing the diagrams to the same thickness of the GDL but different RHc, can be seen that in the case of RHc=80% the detachment of the curves happens before (greater ΔV and smaller current densities) regarding the same more dry case with RHc=30% of the reactant flow inlet; this phenomenon can be explained taking into account that the problem of flooding is greater when I have a higher input RH, because the water that is formed by the reactions to the catalyst layer adds a greater amount related to the relative humidity already present in the input. As a result, flooding already occurs under operating conditions that are not too severe. The geometric presence of rib therefore entails an unevenness, increasing with the growth of the R/C ratio, which it is important to investigate thanks to a local analysis of selected variables. From the figure 5.11 it is noted how the maximum of the current density is in correspondence of the channel, along its symmetry plane, and, as R/C increases, also the gradient of the current density grows. Therefore the average value of the current density profile tends to decrease with the increase of R/C. This trend can be explained by considering that current production depends locally upon reactant concentration and cathodic overpotential.

At high values of the R/C ratio, in this work R/C=3, mass transport results to be a limiting factor, since oxygen is impeded to reach reaction sites in the region placed under the rib, because of higher diffusion path and higher level of liquid saturation. Instead at low values, malgrado a high electrical conductivity, the limiting phenomenon is the electron transport resulting from a decrease in the portion of the region in contact with the current collector and therefore from the higher overpotentials, needed for electrons to reach the reaction sites present under the channel. The increasing difficulty in the diffusion of reactants with the increase in the R/C ratio can be seen in the figure 5.8 showing the mole fraction of oxygen in the layers. In the same way it is possible to analyze the graphs of the mole fraction of water vapour in figure 5.7 in order to investigated how multiphase water transport is affected by a change in R/C ratio.

Water vapour mole fraction has a maximum where reaction rate is maximum, since it is being produced in active sites. This condition occurs in the CCL in correspondence of the Channel-Rib interface which moves when moving its position in the three cases analysed. In GDL instead the trend is reversed since the presence of rib leads to a decrease in pressure below the rib itself and, thus, a tendency of water to accumulation resulting in an increase of the value of the mole fraction and liquid saturation. Figure 5.7 shows this behaviour. The liquid saturation contour is instead shown in figure 5.6. Liquid water, as water vapour, tends to accumulate in region not directly contacted by channel. GDL flooding is very relevant, growing size of the rib, because at the same time the GDL-Ch contact area, which is the only way to allow the water to be expelled thanks to the gas flow in the channel, decreases. In figure 5.9 the evaporation volumetric rate,

m_{EVA}, has been reported. In these operating conditions, both condensation and evaporation phenomena are present. Therefore, in case of condensation, m_{EVA} is negative, positive if evaporation occurs. This variable depends directly upon liquid saturation and water vapour concentration and therefore a similar trend is obtained. For high R/C ratio, condensation is obtained in cathode CL under the channel distributor, where activity of water is high, as well as liquid saturation. However condensation affects strongly also the GDL region under rib where water vapour and liquid saturation are accumulating. The maximum value of m_{EVA} increases with R/C but its range decreases because only in the small region contacted by channel, where activity of water vapour is low, evaporation occurs. For decreasing ratios instead, condensation is shifting towards the region under the rib since water vapour mole fraction reaches its maximum there. In GDL, most of liquid water tends to evaporate more and more, as R/C decreases.

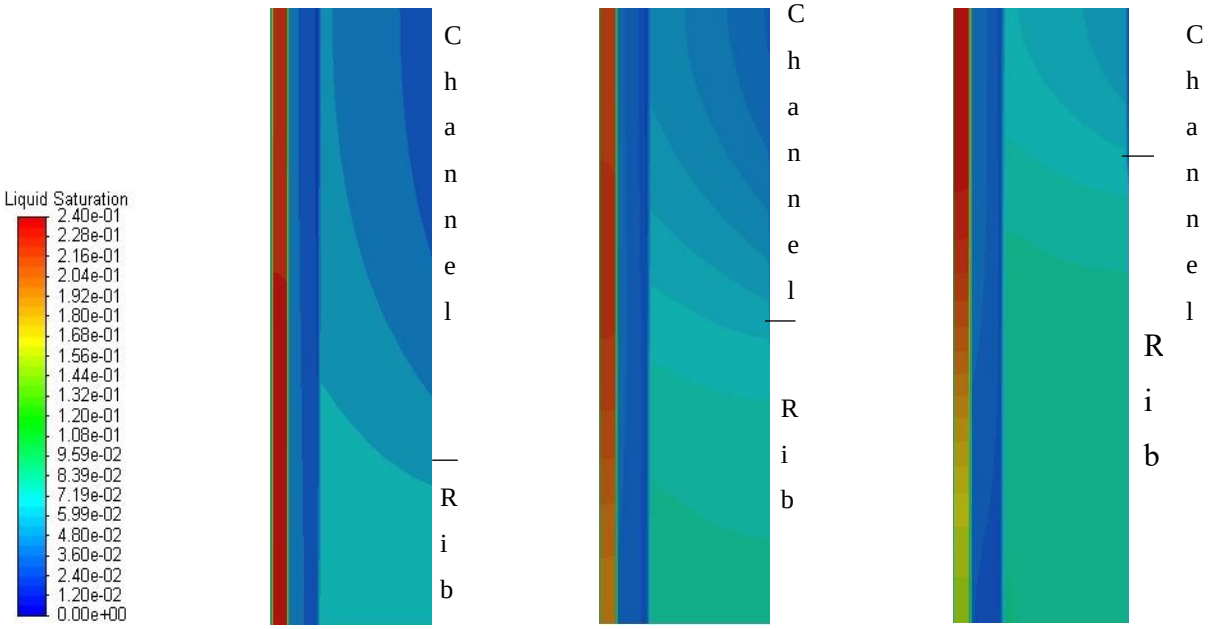

Figure 5.6 Liquid water saturation contour plot on a section placed at 50 % of channel length, varying R/C ratio-ΔV=0.30V.

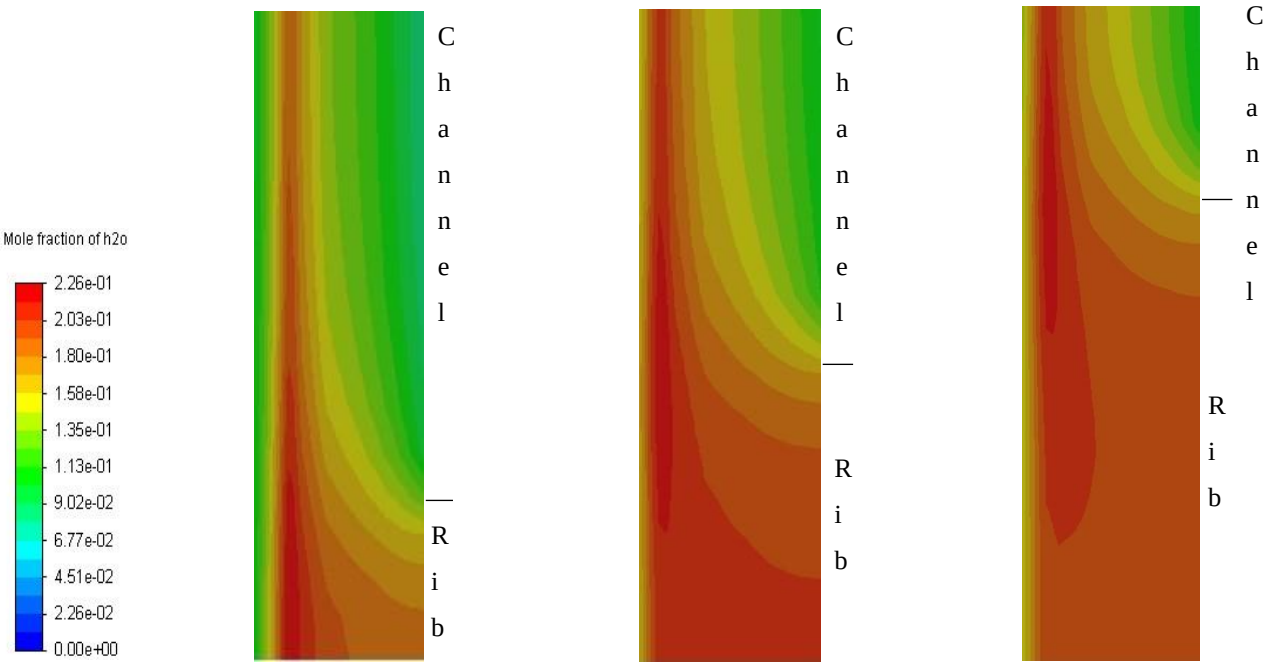

Figure 5.7 Water vapour contour plot on a section placed at 50 % of channel length, varying R/C ratio-ΔV=0.30V

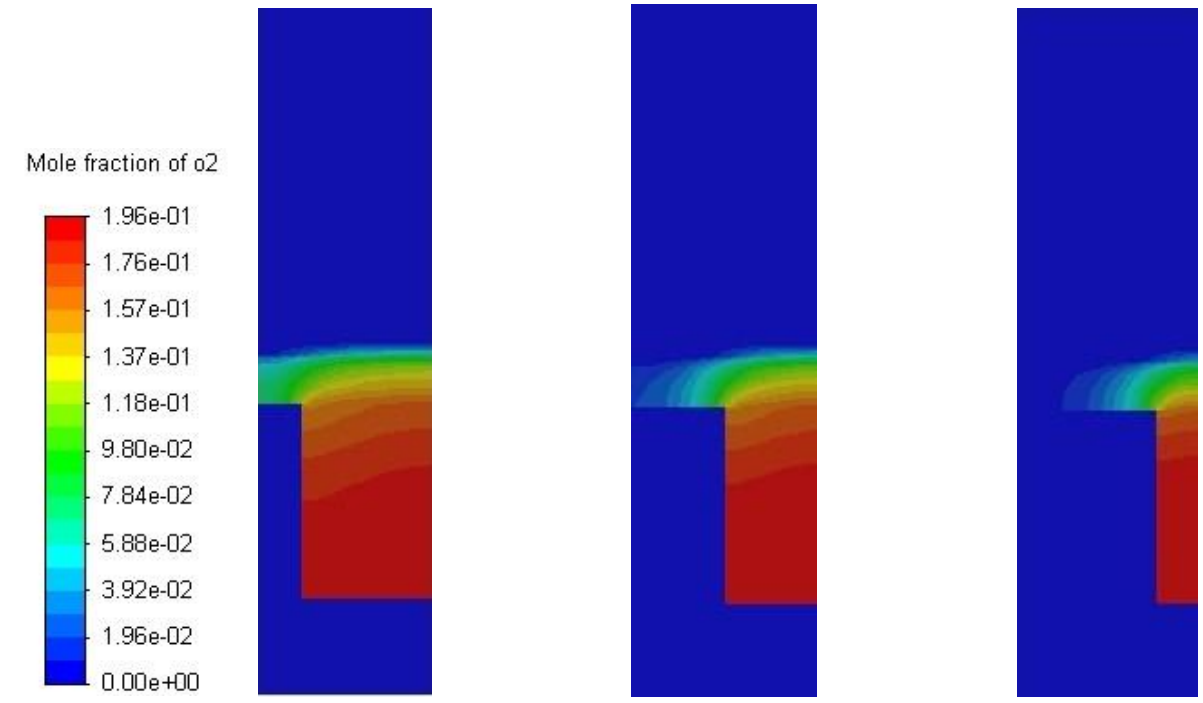

Figure 5.8 Oxygen mole fraction contour plots on a section placed at 50 % of channel length, varying R/C ratio-ΔV=0.30V.

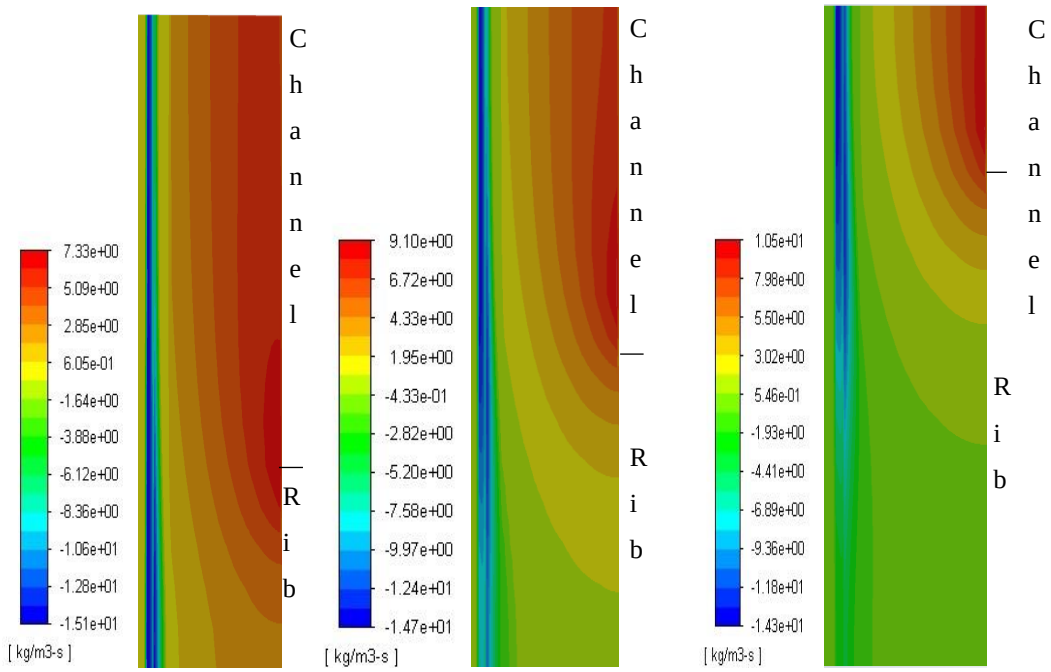

Figure 5.9 Contour plots of evaporative volumetric rate on a section placed at 50% of channel length-$\Delta V=0.30V$.

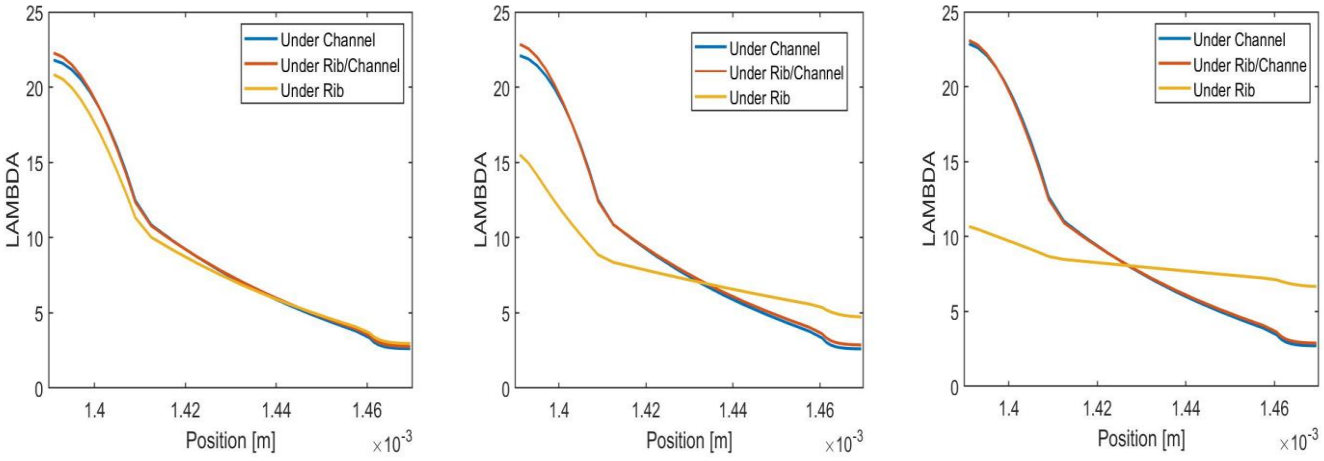

Figure 5.10 Local profiles of water content, exported from lines oriented parallel to y-directions through ACL-Mem-CCL placed on a section at 50% of channel lenght in correspondence of the center of the channel, the center of the rib and the interface rib-channel, for three different case, changing R/C ratio-$\Delta V=0.30V$. Starting from the left R/C=1/3, R/C=1, R/C=3.

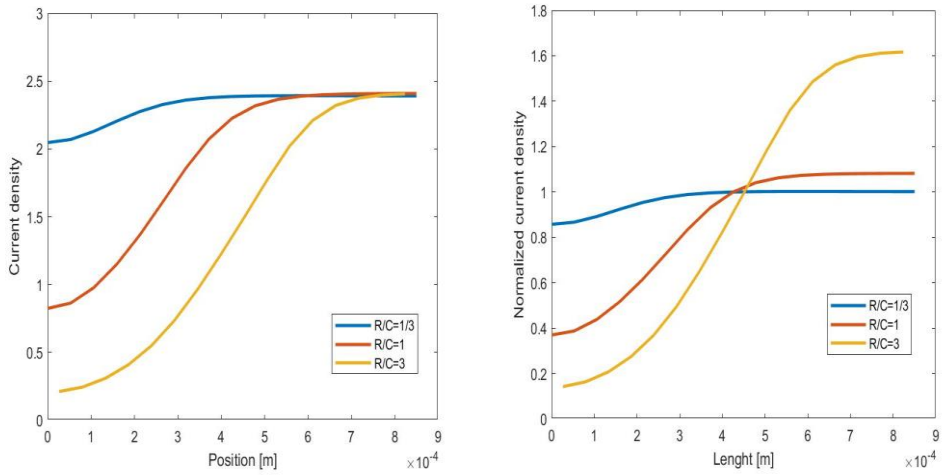

Figure 5.11 Local profiles of current density magnitude and normalized current density, exported from a line oriented parallel to x-direction in the middle of membrane region placed on a section at 50 % of channel length-ΔV=0.30V.

5.2.2. Effects of GDL thickness variation

In this paragraph the influence of GDL thickness on cell performance is analysed. The increase or decrease of this geometric parameter changes the distance made by the reactants to reach the active area. The effect of a change in GDL thickness does not have a strong impact on performance such as the R/C parameter, discussed above, however, polarization curves show a different behaviour depending on whether low R/C cases are analysed rather than high value ones. As shown in the first two lines of Figure 5.12 at low R/C values the best performance is guaranteed by choosing a smaller thickness (150µm). A finer thickness implies an increase in the mass transport through it and consequently a decrease in the losses of mass transport. The contour plot of the mole oxygen fraction at the CCL and GDL is also presented to support in Figure 5.13, showing how the unevennes in the diffusion of reactant increases with the decrease of the thickness of the GDL due to the smaller distance of the diffusion of the oxygen. Increasing the thickness of GDL instead the mole fraction tends to homogenise, also under the rib, as well as the gradients in the direction parallel to the axis-x, resulting in more flat profiles, because are less affected by the presence of rib. In figure 5.14 the evaporation volumetric rate, m_{EVA}, has been reported. It can be seen that, even condensation, which takes place in the CL, becomes more homogeneous with the increase of the thickness, going to affect also the zones under the channel. The maximum value of m_{EVA} between the three configurations is reached in the case

of finer GDL, therefore the use of combination of low values R/C and GDL guarantees the best performances as expected from the polarization curve.

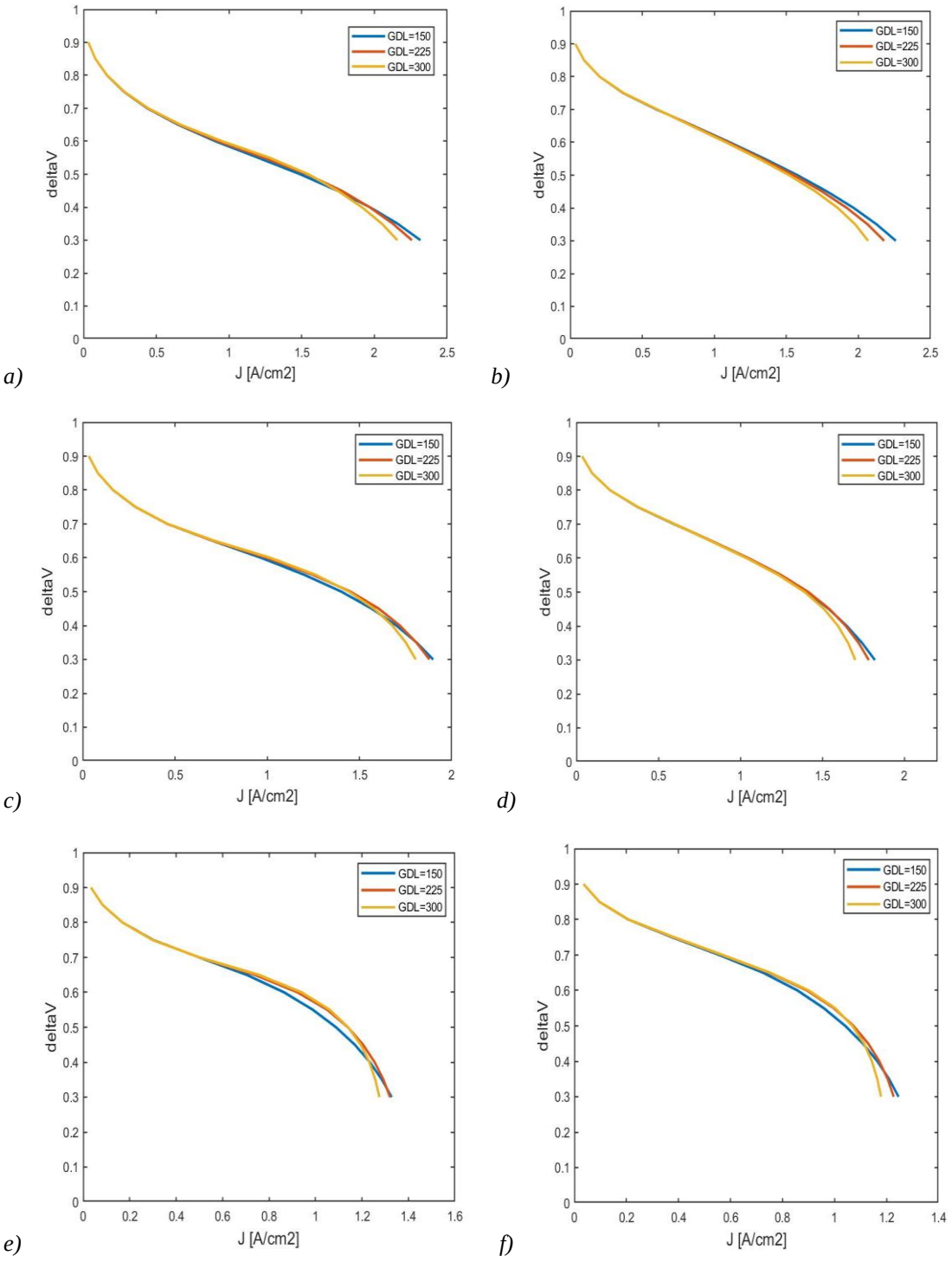

Figure 5.12. Polarization curves a) R/C=1/3 RH=30%, b) R/C=1/3 RH=80%, c) R/C=1 RH=30%, d) R/C=1 RH=80%, e) R/C=3 RH=30%, f) R/C=3 RH=80%

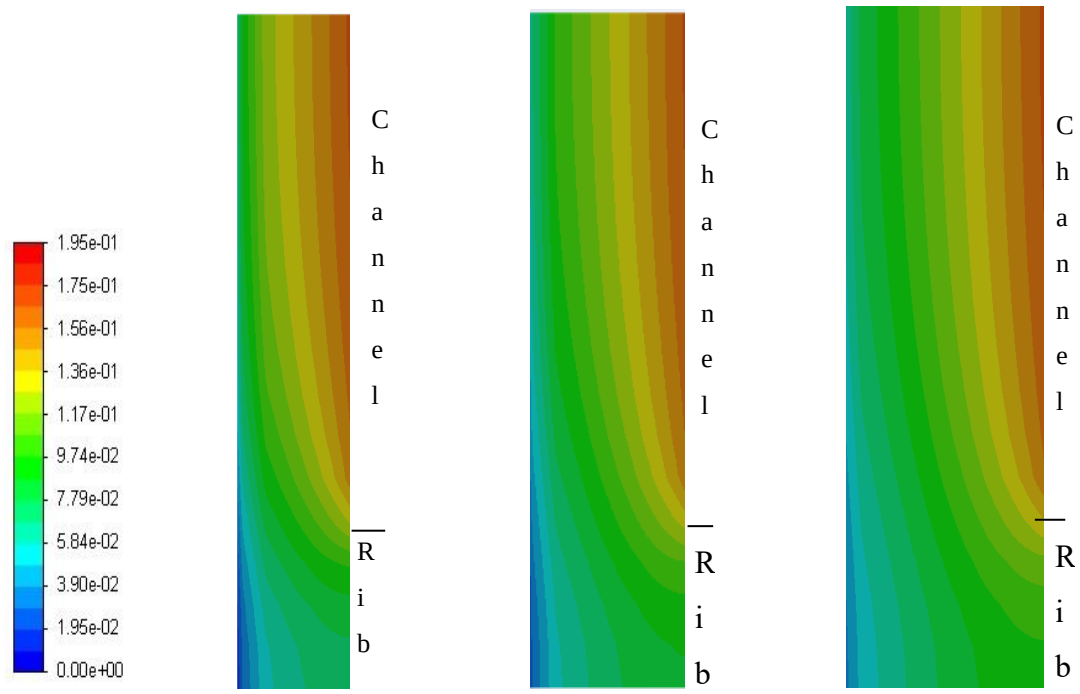

a) GDL=150 *b) GDL=225* *c) GDL=300*

Figure 5.13 Case R/C=1/3. Water vapour mole fraction contour plots on a section placed at 50 % of channel length-ΔV=0.30V.

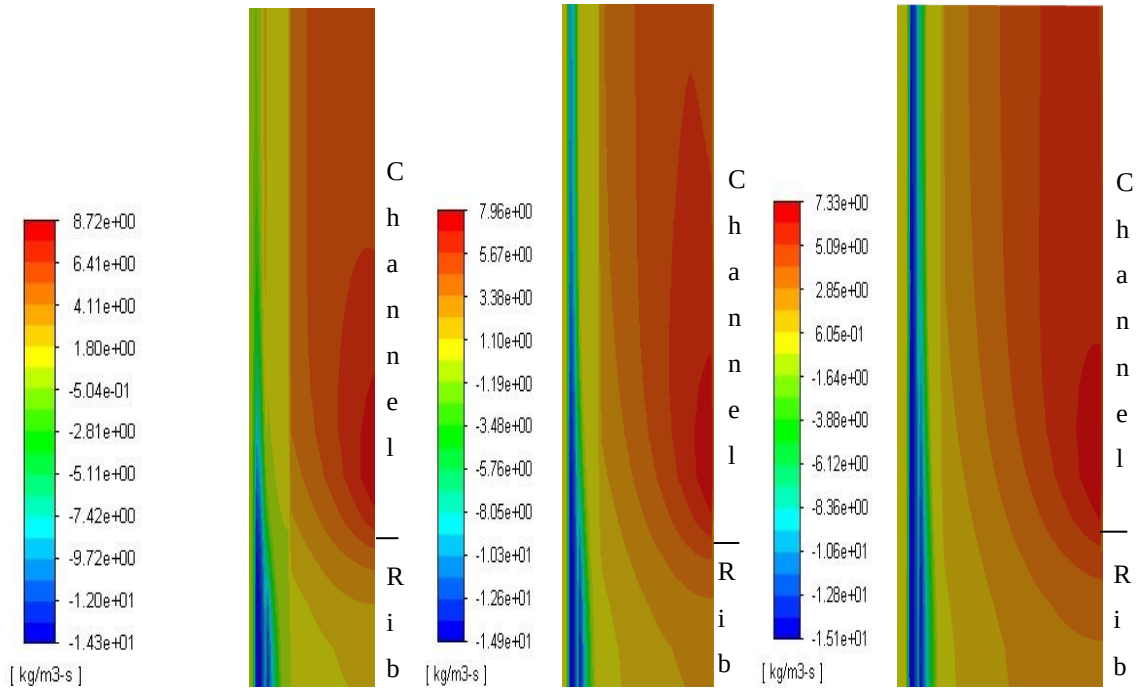

a) GDL=150 *b) GDL=225* *c) GDL=300*

Figure 5.14 Case R/C=1/3. Contour plots of evaporative volumetric rate on a section placed at 50% of channel length-ΔV=0.30V.

At high values of R/C the behavior of the cell is strongly affected by the three-dimensional effects related to the presence of a wider rib and so also the behavior considering different thickness of the GDL changes. A thinner thickness in fact disadvantages the performances, with the exception of the conditions of high current density, because it associates to the diffusion problems related to the high value of R/C, also a less space for diffusion resulting in an increase in the disomogeineity in the exploitation of the active area as well as in the diffusion of reactants. A greater thickness instead allows a more homogeneous diffusion guaranteeing a greater medium distance for the gases. At high current densities also problem of managing liquid water arises, which tends to accumulate in GDL. A finer thickness favours the expulsion of the products, given the least average path that the liquid water must permeate in order to be expelled from the gas stream to the GDL-channel interface.

Figure 5.15 – 5.16 – 5.17 shows contour plots of the water vapour and oxygen mole fractions and m_{EVA} in a case R/C=3 and V=0.3 V corresponding to high current densities. As explained above, in these conditions it is not easy to tell a priori which configuration gives the best performance because on the one hand a GDL more often facilitates a more homogeneous diffusion of the oxygen allowing therefore a better exploitation of the active area, on the other hand, the difficulties encountered by liquid water on its way to the channel-GDL interface increase. Moreover, as shown in figure 5.17 in the configuration with finer GDL the maximum value of m_{EVA} is higher than in the other two cases and the condensation is lower. The best performances are therefore guaranteed by the configuration that guarantees a better balance between these phenomena.

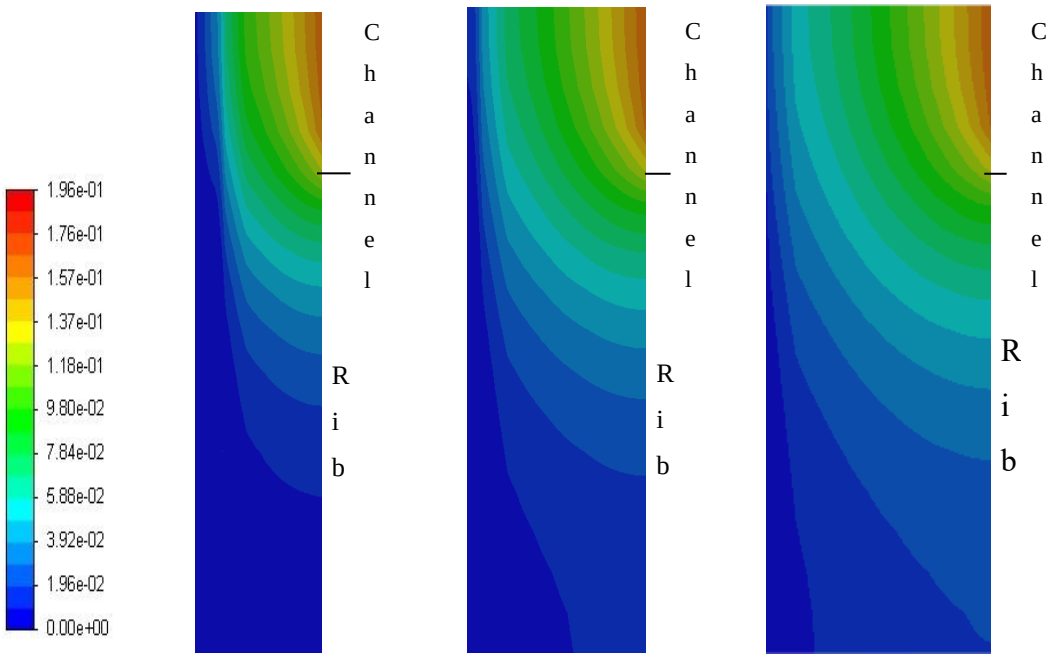

a) GDL=150 *b) GDL=225* *c) GDL=300*

Figure 5.15 Case R/C=3. Oxygen mole fraction contour plots on a section placed at 50 % of channel length-ΔV=0.30V.

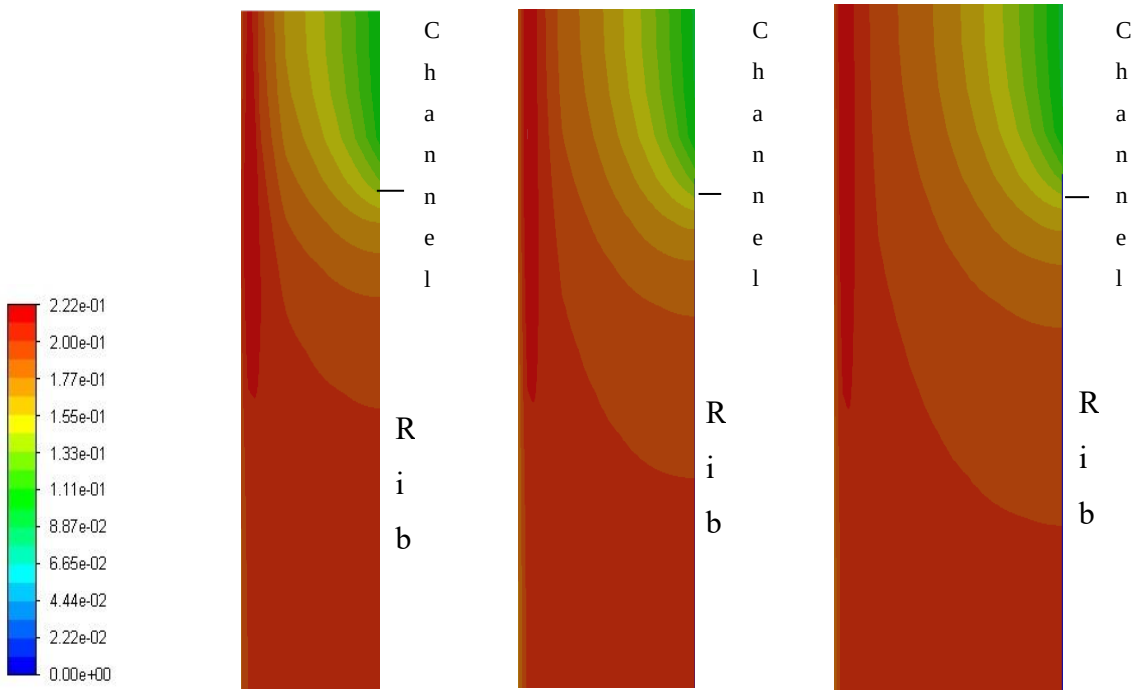

a) GDL=150 *b) GDL=225* *c) GDL=300*

Figure 5.16 Case R/C=3. Water vapour fraction contour plots on a section placed at 50 % of channel length-ΔV=0.30V.

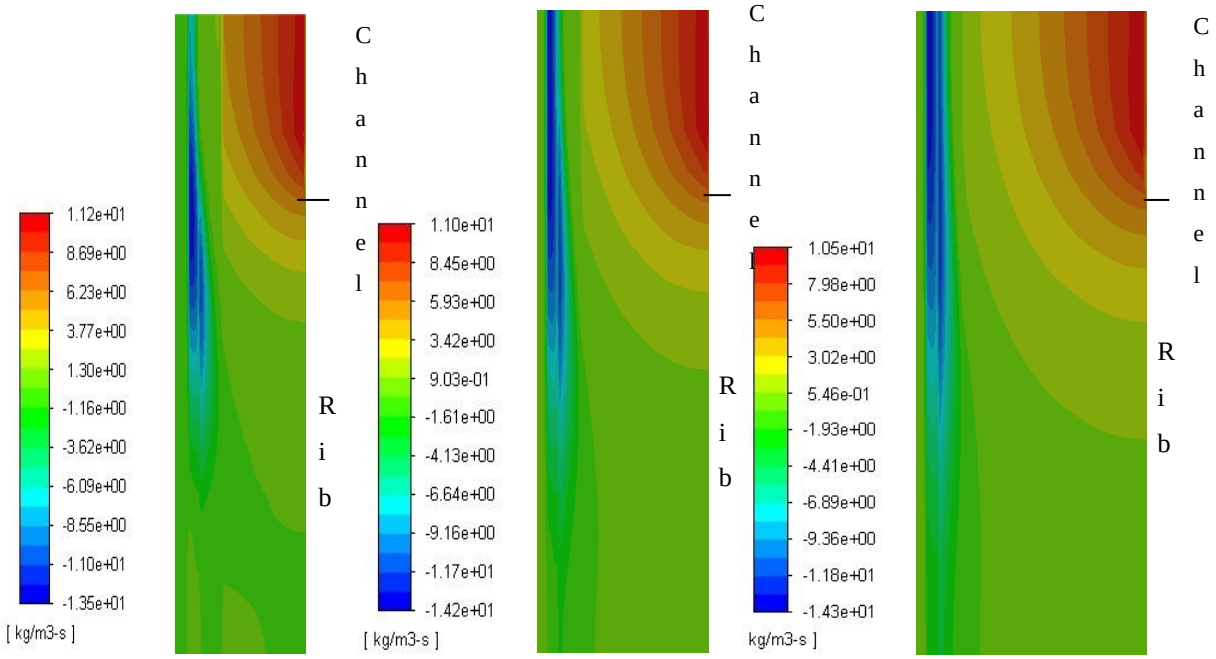

Figure 5.17 Case R/C=3. Contour plots of evaporative volumetric rate on a section placed at 50% of channel length-ΔV=0.30V.

5.2.3. Effects of cathode relative humidity (RHc)

PEMFC performance is strongly dependent on the water management in the cell. The aim is to achieve a delicate balance between the two conflicting requirements: achieving membrane hydration and avoiding electrode flooding. The membrane hydration must be maintained for proton transport given that the ohmic resistance of the membrane increases as the membrane water content decreases, thus reducing cell performance. The electrochemical reaction on the cathodic side produces water in dissolved phase. When the partial pressure of the water is higher than its saturation pressure, it tends to condense in liquid phase. A key role in ensuring water management is played by the humidification of incoming reactant flow, by the operating conditions on which the electrochemical reactions occurring in catalyst layers depend, and the phenomena of water transport within the membrane. Water transport in membrane is determined by two mechanisms, electro-osmotic drag that generates a water flux from Anode to Cathode, strictly related to protonic flux in which protons traveling through the pores of electroyte generally drag one or more water molecules along with them, and the so-called back-diffusion transport that determines water transport from high water content

region, typically Cathode CL, to low water content region, typically Anode CL. Indeed, at Cathode CL, water produced by ORR is in the form of dissolved phase, thus determining that the water content is greater in this region.

The aim of this paragraph is to study polarization curves, the liquid water distribution, liquid saturation and water content, oxygen mole fraction and local current densities in order to understand the effect of a RHc variations.

In Figure 5.18 two polarization curves of a fixed geometry cell (R/C and δGDL parameters) are shown, varying the RH input to the cathode. Two RHc values are taken into account: a dry case with RHc=30% and a more humid case with RHc=80%. The two polarization curves show an interesting behavior. At high voltages and consequent low current densities produced the performance guaranteed by a high RHc inlet value is better compared to the dry case one. At low voltages and therefore in high current density region instead, the trend is reversed because the operating condition, which allows to reach higher values of produced current density, is the smaller RHc. This trend is repeated for all simulated geometric configurations, varying R/C and δGDL values, as shown in Figure 5.18.

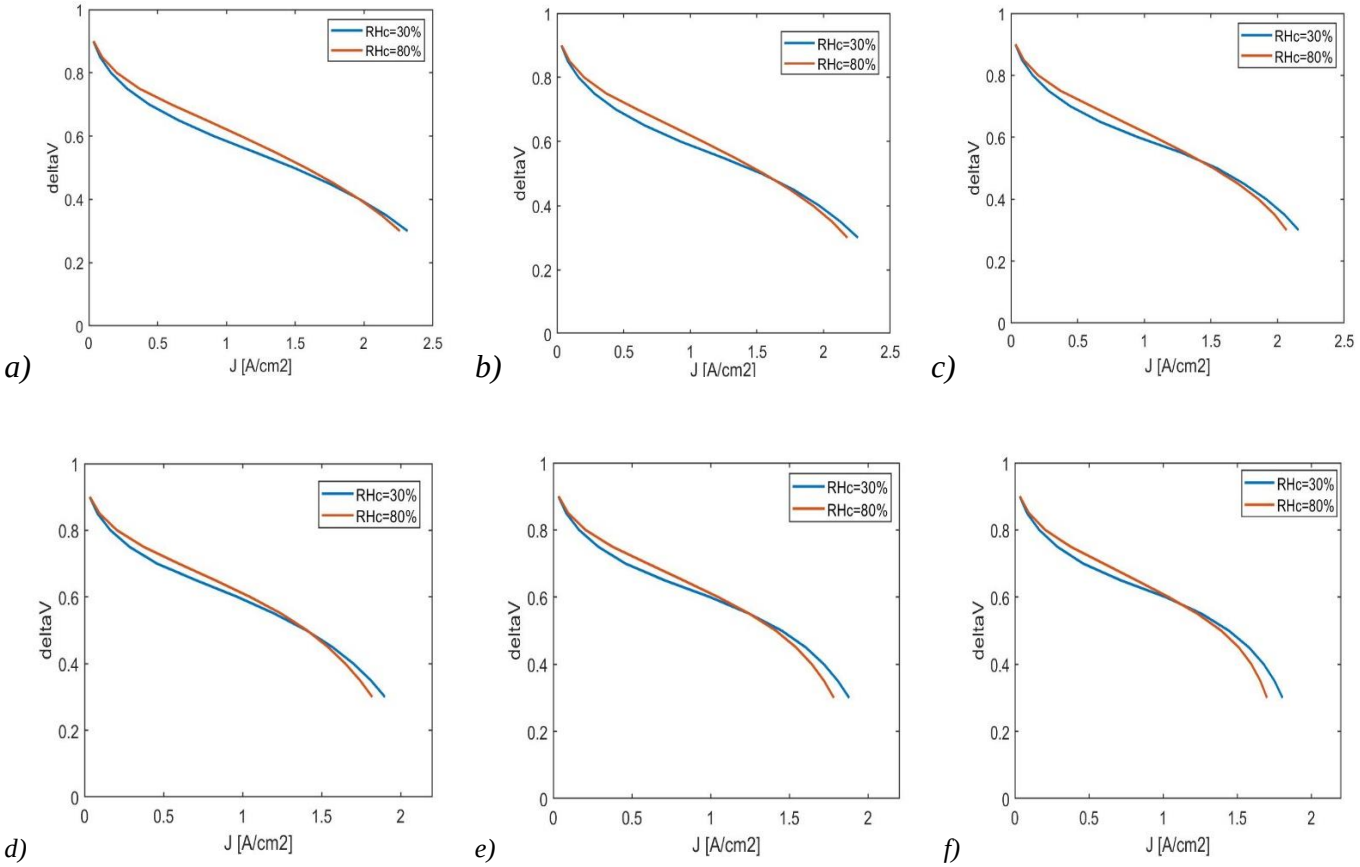

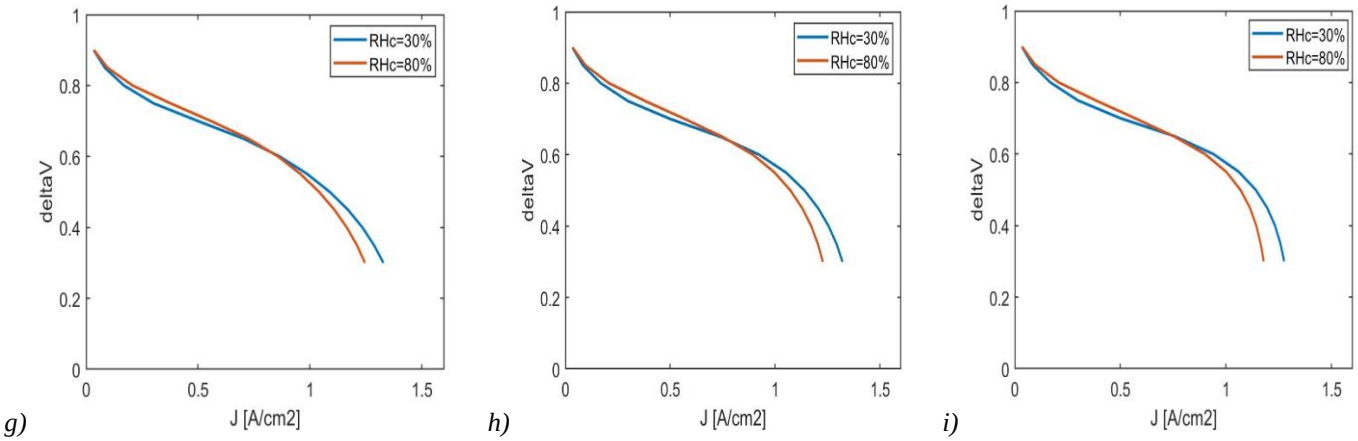

Figure 5.18. a) R/C=1/3 GDL=150µm, b) R/C=1/3 GDL=225µm, c) R/C=1/3 GDL=300µm, d) R/C=1 GDL=150µm, e) R/C=1 GDL=225µm, f) R/C=1 GDL=300µm, g) R/C=3 GDL=150µm, h) R/C=3 GDL=225µm, i) R/C=3 GDL=300µm.

A more in-depth analysis is then carried out considering two different situations: high current densities and low current densities. Local trends of solution variables are analyzed in order to understand better the effect of RHc in both the region of polarization curves. Since the simulations have been carried out in potentiostatic are taken for the analysis two voltage values: 0.8 V for describing in low current densities region the effect of membrane hydration and 0.3 V for describing in high current densities region the effect of flooding.

At low current density membrane hydration is the limiting phenomenon in current production. The production of water to the cathode from the half-reactions is low and to ensure a good proton conductivity of the polymeric membrane is necessary a correct degree of membrane humidification that depends on the balance of electro-osmotic drag, back pressure transport and RH of reactant gases contributions. The electro osmotic drag causes a dehydration of the membrane on the anodic side and an increase of ohmic losses that can be countered by the phenomenon of pressure back transport. The reactant flows with their relative humidity play a decisive role because the higher the input RH, the higher the mole concentration of water on the cathode side, and the more back pressure transport is favoured. For this reason, at low current densities the best performance is achieved with a high RHc value. As can be seen from Figure 5.19, the dissolved water mole concentration is higher at the anode than the cathode at low RHc inlet while the opposite occurs at high RHc inlet. Only with higher RHc inlet the global flux resulted to be directed from cathode to anode. As a result, the phenomenon of back pressure transport is present at low current densities only with more humidified inlet conditions and counterbalance the disadvantage, explained above, related to electro osmotic drag.

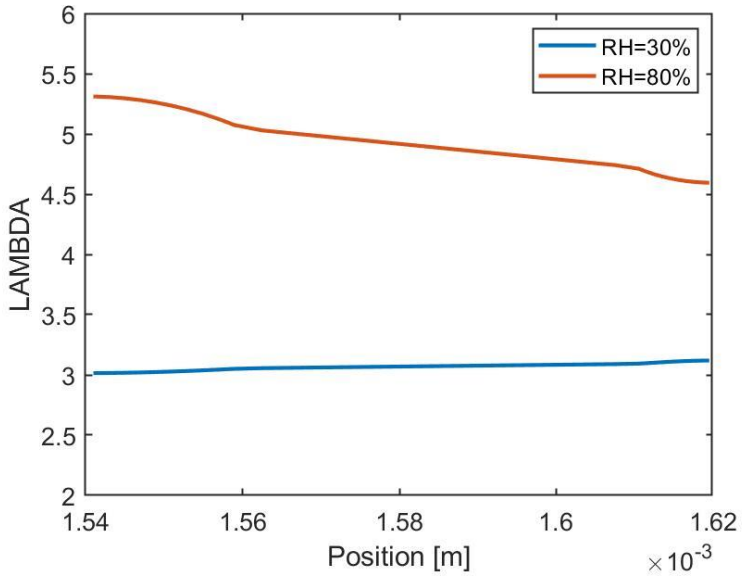

Figure 5.19 Water content through the membrane exported from a line oriented parallel to y-direction from ACL-membrane to membrane-CCL interfaces placed on a section at 50 % of channel length.

In Figure 5.20, contour plots of current density are shown on a section in the middle of membrane. As it can be seen, the maximum of current density for RHc equal to 30%, is at the end of channel, while for more humidified inlet condition it is at the beginning. In the first case, membrane presents a lower hydration because of lower RHc and as water content in ionomer is increasing along channel direction, this favours the increase in protonic conductivity and therefore a higher current density while, for RH=80%, membrane is well hydrated also at the beginning of the channel region for the whole length and liquid water starts comparing in the last part of channel, determining a higher diffusion resistance and lower ECSA in cathode CL. Therefore, this determines a decreasing trend in current density from inlet to outlet. The maximum value of the current density remains below the rib because the simulations have been performed both with very high stechiometries, in great excess, and the considered case is characterized by a low R/C ratio, in which the effect of the rib is limited. For these reasons for more humidified inlet condition the amount of oxygen present in the reactant gases is high enough to not prevent its diffusion towards the CL. In Figure 5.24 the same contour plot is reported but considering a different flow field geometry, in terms of higher R/C ratio, to evaluate the effects of a RHc variation in a case where the presence of a large rib plays a decisive role, as explained in paragraph 5.2.1. The variation of RHc in this case causes a displacement of the higher values

of the current density from below the rib to below the channel in almost all the active area.

Figure 4.20 *Figure 4.21*

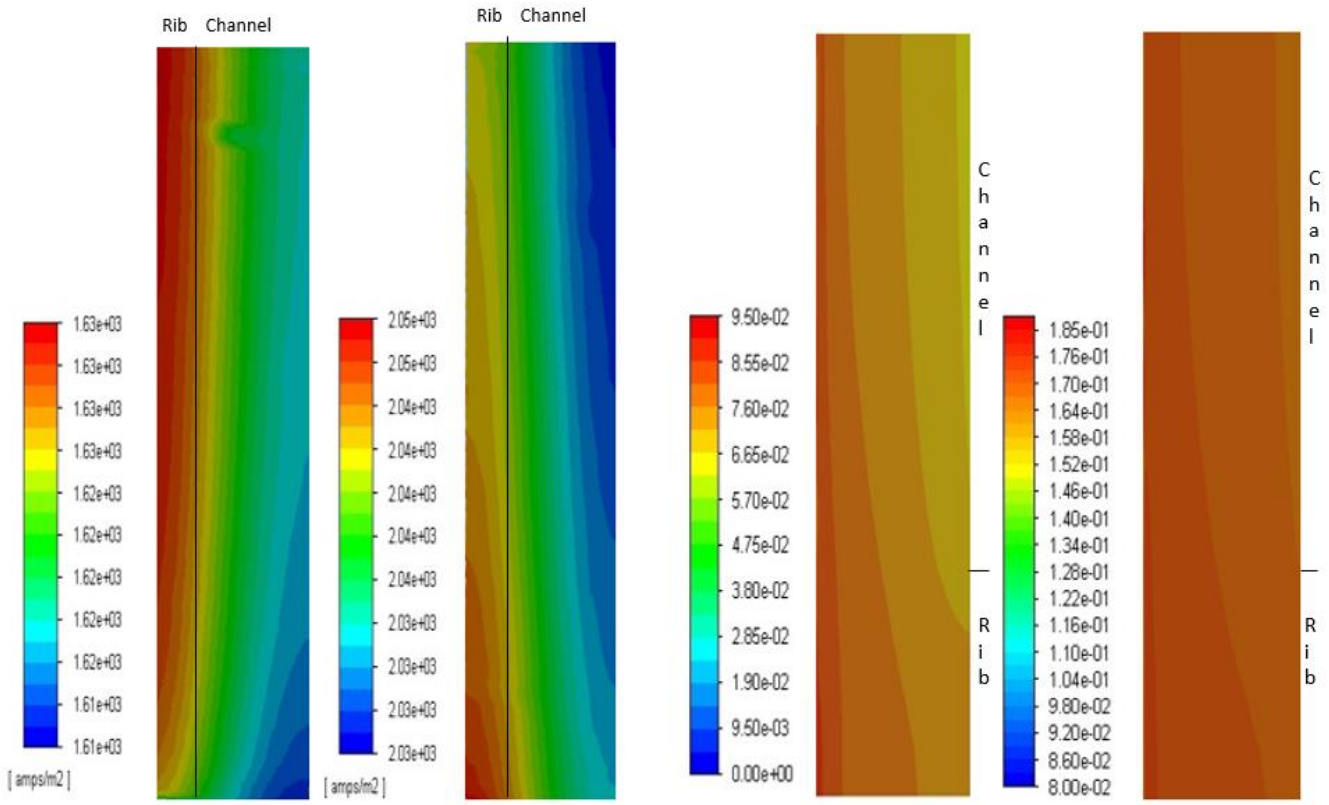

a) RH=30% b) RH=80% a) RH=30% b) RH=80%

Figure 5.20 ΔV=0.80V. Current density contour plots on a section parallel to membrane placed in the middle of it.
Figure 5.21 ΔV=0.80V. Water vapour mole fraction contour plots on a section placed at 50 % of channel length.

Figure 4.22 *Figure 4.23*

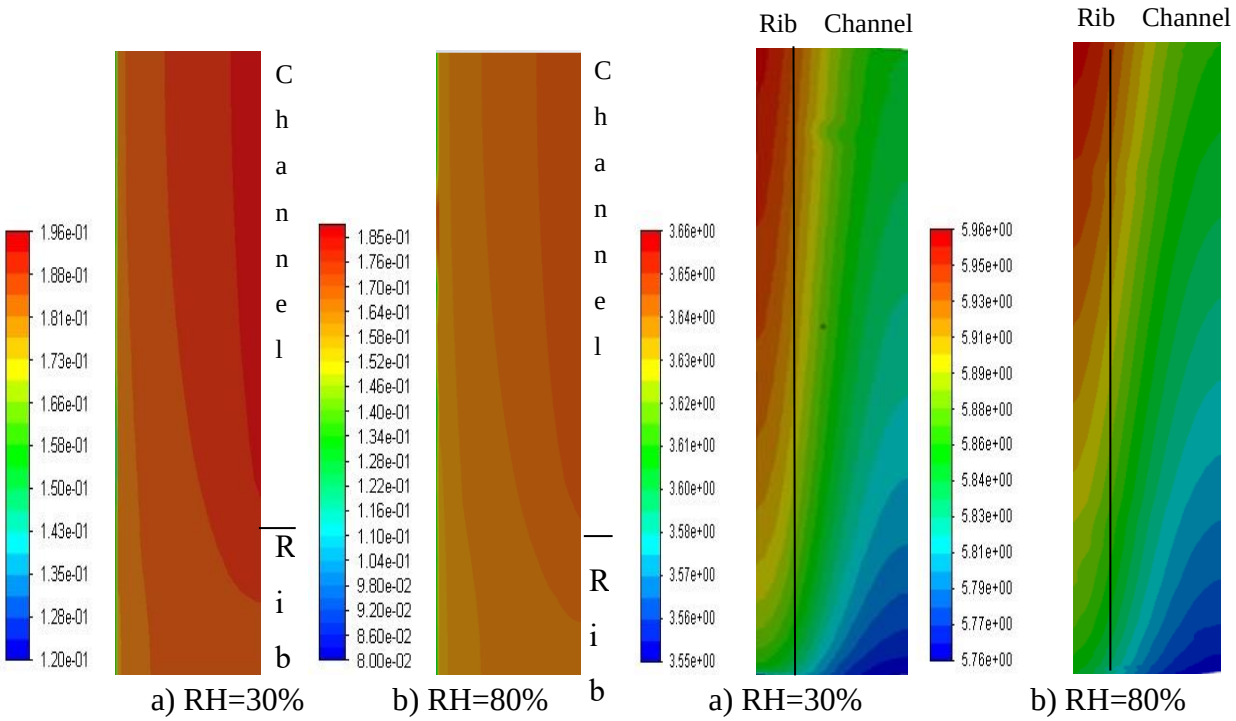

a) RH=30% b) RH=80% a) RH=30% b) RH=80%

Figure 5.22 ΔV=0.30V. Oxygen mole fraction contour plots on a section placed at 50 % of channel length. Figure 4.23 ΔV=0.30V. Water content contour plots on a section parallel to membrane placed in the middle of it.

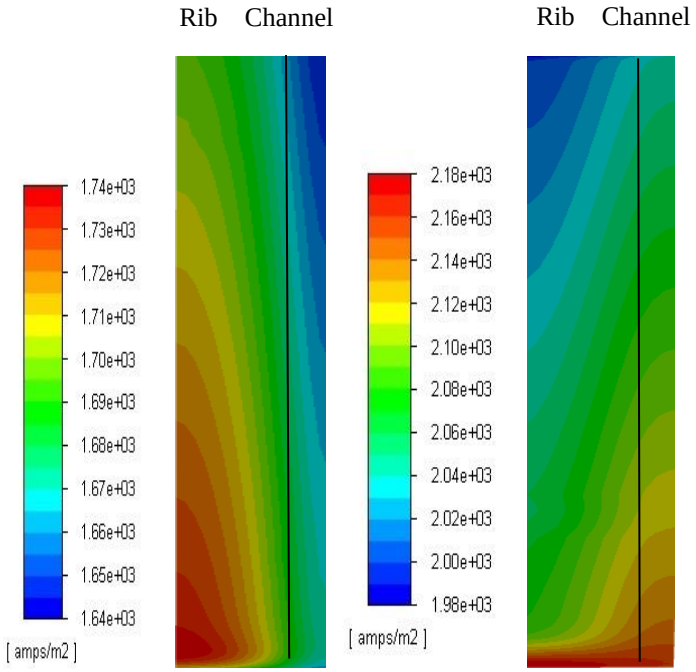

a) RH=30% b) RH=80%

Figure 5.24 Case R/C=3, GDL=150-ΔV=0.80V. Current density contour plots on a section parallel to membrane placed in the middle of it.

In Figure 5.22 and 5.21 respectively, contour plots of oxygen and water vapour mole fraction, from a section placed at 50 % of channel length, are reported. As expected, the oxygen mole concentration is lower as RHc increases and the same occurs under the rib. Water vapour is higher in CL region for the two lower values of RHc, therefore it is exiting GDL. For RHc equal to 80% and water concentration is higher in channel and this determines that is diffusing into GDL. Figure 5.23 shows water content trend in a plane placed in the middle of membrane. For all the values of RHc considered, it can be seen that membrane hydration is increasing along channel direction since water vapour concentration gets higher as well and presents a maximum under the rib.

At high current density instead, a different behavior is observed, the limiting phenomenon is the onset of mass transport issues associated with water formation and distribution limit cell output. Without sufficient water management, an imbalance will happen between water production and evaporation within the cell. When the water generation rate on the cathode side by electro-osmotic drag and oxygen reduction reaction exceeds the water removal rate from the cathode by back-diffusion to the anode, evaporation, and capillary transport of liquid water through the cathode GDL and CL, the cathode becomes flooded. Excess accumulated liquid water blocks the gas pores in the GDL and CL, forming a barrier over the catalyst active surface in the CL and worsening PEMFC performance. In general, humidification of the reactants can ensure membrane hydration, but this may produce cathodic flooding. the effect of RHc on flooding and, thus, on mass transport have been analysed.

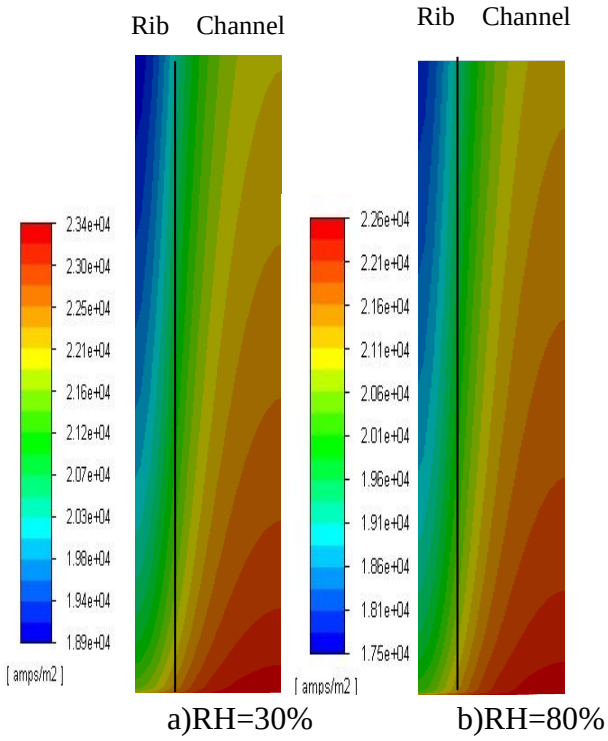

Figure 5.25 Case R/C=1/3, GDL=300-ΔV=0.30V. Current density contour plots on a section parallel to membrane placed in the middle of it.

In figure 5.25, local current density trend in membrane along channel direction have been reported for the two different values of RHc. It can be seen that the maximum value is reached by the lower RHc simulation, consistently with what is seen in figure 5.18. Moreover, the maximum of current density is near the inlet where oxygen concentration is maximum in cathode CL but, by proceeding downstream, current density is decreasing because of lower oxygen concentration and increase in liquid water content that worsens diffusion resistance for reactant species. This occurs because of a more significant flooding under the rib. The larger RHc, the stronger the flooding under the rib and, thus, the lower the values of current densities in that region.

In figure 5.26 and 5.27 respectively, contour plots of oxygen and water vapour mole fraction, from a section placed at 50% of channel length, are reported. The oxygen mole concentration is lower as RHc increases. By looking at water vapour, the maximum of water mole fraction is always in CL zone under channel, where the maximum of current density is present and current production is highly heterogeneous there. The maximum in water vapour mole fraction increases as RHc increases, but it diffuses towards the current collector region and it is accumulating there more and more. Because of a higher water vapour activity, as RHc gets higher, liquid saturation in the rib region is increasing and, thus, the flux of liquid water comparing at GDL-channel interface.

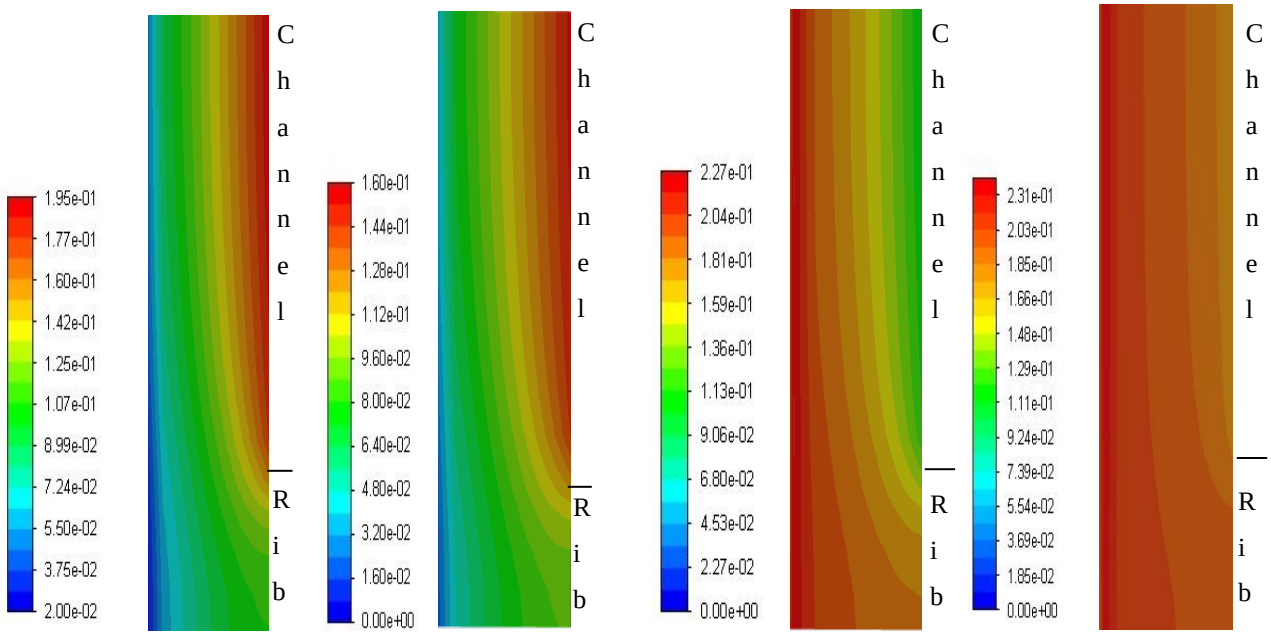

Figure 5.26 Oxygen mole fraction contour plots on a section placed at 50 % of channel length. Figure 5.27 Water vapour mole fraction contour plots on a section placed at 50 % of channel length.

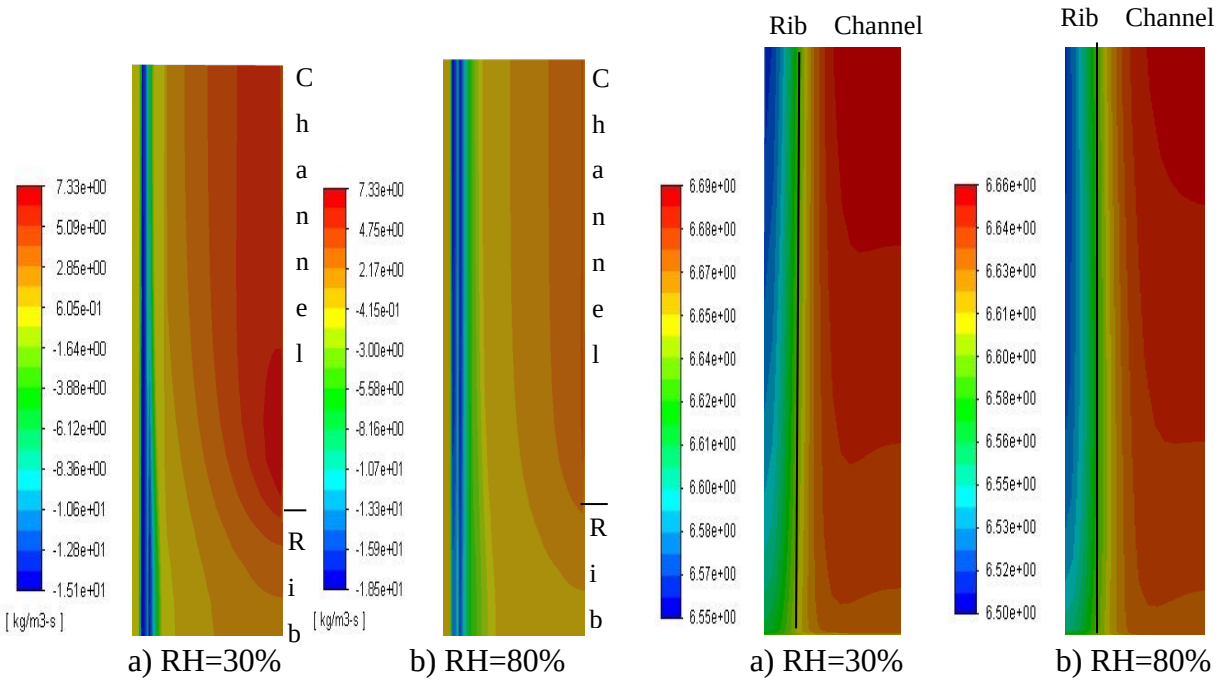

Figure 5.28 Contour plots of evaporative volumetric rate on a section placed at 50% of channel length-$\Delta V=0.30V$.
Figure 5.29 Water content contour plots on a section parallel to membrane placed in the middle of it. $\Delta V=0.30V$

In figure 5.28 the evaporative volumetric rate per unit volume,m_{EVA}. It is visible that condensation occurs always in CL portion under the channel, where maximum of liquid saturation and water vapour concentration is present. At RH=30% condition m_{EVA} is positive in GDL and almost all MPL and increases as getting closer to GDL-channel interface, thus favouring liquid water removal and limiting flooding of diffusion layers. At RH=80% m_{EVA} is still positive for the GDL-channel interface but reaches lower values compared to the dry RHc case and it is reducing further till condensation becomes relevant in the whole cathodic region.

5.2.4. Effects of dry partial pressure of oxygen

In this paragraph the effect of dry partial pressure of oxygen is investigated. The analysis has been performed assuming same relative humidity at cathode and anode sides, as for the previous cases, that is RH=30% and 80% for the cathode while RH=50% for the anode. Costant mass flow rate are considered obtained from the assumption of the same stoichiometric coefficients at the same reference current, equal to 1 A/cm2. Comparison between the two different cases, the reference case and a $p_{O2,dry}^{in}$= 0.10 one, has been performed at the same voltage, equal to 0.30V. The considered geometric configuration is R/C=1/3 GDL=150. Current density has been considered firstly and in Figure 5.30, contour plots of current density and water content in membrane are shown.

As dry inlet partial pressure of oxygen, $p_{O2,dry}^{in}$ decreases, availability of oxygen becomes more limiting. Indeed, with $p_{O2,dry}^{in}$ equal to 20.9%, current density trend is determined by both membrane hydration and oxygen concentration and its value is higher where water protonic conductivity reaches its maximum and oxygen availability is high, that is under the channel in the middle of its development, as it can be seen from figure 5.30.

Despite high values of mass flow rate, oxygen concentration tends to decrease along the channel, resulting in a limiting condition not only under the rib, but also under the channel near the outlet. In the region under collector, ionomer hydration is higher but oxygen concentration is low while under channel, oxygen concentration is higher but protonic conductivity is lower. This condition combined with the presence of a slight flooding results in a decrease of current density near the channel outlet while at inlet, low hydration state of membrane is not favourable to reach high current density. It is possible to see this feature by looking at Figure 5.31 where oxygen mole fraction is reported on a section at 50%

from inlet. In the case of lower $p_{O2,dry}^{in}$, that is equal to 10%, oxygen concentration, instead, becomes limiting and dictates current density profile figure 5.30 The maximum is reached where oxygen concentration is at its highest value, under the channel near the inlet, and, proceeding along channel, it is decreasing. Indeed, as it can be seen from figure 5.31, in the portion of CL under the current collector, oxygen mole fraction is very low. This determines that reaction sites under rib are quite inactive.

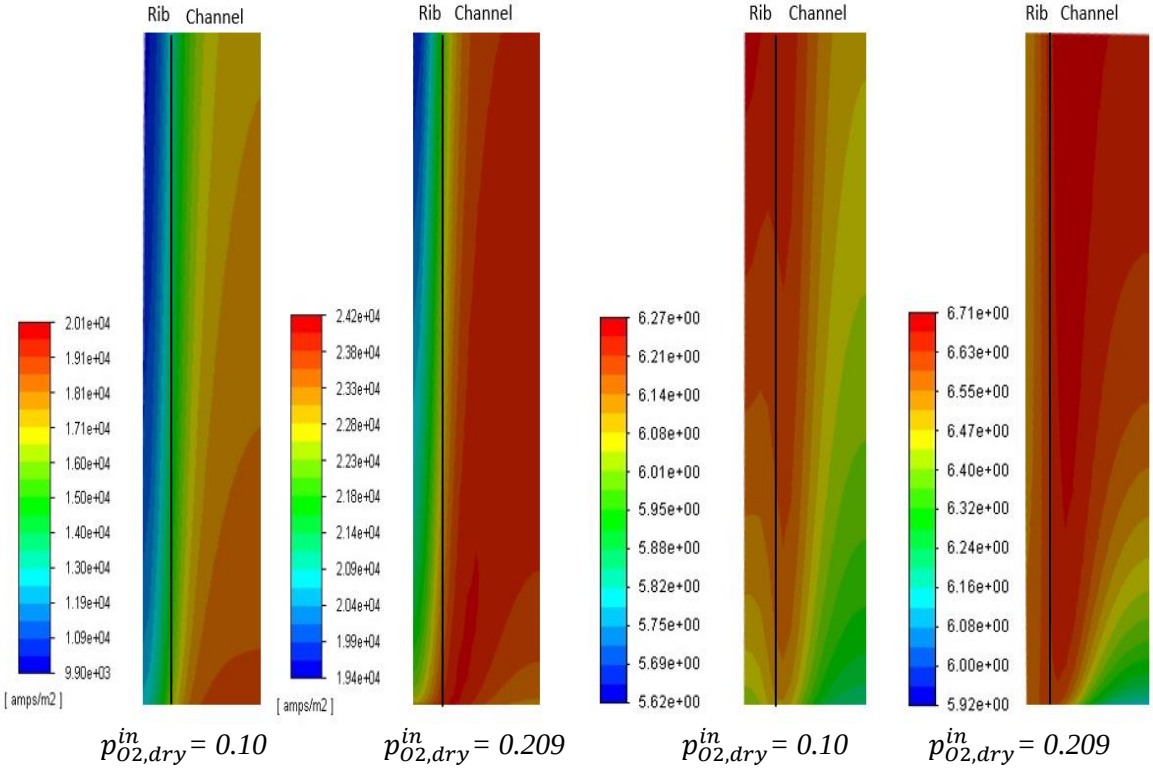

$p_{O2,dry}^{in}$ = 0.10 $p_{O2,dry}^{in}$ = 0.209 $p_{O2,dry}^{in}$ = 0.10 $p_{O2,dry}^{in}$ = 0.209

Figure 5.30 Current density (left-a) and water content (right-b) contour plots on a section parallel to membrane placed in the middle of it. ΔV=0.30V

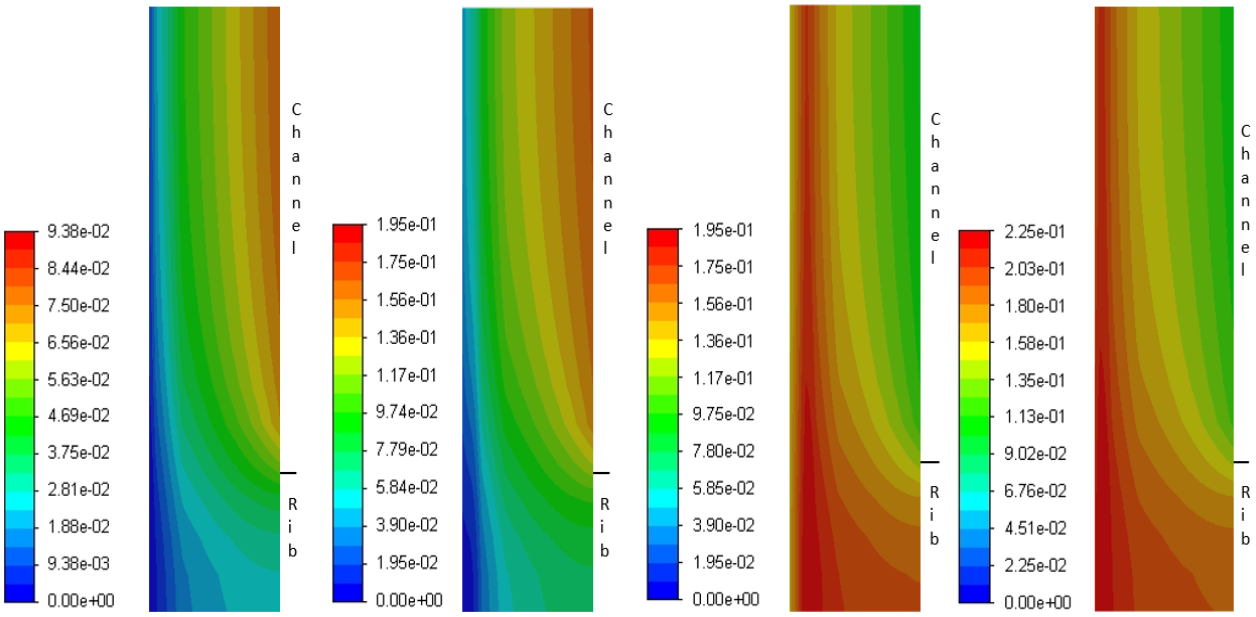

$p_{O2,dry}^{in}$ = 0.10 $p_{O2,dry}^{in}$ = 0.209 $p_{O2,dry}^{in}$ = 0.10 $p_{O2,dry}^{in}$ = 0.209

Figure 5.31 Oxygen mole fraction (left) and water mole fraction (right) contour plots on a section parallel to membrane placed in the middle of it. ΔV=0.30.

What has been said above is confirmed by figure 5.30-b where membrane hydration state is reported. The water content is getting higher moving downstream and the gradient of growth is from channel inlet region to outlet rib region as usually occurs in PEMFC. Analysing the case of lowest $p_{O2,dry}^{in}$, it is visible that the maximum of water content is not under the rib region but between current collector and channel. This occurs because of the lower current density there that determines a lower osmotic drag coefficient in that region and, therefore, a lower gradient in water content along membrane, as shown in figure 5.32, where water content trends are reported from lines, crossing electrodes and membrane, placed respectively in the middle of rib region, of the channel one and between them. Figure 5.31 shows the profile of water vapour mole fraction on section placed at half of channel length. The maximum in water mole fraction is always under the rib as expected.

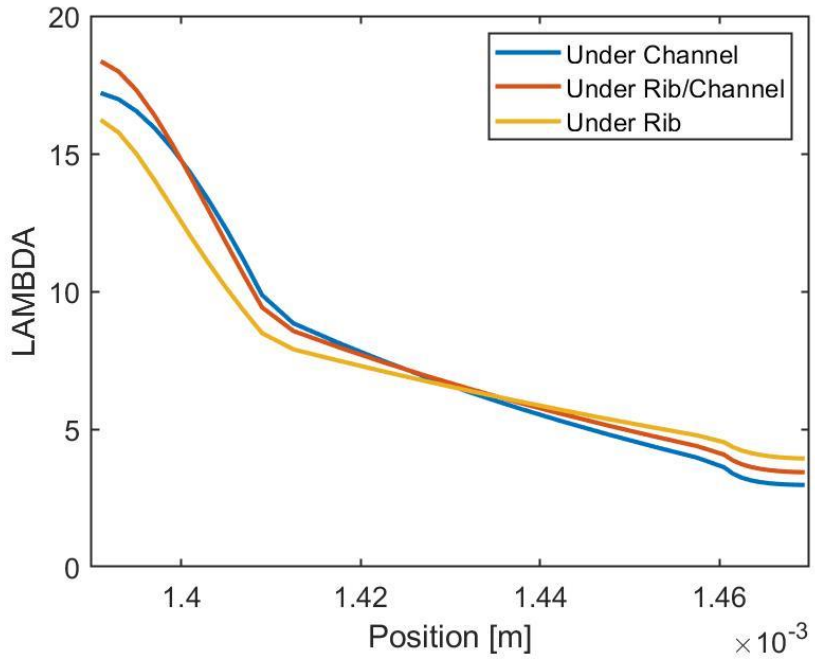

Figure. 5.32: Water content profiles through electrodes and membrane placed in the middle of channel region, in the middle of rib region and between them, considering $p_{O2,dry}^{in}$ *= 10 %.*

5.3. Summary of 3D Analysis

A 3D model has been implemented and different geometrical configurations have been simulated, considering a straight single channel. The analysis has been useful for understanding better the two-phase physics on a three-dimensional domain and how it is
affected by the presence of geometrical elements. The main conclusions from this Chapter are listed below.

- Simulations on a single channel geometry have been performed. Including the presence of rib, it has been possible to investigate oxygen availability as well as on multiphase water transport in a region region not directly supplied by channel. It is concluded that a large rib can favour flooding phenomena; whereas a larger channel width can allow an easier removal of liquid water from porous media and with materials with high electrical conductivity can allow a quite homogeneous current production inside CL.
- A variation in GDL thickness does not have a strong impact on PEMFC performance, as opposed to R/C one; however, in presence of a wider channel

a finer GDL reduces mass transport losses whereas in presence of a wider rib a thicker GDL allows a more homeogeneous reactants diffusion towards the active area, improving the performance.

- Simulating two different values of cathode relative humidity it has been possible to investigate its effect on water management inside PEMFC. A distinction has been made between low and high current density region. In high current density region, a low RHc value guarantees better perfomance whereas at low current densities increasing RHc value, also protonic conductivity increases and, thus, PEMFC perfomance.

Chapter 6

1D models are less time-consuming but on the other hand they can not take into account the 3D geometry of the problem. An analysis and methodology for a consistent comparison between the two models is reported.

6. Comparison 1D-3D model

This chapter deals with the numerical modeling of the PEMFC through a 1D approach, comparing the results obtained here with the one reported in the previous chapter for the 3D approach. Starting from the 3D analysis and from an investigation of the parameters of the models, a calibration of parameters among the two approaches is presented for a wide range of operating conditions. Investigation of parameters, and validation of calibration methodology are the key points of this chapter. Structure and methodology of the Chapter are listed below.

- 1D model description.
- Results of local and global comparison between two models discussion.
- Introduction of parameters used for the calibration and sensitivity analysis.
- Description of the calibration methodology.
- Validation of the methodology results on wide range of geometrical features and operating conditions trying to obtain a deeper understanding 1D model prediction.
- Conclusions.

6.1. 1D – Model

The system of governing equations, presented in the second chapter, has been implemented into a one-dimensional configuration, using the software MATLAB®. This model, as usually done for 1D models present in literature, describe the physical phenomena occurring along through-plane direction, across the Membrane Electrode Assembly (MEA). The through-MEA direction includes the discretization of Anode and Cathode GDLs, Anode and Cathode MPLs, Anode and Cathode CLs and membrane. Some simplifying assumptions has been done for 1D modelling of PEMFC, described shortly.

- Channel volumes are not resolved in this model, so is impossible to take into account the presence of the rib and in general R/C ratio as well as the depth and three-dimensional development of the channel. Domain boundaries are represented by Anode and Cathode GDL-channel interface.

Thus, Dirichlet type boundary conditions are used for species concentration.

- Velocity is assumed to be zero along through-plane direction, thus Equation (3.3) has not been solved.
- Pressure drop along through-plane direction and, thus, permeation of gases, described by (3.11), are considered negligible.
- 1D Stefan-Maxwell equation with constant pressure has been used to describe flux of species across porous media.
- Binary diffusivities, D_{ij}, are computed by means of the correlation by Chapman-Enkog et al. as reported in (3.7).
- It has been decided to neglect the contribution of Knudsen diffusion to transport of gas species inside porous media. This choice has been done because of the difficulty to implement this equation in the commercial software used in this work. However, the absence of Knudsen diffusion has been compensated by an increase in transport resistance inside regions where Knudsen diffusion contribution is non negligible, that is MPL and CL.
- Electric charge transport is not solved along Anode and Cathode GDLs and MPLs, thus determining that potential, ϕ_s is only defined in CLs and membrane. However, electrical conductivities of carbon materials are assumed to be high enough to determine a voltage loss of less than 10 mV.
- Another assumption is that the processes of adsorption and desorption from vapour and from liquid water to dissolved phase are symmetric, therefore $k_{ads,g} = k_{des,g}$ and $k_{ads,l} = k_{des,l}$.

The above-mentioned simplifications are not enough to tackle the stiffness of PEMFC model, that is caused principally by multiphase water transport. Permeability of liquid water, described by Equation (3.36), is a strongly non-linear function of saturation through use of correlation Pc(s). Actually, when saturation approaches zero, these terms generate very large gradients in saturation, making Equation (3.38) highly stiff.

6.2. Introduction to local and global comparison

An important step for the development of this work has been represented by the comparison between 1D and 3D models. The objective of this phase has been to verify the correct implementation of equations described in Chapter 3, adapting PEMFC model, already present in Fluent to our needs. Indeed, this allows to have a better comprehension of the implemented equations.

The comparison between the models seems to be complicated given the differences between the two. 3D model is more completeand more computationally expensive, allowing to simulate the performance of a PEMFC with different geometric configuration of flow field characteristics and operating cconditions, provided the use of a mesh refined enough to consider the solution obtained by convergence as independent of the mesh itself. The 1D model instead is less onerous computationally but, as explained in the previous paragraph, it has intrinsic limitations due to the inability to resolve the channel and simplifying hypotheses. First of all, same values for model parameters have been assumed for 1D and 3D model, contained in Table 6.1. It has been adopted the reference Mesh, assuming, as operating conditions,

- high excess of reactants, trying to limit gradients of species concentrations and to get homogeneous conditions along channel direction.
- The feed is co-current.
- Constant flow rate approach has been used for 3D model boundary condition, considering the operating conditions described in Table 4.2, at a certain reference current, jref.

Parameter	Value	
Operating temperature T	353.15	K
Gaseous pressure at anode P_{an}^{in}	2.5	bar
Gaseous pressure at anode P_{cat}^{in}	2.3	bar
Relative Humidity at anode, RHa	50%	
Relative Humidity at anode, RHc	30% - 80%	
Stoichiometric ratio at anode λ_{an}	10	
Stoichiometric ratio at cathode λ_{cat}	10	

Tabel. 6.1 Operating conditions used in the base case study.

Then, a valid comparison procedure has been developed, as described in the following lines.

- Identification of the geometric configuration of the 3D reference case.
- Introduction of comparison variables.
- Analysis of local and global comparison results

Starting from the 3D analysis carried out in the previous chapter, first step is the selection of the geometric configuration that allows a better comparison between the two models. Thus, the comparison between begins with the identification of

the 3D simulation that has the most monodimensional characteristics. Indeed, the 1D model does not resolve channels and does not take into account the presence of rib.

The 3D case data on water content, liquid saturation and oxygen mole fraction profiles in a direction parallel to the x axis in a through plane placed at 50% of channel development at half GDL and half CCL, are analysed. The 3D case searched is the one that turns out to have flatter profiles of the above-mentioned quantities, that is whose gradients in direction-x are small, since they suffer less of the presence of the rib. In the first line of Figure 6.1 the results of a comparison between three cases with GDL=150µm and R/C different from case to case are presented. It appears that among the three R/C values studied, the case where the rib impacts less on the profiles is the case R/C=1/3. This result reflects what is expected, since the R/C=1/3 value is associated with the flow field configuration where the rib covers a smaller portion of the interface with the GDL. Fixed the R/C, in the second line instead the same graphs of three cases are analyzed with R/C=1/3 varying the thickness of the GDL. Among the three GDL cases studied, the largest layer thickness (300µm) ensures flatter profiles. Although the configuration with GDL=150 together with low R/C values ensures the best performance, as explained in Chapter 5, a finer thickness forces the reactants to diffuse to the active area covering a smaller distance, thus leading to greater gradients in the area below the rib.

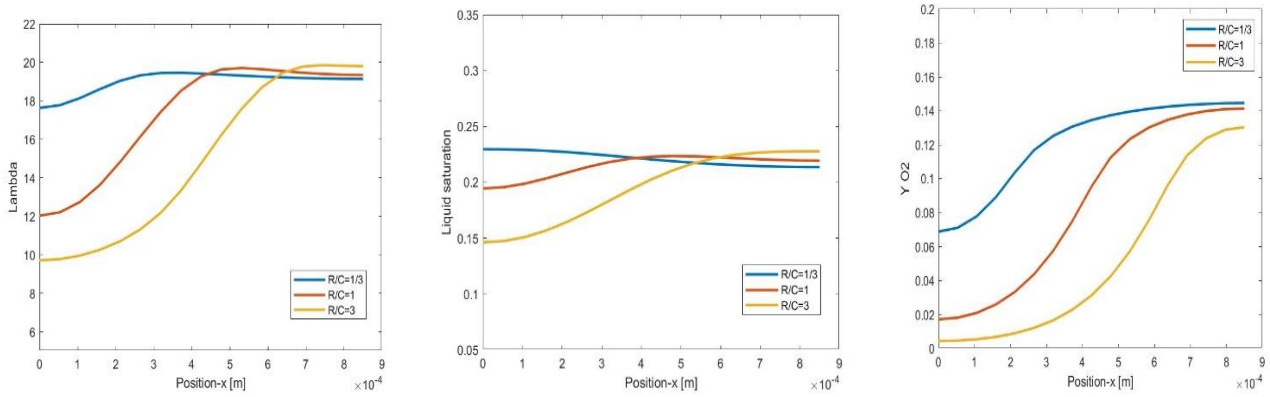

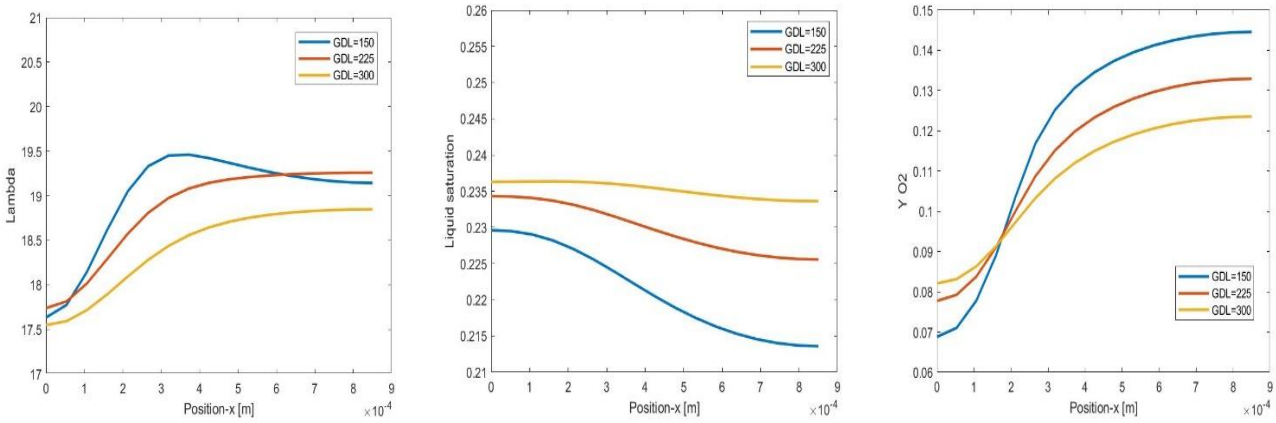

Figure 6.1. Case R/C=0.33 GDL=300 µm RH=30%. Local profile of water content and liquid saturation in the middle of CCL and oxygen mole fraction in the middle of GDL, comparing different R/C ratio on first line, and different GDL thickness on second line.

The configurations selected are R/C=1/3, GDL=300, RH=30% and 80%.
Data have been collected in 3D model along lines drawn on the symmetry plane, visible from Figure 6.2, i.e. on the plane placed in the middle of channel, at 50% from inlet boundary, because it allows to have a better understanding of how models behave at different operative conditions. 1D model takes into account what happens along the through plane direction. Velocity field, as well as species distribution and depletion inside channel region are not resolved in 1D but proper boundary conditions has to be set in order to be consistent in comparing results. Local values of species concentrations, evaluated at GDL-channel interface from data obtained by 3D model, are used as BCs for the 1D model. Electrical potential difference represents an input variable for 1D model, since it simulates operation of PEMFC in Potentiostatic mode.
To ensure a proper comparison has been decided to show local trends of several characteristic variables and source terms of governing equations and they are the following:

- Species mole fractions, Y_{H2O}, Y_{O2} and Y_{H2}, to verify correct implementation of Equations describing transport of gas species and their related properties reported in Paragraph 3.2.
- Water content, λ, across Catalyst Layers and membrane, together with the source terms for dissolved phase, S_{vd}, to verify consistency in having implemented dissolved phase model described in Paragraph 3.2.4.1 and properties affected by the hydration state of membrane, like σ_m.
- Liquid saturation s in cathode porous region, described in Paragraph 3.2.4.2.

This represents a complete list of characteristic quantities for purpose of comparison.

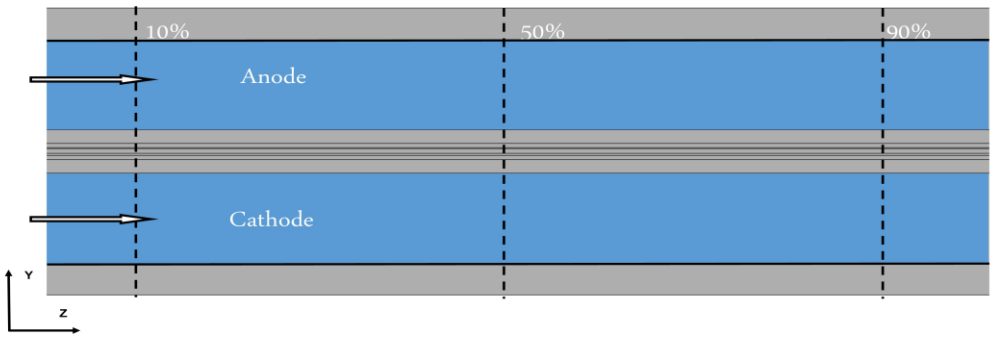

Figure 6.2. Detail of reference Mesh in z-direction with indication of line (50%) used for comparison purposes.

Local and global comparison

Fixed the geometrical configuration, two situations have been analysed, the first one at 0.90V in which the amount of water produced to the cathode is very limited and therefore also the presence of liquid water is minimal, and the second one at 0.30V in water which is present also as liquid. The results of the analysis at 0.90V are shown in Figure 6.3 and Figure 6.4.

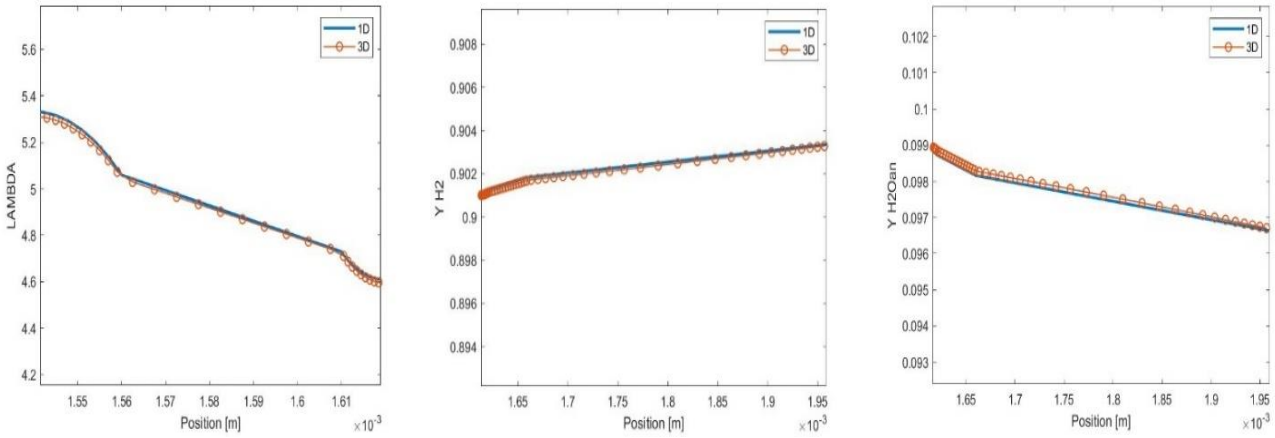

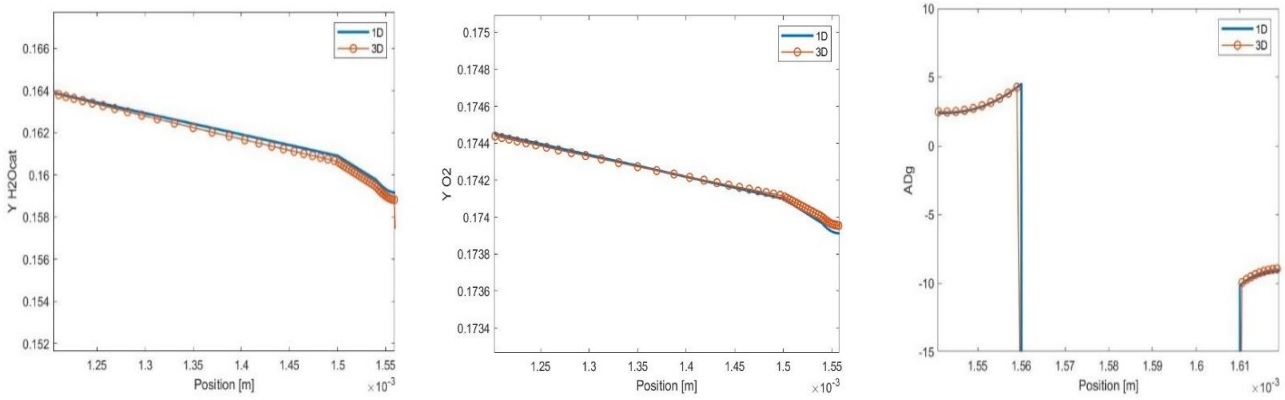

Figure 6.3 Case R/C=1/3, GDL=300, RH=80%. Local profiles of solution variables at 0.9 V across-through plane direction in 1D and 3D, without presence of liquid phase, under operating conditions described in Table 3.3.

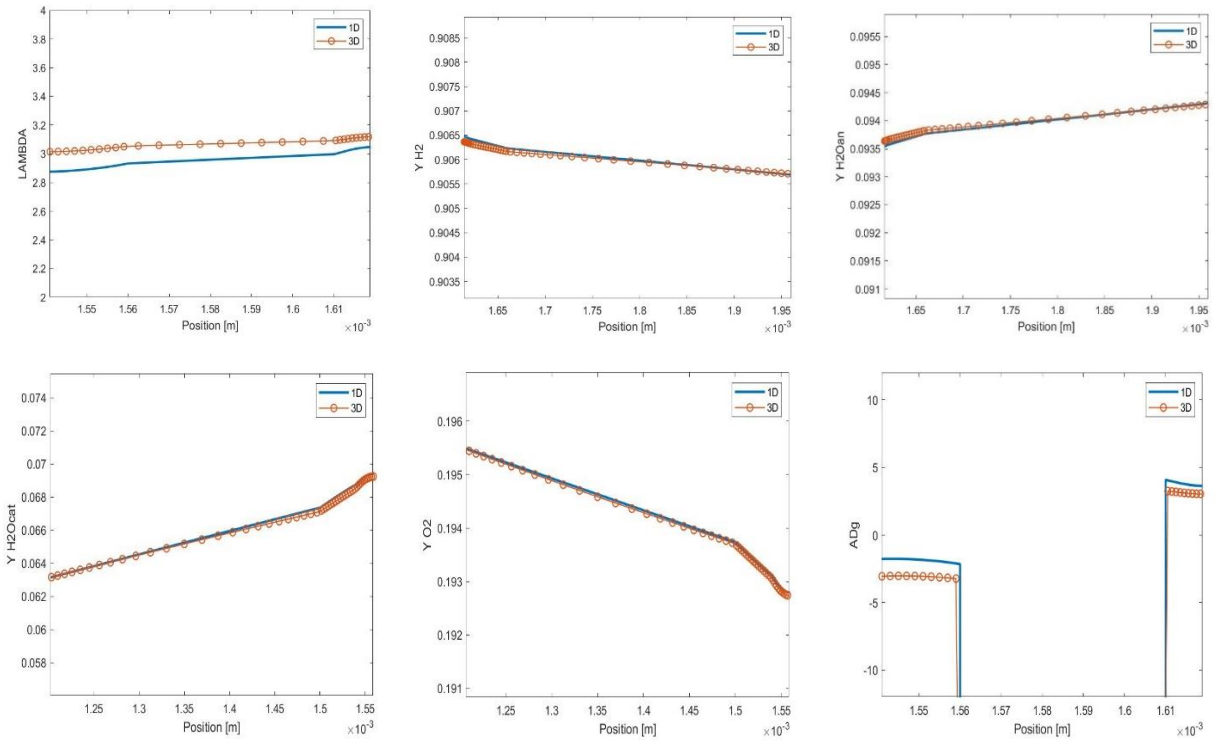

Figure 6.4 Case R/C=1/3, GDL=300, RH=30%. Local profiles of solution variables at 0.9 V across-through plane direction in 1D and 3D, without presence of liquid phase, under operating conditions described in Table 4.2.

Trends and gradients of species molar fractions are consistent and follow the diffusion correction as declared in Chapter 3. Thus there is a good accordance

between 1D and 3D model and comparison method works well. Species transport in porous media is described in the same way between two models, as observed in molar fractions charts in Figures 6.3 and 6.4. At 0.90V 1D is able to simulate the behavior of a real PEMFC in a 3D model without any change in its parameters. It can be concluded that equations related to dissolved phase model have been correctly implemented and the problem solved consistently.
The second part of the analysis concerns instead the comparison to 0.30V to the high density of current in presence of liquid water. The results are presented in Figures 6.5 and 6.6. Differences between the profiles are much more visible and need to be analysed.

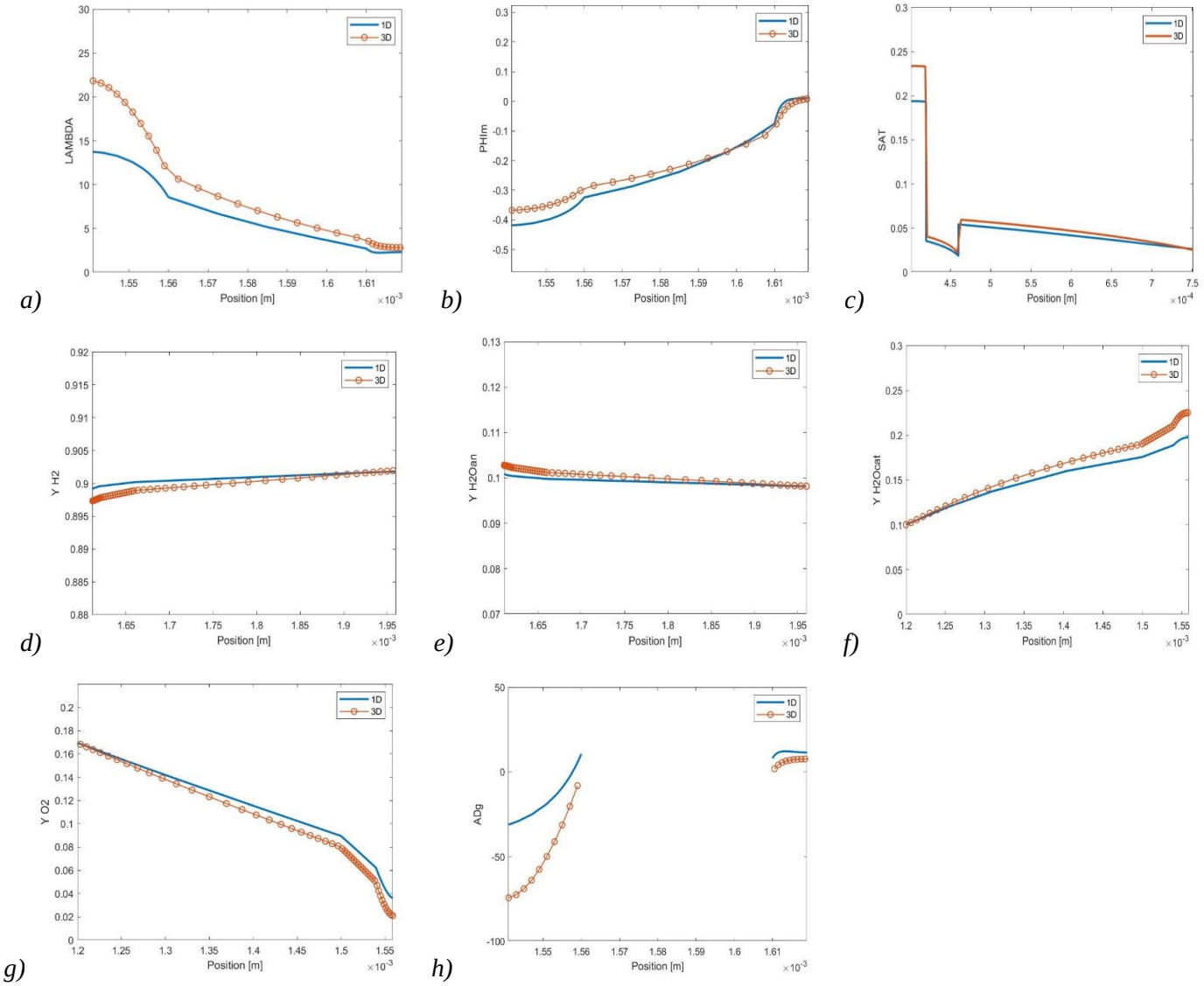

Figure 6.5 Case R/C=1/3, GDL=300, RH=30%. Local profiles of solution variables at 0.3 V across-through plane direction in 1D and 3D, with the presence of liquid phase, under operating conditions described in Table 4.2.

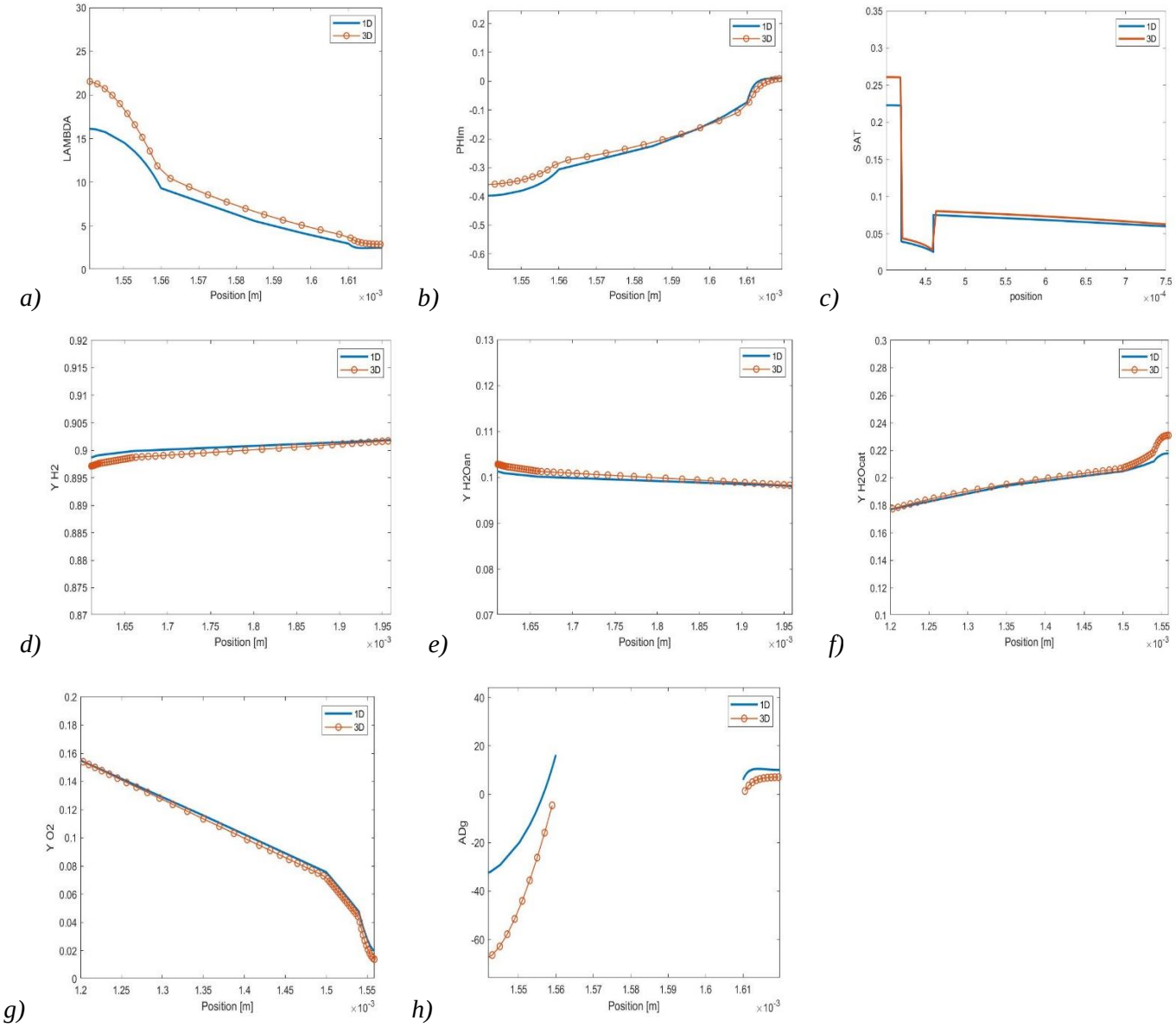

Figure 6.6 Case R/C=1/3, GDL=300, RH=80%. Local profiles of solution variables at 0.3 V across-through plane direction in 1D and 3D, with the presence of liquid phase, under operating conditions described in Table 4.2.

First of all, liquid saturation profiles (*s*) have been taken into account. As it can be seen from Figures 6.5-c and 6.6-c, 3D model slightly over-estimates the saturation value (s|GDL−Ch) in Cathode GDL. This behaviour is determined by 2D geometrical effects under the rib region and 3D effects related to reactants depletion along the channel. Liquid saturation gradient, firstly, along in-plane direction and, secondly, along channel, are not negligible. In the last part of

Cathode GDL at 0.3V, results of 1D and 3D model are the same, as well as in Cathode MPL. In Cathode CL, average saturation value is under-estimated by 1D model of a quantity equal to 20% of value predicted by 3D model.
These discrepancies have been analysed and they can be attributed to a 2D diffusion effect that determines a slight lower value of saturation in MPL side next to the interface with CL region in 3D model. As described in Paragraph (3.2.4.2), continuity of capillary pressure needs to be guaranteed at interface between MPL and CL. From Leverett relation (3.42), Pc(s), it is noted that Pc depends directly upon the value of liquid saturation s through the term cos(ϑ_c). Thus, a small variation in Pc, determines, as a consequence of the fact that term $|cos(\vartheta_{CL})| \ll |cos(\vartheta_{MPL})|$, a larger variation of saturation in CL. A slight difference is present in the S_{ld} formulation, implemented in 1D model, for reasons of stability of the model itself. Values of S_{ld} depends on saturation as well, because of their strict dependence, as shown in paragraph 3.2.4.1, and this leads to a difference in the simulation of the liquid saturation value. For this reason also the water mole fraction at CCL is underestimated by 8% causing in turn a difference in the value of the activity of water and consequently in the determination of the value of λ_{eq} (3.29). Those differences in saturation do not affect other species mole fraction, whose maximum discrepancy between model is about 3%.

In terms of overall performance, the polarization curve is used as comparison tool. The results for the two cases analysed are shown in Figure 6.7. Low-current region of polarization curves is well described by 1D model but the curves starts diverging because of the lower hydration state predicted by 1D model at cathode side and also at the interface CLc-membrane. As visible in figure (6.5-b) and (6.6-b), protonic potential on the cathode side is underestimated resulting therefore in increased ohmic losses. The main difference is determined by the presence in 3D of the rib of current collector that prevents the GDL to be completely in contact with the channel, therefore creating space under the rib where the reactant diffusion is much more difficult and also liquid water can accumulate, thus increasing water content in membrane and limiting ohmic losses. Morover flooding phenomenon becomes stronger as current density increases and along the channel. The current density obtained also in the 3D case comes from considering all the active area including also the portion in correspondence of the rib that is exploited less because more difficult reached from the reactants. 1D model instead is unable to consider tridimensional effects like geometrical presence of ribs or oxygen depletion along the channel.
Local and global comparison has shown the effects of geometrical elements on cell performance and it can be concluded that at high current density or low voltages 1D model fails to accurately predict cell behavior, although transport equations are implemented correctly, as visible from 0.90 V analysis. For these

reasons a methodology needs to be found in order to include these effects in 1D model.

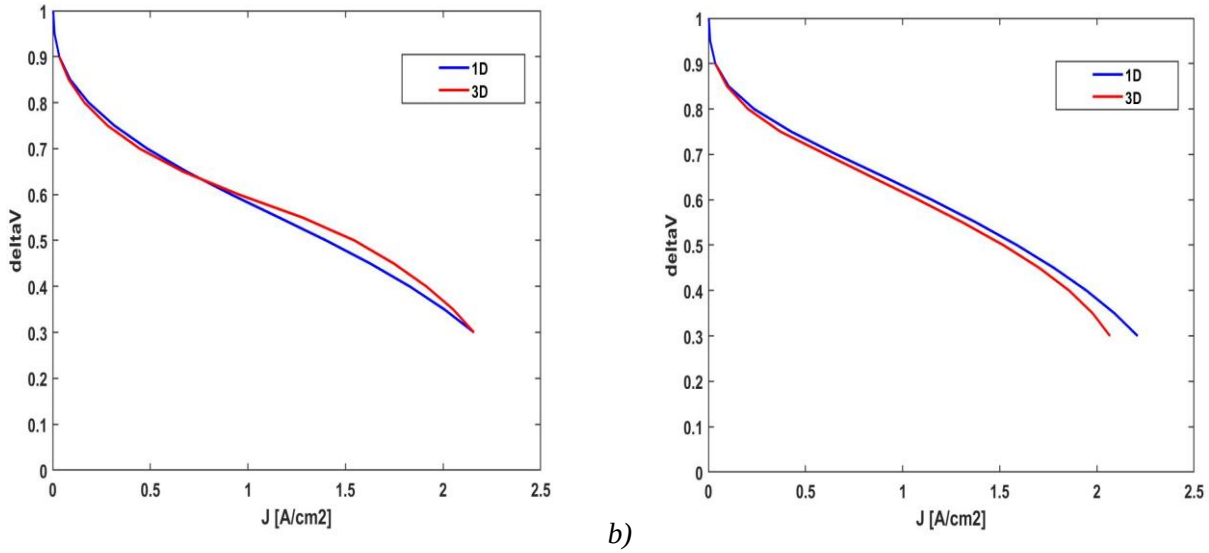

a) *b)*

Figure 6.7 a) Case R/C=1/3, GDL=300, RH=30%. b) Case R/C=1/3, GDL=300, RH=80%. Polarization curves.

6.3. Calibration parameters

From the previous paragraph it is evident that it is necessary to find a methodology, regarding one or more parameters of the 1D model to be corrected, in order to take into account the effects related to a three-dimensional geometry in a one-dimensional simulation. The first important step is the identification of the objectives that need to be achieved by a 1D simulation to be able to confirm that the results obtained are consistent with the 3D simulation of reference. Moreover from the previous paragraph it is clear that the greatest differences between the models reside in the high current densities zone of the polarization curve because of the underestimation by the 1D model of the level of hydration of the membrane, therefore of the water content, and liquid saturation related to the presence of rib. The objective of 1D simulation is, therefore, to ensure an estimate of the value of water content and saturation when closer to the simulated value with the 3D model. The achievement of a good correspondence of water content profile in the membrane also guarantees a good prediction of the proton conductivity profile σ_m and performance. Another important objective is therefore the polarization curve. The simulated curve in the 1D model must be as close as

possible to the 3D model one, so the current density produced is the same between the two models. In order to achieve the objectives at the same time, it is necessary to identify as few parameters as possible of the 1D model to be taken into account. The parameters shall not belong to material characteristics nor to operating conditions in order to not distort the simulation itself. The parameters selected to improve 1D model prediction capability are:

- δ_{GDL} multiplier of GDL thickness
- $k_{ads,l}$ adsorption/desorption rate constant from liquid phase $[s^{-1}]$
- $k_{ads,g}$ adsorption/desorption rate constant from vapour phase $[s^{-1}]$,

By analysing the three parameters considered the multiplication factor δ_{GDL} allows to simulate, increasing its value, an increase of the difficulties of diffusion of the reactants towards the active area and a greater difficulty in the expulsion of the products related to the presence of a wider rib in the 3D model. A factor δ_{GDL} greater than 1 in fact causes in the 1D model an increase of the thickness of the GDL that therefore involves greater losses of mass transport. The values of $k_{ads,l}$ e $k_{ads,g}$ instead have been chosen mainly to ensure a correct relationship between the phases that allows the 1D model to correctly simulate the values of water content, protonic potential and liquid saturations.

6.4. Sensitivity analysis on model parameters

Before calibrating and validating 1D model coefficients on 3D model results, it is important to understand what is the effect of parameters on performance of PEMFC thanks to sensitivity analysis. Polarization curves have been obtained under the same operating conditions, described in Table 5.1. It has been decided to use fixed BCs as current increases, such that no effect of operating conditions is present. The aim of this part is to assess the global effect of selected parameters on steady-state performance of PEMFC, as visible from polarization curve, and also to understand which physical phenomena are affected by a change in parameters. Indeed, local profiles are analysed to get insight into physical aspects.

6.4.1. Adsorption/desorption rate constant from vapour phase

The adsorption/desorption rate constant from vapour phase, $k_{ads,g}$, adjusts velocity in water desorption from ionomer to water vapour in cathode side, generally, and adsorption from vapour to ionomer in anode side. Equation 3.30 shows that if this process reaches equilibrium, water content λ coincides with its thermodynamic value λ_{eq}, while if it differs $k_{ads,g}$ and $k_{des,g}$ have a key role. In this model, it has been assumed that water adsorption and desorption are symmetric; thus, it is needed to analyse only one parameter. In order to understand how this parameter impacts on the performance of the PEMFC besides the reference case, are analyzed other two where the parameter changes of an order of magnitude. 1D simulation are performed considering a initial value $k_{ads,g}$= 0.2 and $k_{ads,l}$= 0.8. The polarization curves are shown in Figure 5.8-a. The parameter $k_{ads,g}$ mainly influences water mass transport in membranes. At high current density, for low rate $k_{ads,g}$, water has more difficulty in being desorbed from ionomer in Cathode CL and this determines a higher water content inside membrane, thus, a lower protonic conductivity. For high values of $k_{ads,g}$ instead a faster desorption process occurs, the water content λ decreases thus, a lower protonic conductivity is obtained in membranes. Analysing the saturation profile in Figure 6.8-c, it is visible that a higher value of $k_{ads,g}$ results in a decrease in saturation in the CL. This occurs because at high current density, where liquid phase starts comparing because of condensation process, the low desorption rate to vapour favours desorption to liquid phase, thus, an increase in saturation values of Cathode CL while for high desorption rate, desorption into vapour is favoured with respect to liquid phase, thus, lower saturation values can be obtained into CL. From the charts in Figure 6.8 it is also visible that the contribution of a variation of $k_{ads,g}$ is small as regards saturation and the profile of λ on anode side. A greater difference is present in the water content on the cathode side. For $k_{ads,g}$ values less than 0.2 the profiles tend to overlap. Indeed, as $k_{ads,g}$ decreases phase non equilibrium is increasingly unbalanced towards the liquid phase, and since the data is unbalanced in this direction also in the reference case, the visible effects in the profiles are very small.

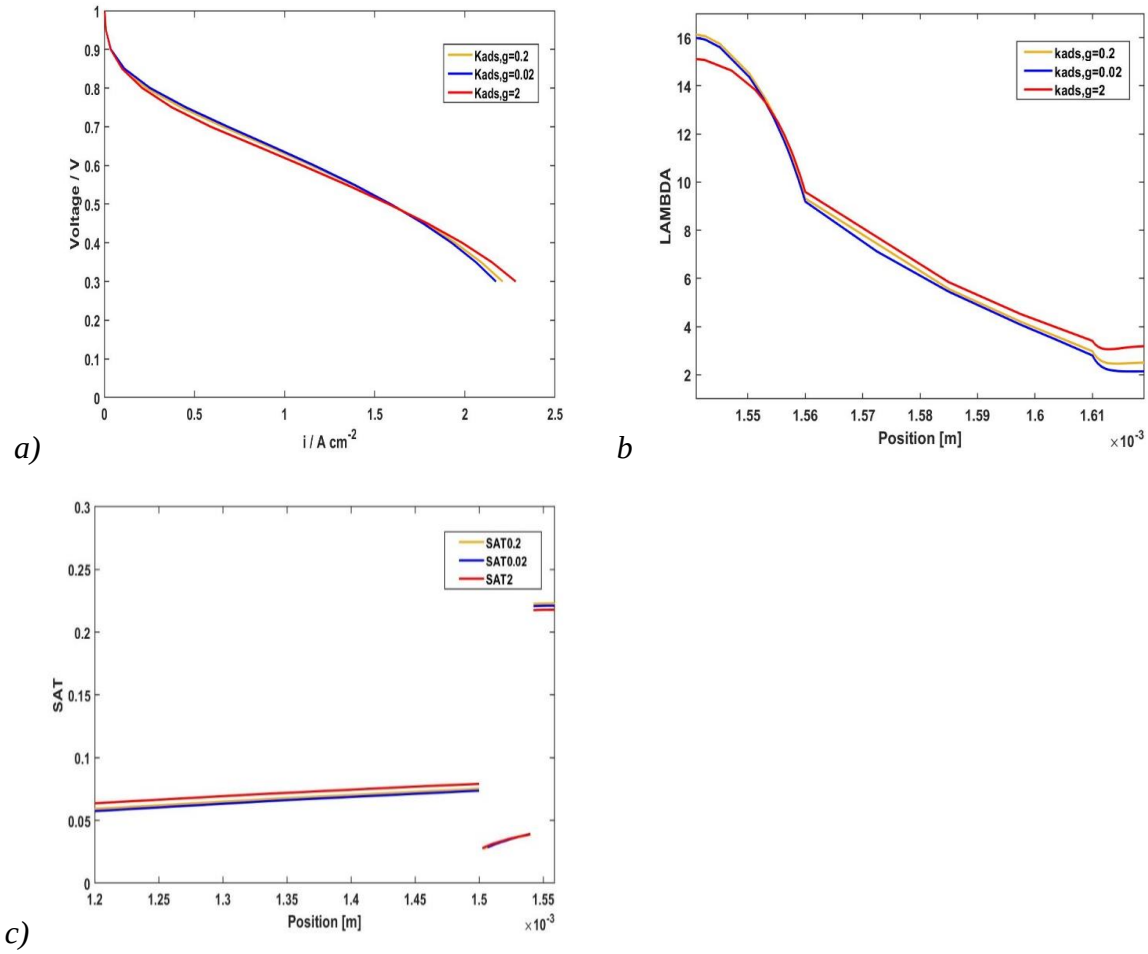

Figure 6.8 Influence of kads,g on local profiles of selected variables simulated with 1D model under operating condition described in Table (5.1). a) Polarization curves b) Water content c) Liquid saturation.

6.4.2. Adsorption/desorption rate constant from liquid phase

The adsorption/desorption rate constant from liquid phase, $k_{ads,l}$, dictates the rate of water desorption from ionomer to liquid phase, and this process becomes important when liquid water is present inside catalyst layer. Also for this parameter two other cases are analyzed, besides the reference one, where its value changes of an order of magnitude. The graphs of the polarization, water content and saturation curves are shown in Figure 6.9. The analysis is carried out in the region of the high current densities where the condensation of the water takes place and therefore there is the presence of liquid saturation. As $k_{ads,l}$ increases, water produced in Cathode CL in the form of dissolved phase inside ionomer

volume, is desorbing more favourably to liquid phase with respect to water vapour and this increases liquid saturation values, mostly in Cathode CL, hindering both ORR and species diffusion. As visible in Figure 6.9 The polarization curve associated with the higher $k_{ads,l}$ value is more penalized in high current densities region due to the increase of flooding phenomenon. Indeed, liquid saturation increases in cathodic porous media, as well as $k_{ads,l}$ increases. Water content profile confirms the above results. For low $k_{ads,l}$values the water produced at the cathode tends to desorb more difficult, thus increasing lambda value. The opposite is true for high $k_{ads,l}$ values, thus encouraging an increase in saturation. Moreover, it is important to remember that phase transfer between vapour and liquid does not guarantee equilibrium among the two phases.

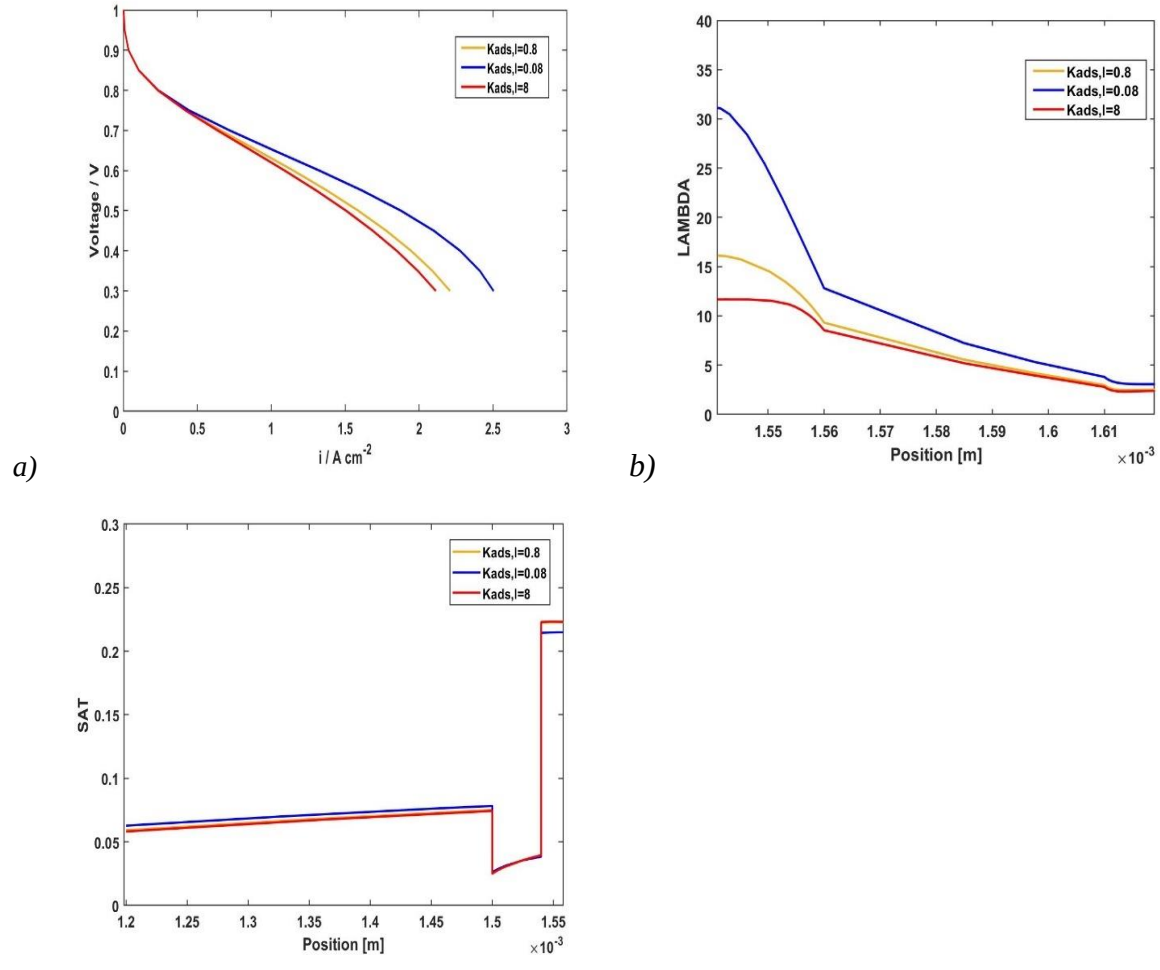

Figure 6.9 Influence of $k_{ads,l}$ on local profiles of selected variables simulated with 1D model under operating condition described in Table (5.1). a) Polarization curves b) Water content c) Liquid saturation.

6.4.3. Multiplication factor of GDL thickness

In 1D model δ_{GDL} parameter has been introduced to take into account the effect of current collector, that determines, as investigated in 3D analysis, non-uniform condition in reactant concentration, since it increases diffusion path and becomes, for its geometrical configuration, a place where liquid water can accumulate. To analyse the effects of a variation of this parameter, two values are considered, multiplying and dividing the thickness of the base case GDL=300 μm by 5 times. The greater effects of such a wide variation in GDL thickness are visible in the graph of polarization curves. A smaller thickness ensures lower mass transport losses and at the same time a greater ease for products to be expelled. The performance improves, increases the current density produced which causes an elongation of the polarization curve. The liquid saturation, with respect to the base case, tends to decrease, although the water produced to the cathode increases considering the increase of the current density. A greater thickness instead causes a strong worsening of the performances due to the increase of the diffusion path and, therefore, of the mass transport losses in the layers. The polarization curve shows this decrease in the produced current density. The liquid saturation simulated by the 1D model is lower than the base case, while in the 3D simulation the maximum value in the CCL is similar to the base case as shown in figure 6.10. This discrepancy in the liquid saturation prediction is a consequence of the increasing difficulties of the reactants' diffusion. In fact, due to increased transport losses, the current density decreases and also the water produced by the cathodic semireaction decreases. In a configuration with a flow field characterized by a high R/C value, the liquid water tends to accumulate under the rib while the 1D model fails to take into account this behavior. The factor δ_{GDL} is therefore effective in ensuring a polarization curve similar to the derived one from 3D simulations but fails to contribute to a correct prediction of the liquid saturation value when R/C is too high. The liquid saturation in fact depends heavily on geometry and three-dimensional effects.

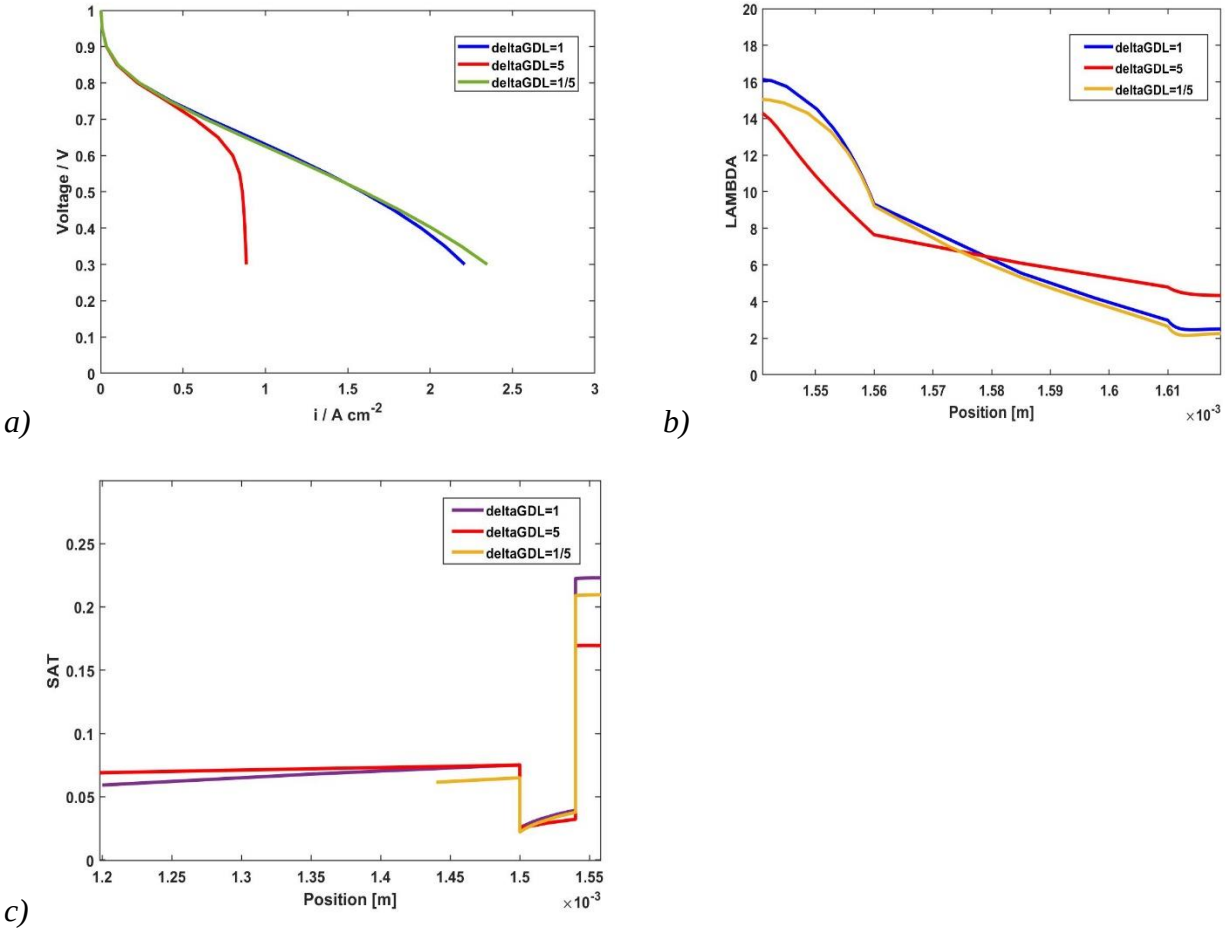

Figure 6.10 Influence of δ_{GDL} on local profiles of selected variables simulated with 1D model under operating condition described in Table 6.1. a) Polarization curves b) Water content c) Liquid saturation.

6.5. Methodology and calibration

As shown in the previous paragraphs, by analyzing the designated parameters, a calibration is needed to ensure a good output result from 1D simulation in terms of polarization curve, water content and saturation value. From the sensitivity analysis emerges that $k_{ads,l}$ is the most impacting parameter on the water content, since the range of variation obtained is wide, while it is more difficult to find a parameter that influences the liquid saturation value in CCL. Liquid saturation in fact depends strongly on the three-dimensional aspects of PEMFC geometry, in particular on the presence of rib, which in a 1D model is not possible to implement. In order to simulate different geometries, parameter δ_{GDL} is introduced, compensating an increase in the difficulty of diffusion of the reactants

due to flooding and therefore to the presence of the rib, as they are strongly related as seen in chapter 3, with increased GDL thickness in the 1D model. The one-dimensionalization of 3D cases therefore involves:

- An increase in the thickness of the GDL according to the geometry
- A deviation from the equilibrium condition between the gas and liquid phases to mimic the spatially non uniform relative humidity (RHc) from channel to rib.

Starting from cases more one-dimensional, a calibration of k_{ads} parameters is presented at both RHc=30% and RHc=80%. Fixed the parameters that influences and modifies the water management in the PEMFC, the changing from one geometric configuration to another is achieved introducing the multiplier factor δ_{GDL}. From the analysis of the first results at 0.30V, shown and explained in section 6.2, it is visible that the liquid saturation and the water content are underestimated by model 1D. The sensitivity analysis of the parameters showed that lowering the kads, the maximum water content values in the CCL are very similar to the result of the 3D. At low $k_{ads,l}$ values, polarization curve tends to stretch as the contribution given by an increase in the lambda value favours an increase in the proton conductivity of the membrane and thus also an improvement in performance. The maximum current density value produced increases with the same voltage considered and the polarization curve deviates more from the result of the 3D. In order to find a good match in the polarization curve it is therefore necessary to influence the simulation by changing δ_{GDL}. Indeed, adopting a value higher than one penalizes the performances contrasting the improvement obtained with a lowering of the $k_{ads,l}$. Finally, the saturation is penalized by a choice of a low value of $k_{ads,l}$ but an increase in GDL thickness also increases the liquid saturation simulated from the 1D model. On the basis of these considerations, a calibration has been made of the parameters, finding the coefficients that best approximate the profiles mentioned. The results of calibration process are shown in tab 6.2. In Figure 6.11 and Figure 6.12 the results obtained with the new parameters for the cases studied in section 6.2, are reported. Both RHc=30% and RHc=80% good matches for the water content profile in the membrane and catalyst layers are achieved. Proton conductivity profile, which is a function of water content, is also good concordance with the 3D one. Liquid saturation, as seen already in the analysis of sensitivity, is the profile less influenced from these parameters, however an improvement is achieved regarding first analysis without the introduction of the calibration methodology.

Parameters	RHc=30%	RHc=80%
kads,l	0.3	0.35
kads,g	0.08	0.15

Table. 6.2. Calibration parameters values

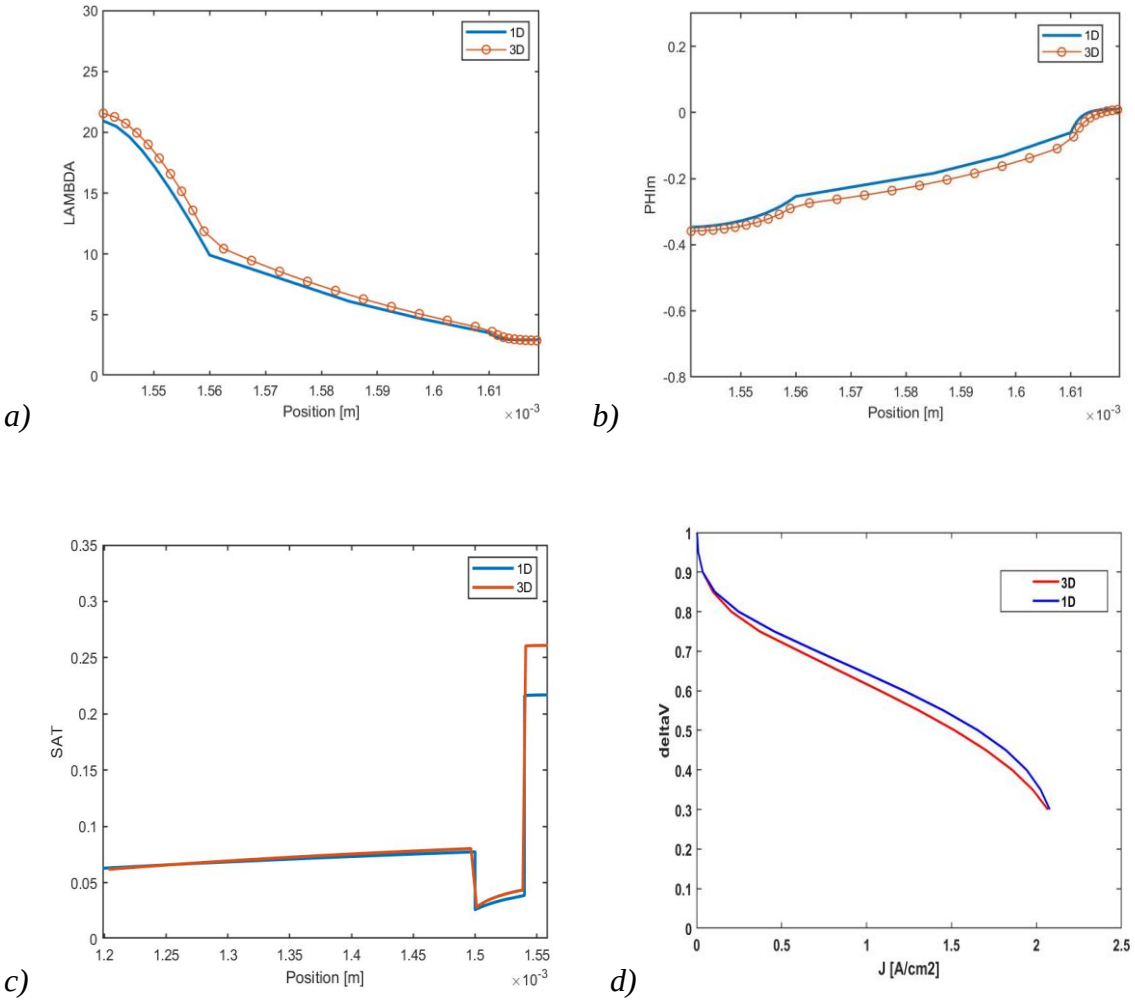

Figure 6.11. Case R/C=1/3, GDL=300, RH=80%. Local profiles of solution variables at 0.3 V across-through plane direction in 1D and 3D, under operating conditions described in Table 5.1.

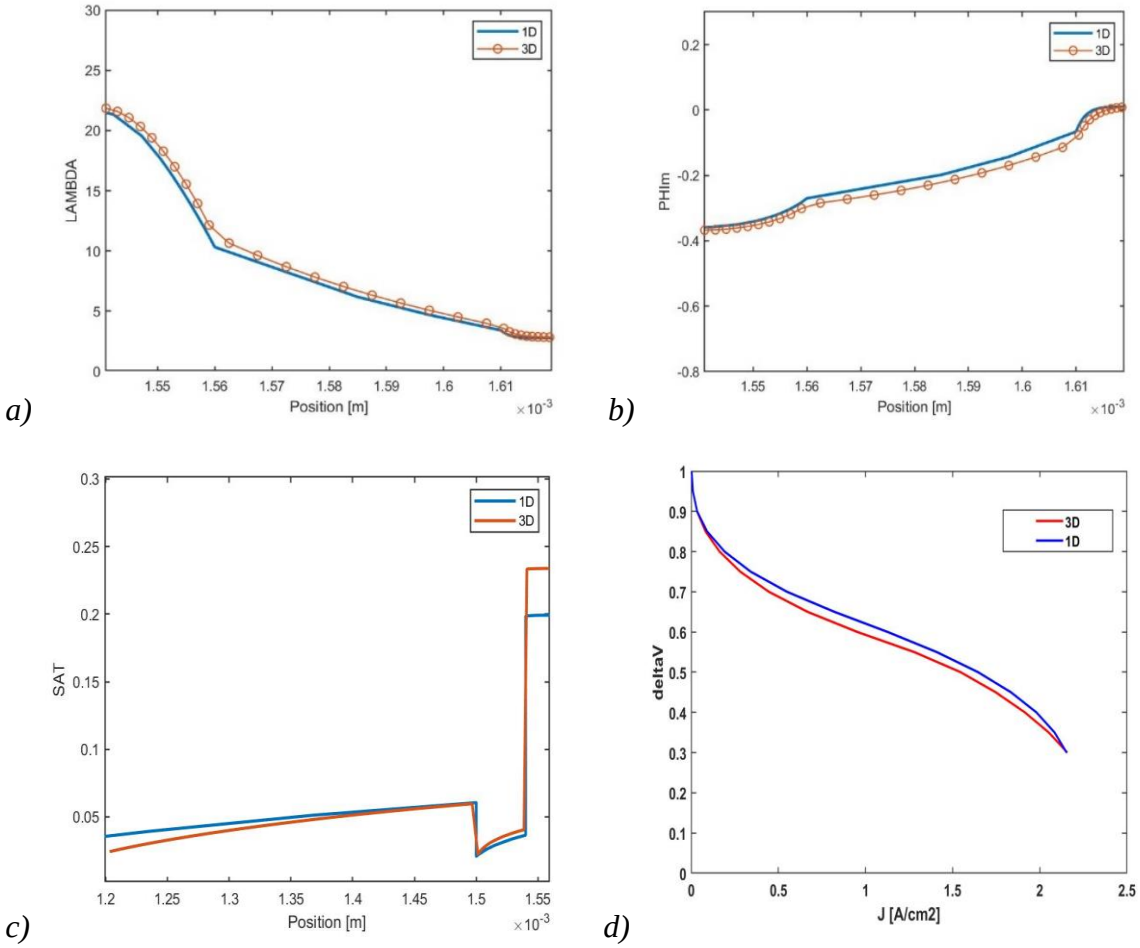

Figure 6.12. Case R/C=1/3, GDL=300, RH=30%. Local profiles of solution variables at 0.3 V across-through plane direction in 1D and 3D, under operating conditions described in Table 5.1.

6.6. Validation in the most critical case

After introducing the coefficients in the previous paragraph, an important step is the verification and validation of the result, taking into account the cases studied in chapter 3. From the 3D analysis, the PEMFC configuration most affected by the three-dimensional effects of flow field geometry, has a high R/C ratio associated with a fine GDL thickness. In fact, the presence of wider rib favours the accumulation of water under the rib region and, therefore, a higher resistance for reactants to reach active sites, while a thinner GDL increases the etherogeneity in the diffusion of reactants. Case R/C=3, GDL=150µm is therefore the most penalized in terms of performance. The case identified is the most critical to predict for the 1D model with calibration methodology, considering that it has

been validated, until now, in the more one-dimensional configuration that considers wider channels and thicker GDL. In figure (6.13) the results of the analysis are shown:

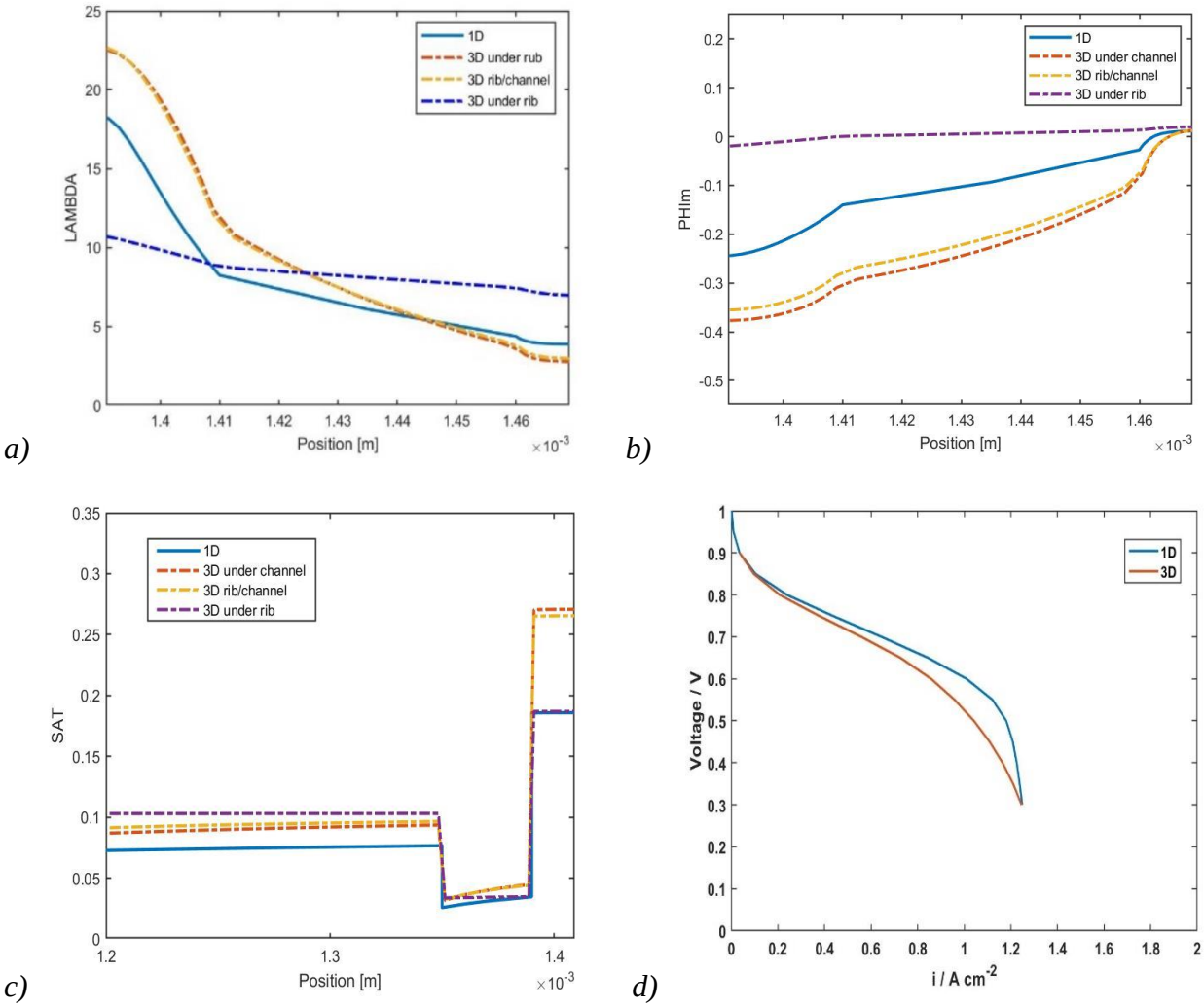

Figure 6.13. Case R/C=3, GDL=150, RH=80%. Local profiles of solution variables at 0.3 V across-through plane direction in 1D and 3D.

Data used for the graph have been collected in 3D model along lines drawn on the through plane in the middle of channel, at different locations, under the rib, under the rib-channel interface and under the channel, because it allows to have a better understanding of how models behaves considering 2D under rib effects. 1D model takes into account what happens along the through plane direction, but it cannot predict the different trend of profiles depending on the position in the 3D model. Flow channel and current collector volumes are not investigated in 1D model.

From the comparison of the results, it turns out that model 1D, using the introduced coefficients, succeeds in mimic correct profiles of the selected variables. Although they are detached from the simulated profiles under the channel, they fall within the range of profiles provided in the through plane. The calibration of parameters is therefore effective in predicting the profiles of the studied quantities within the range of the profiles under rib and under channel. Compared to the more one-dimensional case, the correspondence is less precise, as expected. The polarization curve simulated by the 1D model overestimates the value of the current density produced for majority of the voltage values. This trend is explained by the underestimation that the 1D model provides for liquid saturation.

In figure 6.14 the trends of δ_{GDL} values based on 1D simulation are shown. The comparison between 1D and 3D models has been made for each configuration studied in chapter 3. The case with R/C=3 and GDL=150 μm is associated with the higher δ_{GDL} value, confirming that it is the configuration most subject to three-dimensional effects. In contrast, case R/C=1/3 GDL=300 μm needs a smaller GDL thickness variation, since it is the configuration that more closely resembles the 1D configuration and where the influence of the rib becomes lower. It can be seen that, as R/C and GDL thickness increase, δ_{GDL} increases less than linearly, determining an asymptotic trend.

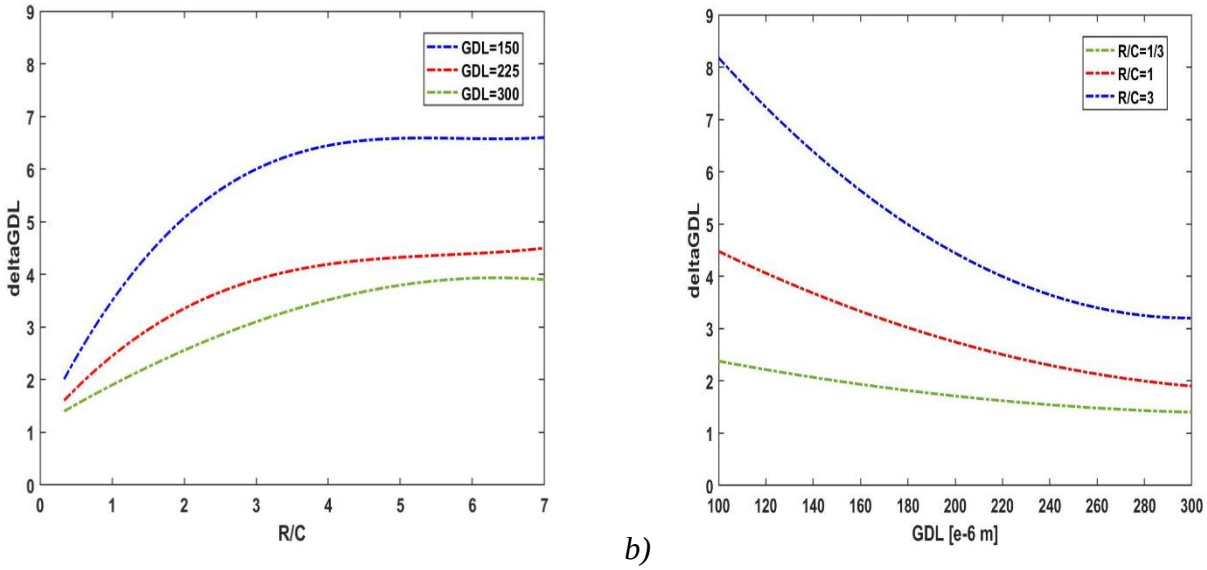

a) *b)*

Figure 6.14. a) Relation between R/C ratio and δ_{GDL} thanks to analysis performed on polarization curves.
b) Relation between GDL thickness and δ_{GDL} thanks to analysis performed on polarization curves.

In order to verify the accuracy of these trends, reported in figure 6.14, the comparison between the two models on a geometry configuration different from those studied in the 3D analysis, in terms of R/C value, but included within the domain of the graphs in figure 6.14, is shown. The simulated case is R/C=2 GDL=300 µm. As a result of this analysis, from figure 6.14a, imposing the value on x-axis, the value of δ_{GDL} for a correct 1D simulation, based on the geometrical thickness of the GDL, is obtained. Thus, δ_{GDL} = 2.3 is needed to reproduce the effects determined by the presence of rib.

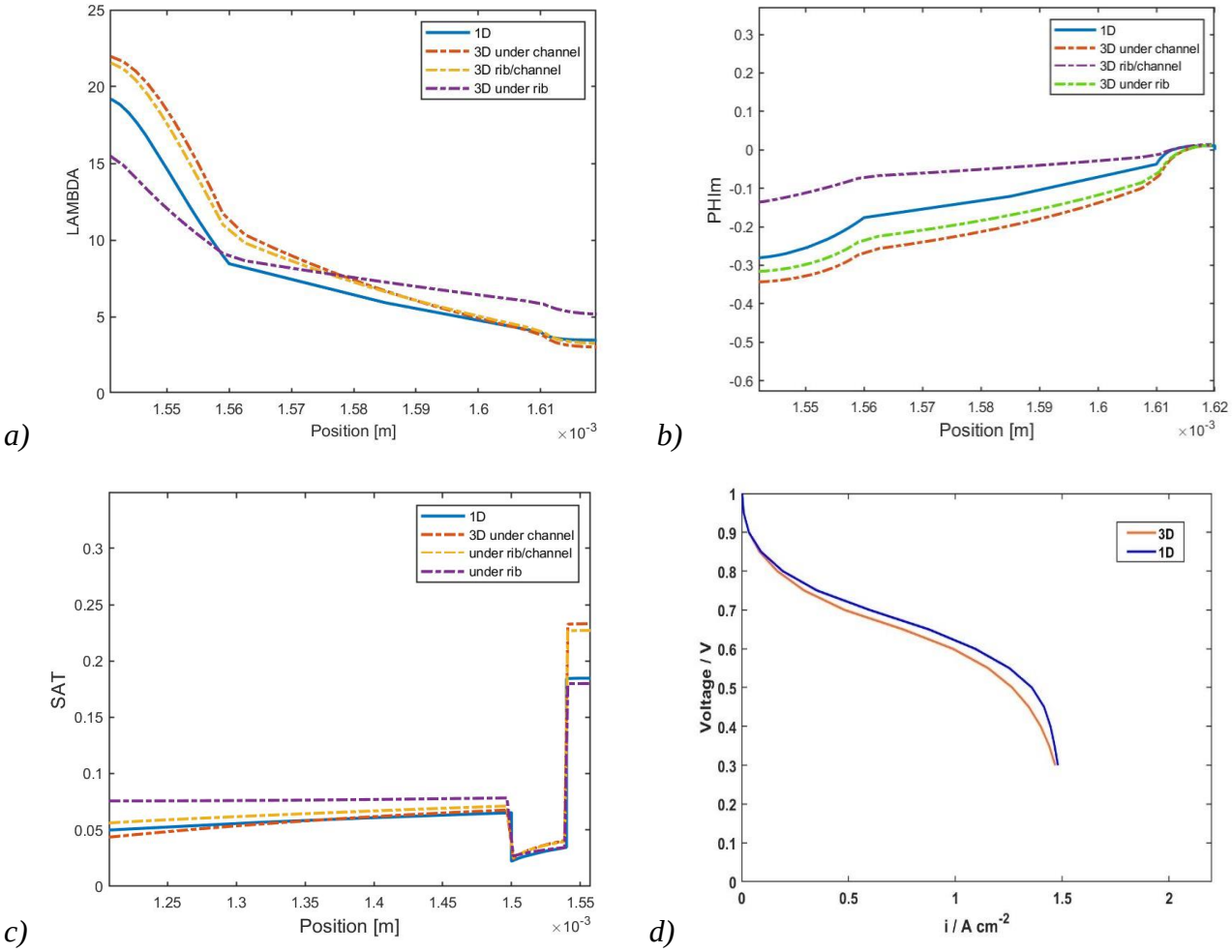

Figure 6.15. Case R/C=2, GDL=300, RH=30%. Local profiles of solution variables at 0.3 V across-through plane direction in 1D and 3D.

From the analysis of the graphs it can be stated that the trend of δ_{GDL}, shown in figure 6.15, predicts correctly the necessary value for every configuration of R/C

and GDL included in the range of values studied in the 3D analysis. It is proved that 1D model, with the coefficients introduced, is able to provide good predictions of the selected variable, as long as the tridimensional effects related to flow field geometry become too accentuated. Its range of applicability, however, has been demonstrated to be wide enough to cover all 3D simulated cases.

6.7. Variation of oxygen partial pressure

In this paragraph the possibility of extending the validity of the calibration methodology to a case where the cathode is fed with oxygen depleted air, is investigated. The dry partial pressure considered is $P_{O2.dry}^{in}$=0.10 while the other operating conditions remain the same as in the previously studied cases, shown in Table 6.1. Geometrical configuration with R/C=1/3 GDL=300 µm is considered. The results are shown in Figure 6.16. In this case of lower $P_{O2.dry}^{in}$ oxygen concentration becomes limiting and dictates current density profile. Indeed, the amount of oxygen which diffuses towards the active area is smaller compared to the air feeding case, as well as the water produced by the semi-reaction to the cathode. Liquid saturation decreases and three-dimensional aspects due to the presence of rib have less impact on performance. The 1D model, using the coefficients found in the preceding paragraphs, manages to guarantee good correspondences in the water content, protonic potential, liquid saturation profiles and polarization curve.

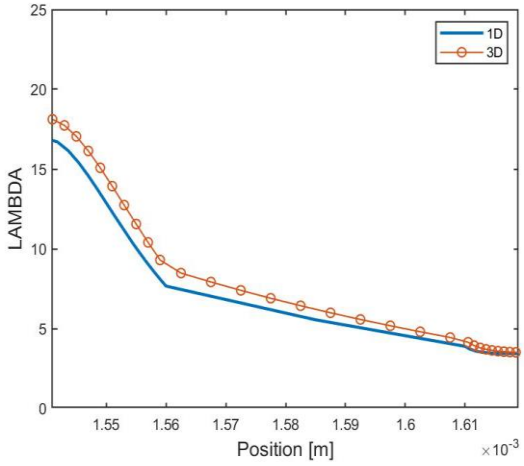

a)

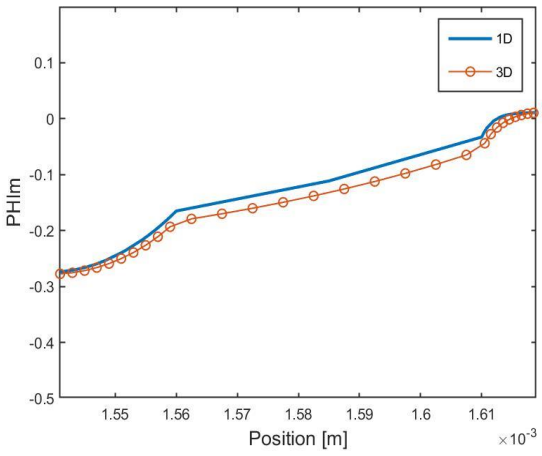

b)

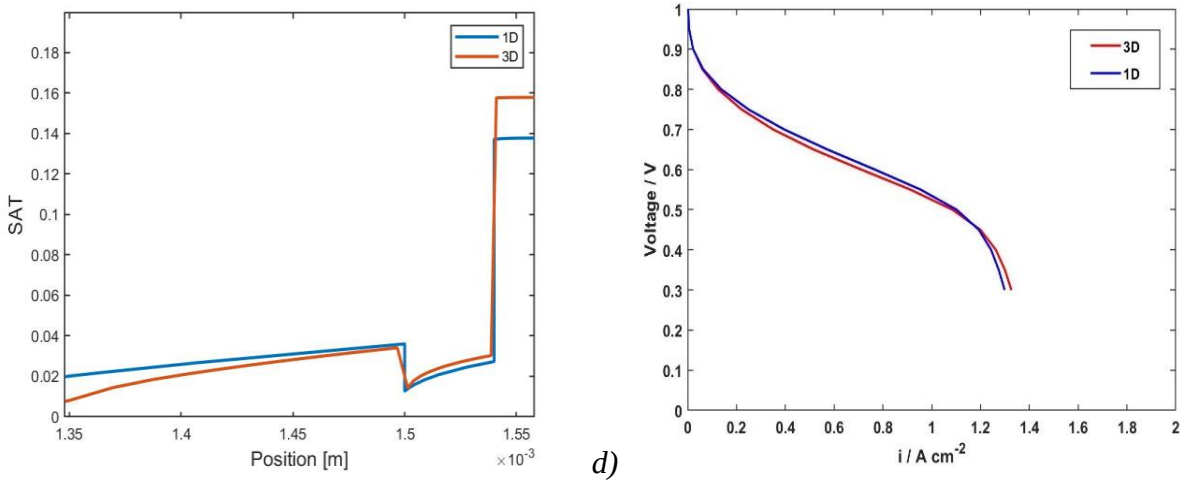

Figure 6.16. Case R/C=0.33, GDL=300, RH=30%. Local profiles of solution variables at 0.3V across-through plane direction in 1D and 3D.

From the results it can be stated that the found coefficients guarantee an acceptable prediction also varying the $P_{O2.dry}^{in}$. This result, therefore, extends the range of applicability of the methodology.

6.8. Conclusions

The main conclusions from this Chapter are listed below.

- Local profiles of solution variables like saturation or water content have been analysed in 1D model.
- Parameters δ_{GDL}, $k_{ads,l}$, $k_{ads,g}$, have been identified and investigated, thanks to sensitivity analysis, and their effect on different regions of polarization curves are analysed.
- A first set of coefficients has been found by means of a calibration phase and it has been tested under different operating conditions in validation phase. Although some discordance in predicting the behaviour of the cases most affected by tridimensional effects, 1D model has provided very good results, matching 3D simulation data, and proving to be a very good tool to reproduce polarization curves, water content and liquid saturation values, unless very important presence of tridimensional effects. The aim of this calibration phase has been to obtain a set of coefficients in a 1D model, in

order to reduce computational time and to achieve a consistency of the results.

7. Conclusions and final remarks

The MSc Thesis reports the detailed analysis of flooding and dehydration issues in PEMFC thanks to 1D and 3D models. Firstly, a 3D model has been implemented and a geometric configuration of a straight 15 cm single channel has been simulated. With 3D configuration, presence of geometrical effects and different operating conditions has been investigated.

By introducing an area of the electrode not directly fed by the channel due to the presence of the bipolar plate, it was possible to study its effects on the availability of oxygen in the catalyst, observing a reduction in the performance of the PEMFC, under the same operating conditions, due to the increased difficulty of oxygen in reaching the catalyst in the area not directly fed by the channel. This geometric element also modifies the local distribution of the current density, which reaches a maximum at the interface between collector and channel. A sensitivity analysis on the geometric parameter of GDL thickness has allowed to evaluate its optimal value depending on the geometry of the flow field. A thinner GDL is found to guarantee better performance when the width of the rib is low, thus decreasing the mass transport losses and favouring the discharge of liquid water. When the rib width value is high, associating a greater GDL thickness has proved to be the best configuration because it ensures a homogeneous diffusion of the reactants counterbalancing the increase of the 2D effects due to the rib. Considering two values of humidity relative to the cathode, it was also possible to evaluate its effect on the water management inside the PEMFC, distinguishing, for each geometric case described, between a dry and a humid case.

Then, an analysis of 1D model has been performed, with a great effort spent on understanding the effects of multiphase physics on PEMFC performance. A comparison between 1D and 3D models has been proposed. Firstly, it has been evaluated whether 1D and 3D model have been implemented in the right way and results have been compared from a local and a global point of view. Among the geometric configurations, in terms of flow field and thickness of the GDL, the case that presents behaviors of selected variables more one-dimensional, thus, whose trend in an through plane placed to 50% of the channel are less influenced by the presence of the rib, has been identified. Fixed the geometry, two different situations are evaluated, the first at 0.90V voltage to study a condition without liquid water, the second at 0.30V voltage to analyze, instead, a condition where

there is liquid water and flooding. Analysing results, at 0.90V it has been concluded that 1D and 3D models are sufficiently identical in numerical implementation. At 0.30V instead the results show some discrepancies in the prediction of the 1D model of the profiles of water content and liquid saturation. From global comparison, it has been understood the importance of the effects of real geometrical elements on performance of PEMFC and the necessity of developing a methodology to include those effects in 1D configuration. Therefore, it has been developed a methodology to include in 1D model the effects of real geometrical elements and of cathode relative humidity. Requirements and parameters that can be varied to be able to consider a 1D simulation consistent with that of reference in 3D, have been identified. To take into account a difference in geometry, it has been introduced the multiplication factor δGDL. Indeed, the presence of a region of GDL directly contacted by solid component determines the increase of GDL effective length and this parameter has been found thanks to an analysis performed on 3D geometry, by varying channel and rib width. To influence water management instead, adsorption/desorption rate constant from liquid phase and adsorption/desorption rate constant from vapour phase have been considered. After a calibration phase, a set of values for adsorption/desorption rate constant has been found to guaranteee a good correspondence with 3D trends. Then, using the multiplication factor δGDL the extensibility of the validity to all the cases studied in the 3D analysis has been verified, proving that the developed methodology allows a consistent comparison between the two models in a wide range of geometrical configurations and operating conditions.

Acronyms and symbols

Acronyms

PEMFC	Polymeric Electrolyte Membrane Fuel Cell
CL	Catalyst Layer
MPL	Micro Porous Layer
GDL	Gas Diffusion Layer
MEA	Membrane Electrode Assembly
HOR	Hydrogen Oxidation Reaction
ORR	Oxigen Reduction Reaction
ECSA	Electrochemically Catalytic Surface Area
RH	Relative Humidity
R/C	Rib widht to Channel width ratio

Symbols

ρ_g	Density of gas phase
ρ_l	Density of liquid phase
$\vec{u}_g$	Velocity of gas phase
$\vec{u}_l$	Velocity of liquid phase
ϵ	Porosity of medium
C_k	Molar concentration of species k
X_k	Mass fraction of species k
Y_k	Molar fraction of species k
J_k	Mass flux of species k
N_k	Molar flux of species k

P_g	Pressure of gas phase
P_l	Pressure of liquid phase
P_c	Capillary pressure
M_{H2O}	Molecular weight of water
K	Absolute permeability
K_{rg}	Relative permeability of gas phase
K_{rl}	Relative permeability of liquid phase
μ_g	Viscosity of gas phase
μ_l	Viscosity of liquid phase
s	Liquid saturation
λ	Water content
λ_{eq}	Equilibrium water content
λ_{cat}	Stoichiometric coefficient at cathode side
λ_{an}	Stoichiometric coefficient at anode side
P_{SAT}	Saturation pressure
P_{H2O}	Partial pressure of water vapour
γ_{HOR}	HOR reaction order
γ_{ORR}	ORR reaction order
γ_s	Exponent of power law for flooding in ORR
δ_s	Exponent of power law for flooding in D_{ij}^{eff}
τ	Tortuosity of porous medium
ϑ_c	Contact angle of porous medium
α	Transfer coefficient for reactions
E	Equilibrium potential for electrode reactions
ϕ_s	Potential of solid phase
ϕ_m	Potential of electrolyte phase
σ_m	Protonic conductivity

σ_s	Electric conductivity
σ	Surface tension of water and air
D_d	Dissolved phase diffusivity
a_w	Water vapour activity
$k_{ads,g}$	Adsorption rate from water vapour to dissolved phase
$k_{des,g}$	Desorption rate from dissolved phase to water vapour
$k_{ads,l}$	Adsorption rate from liquid water to dissolved phase
$k_{des,l}$	Desorption rate from dissolved phase to liquid water
γ_e	Geometric droplet factor related to evaporation
ρ_I	Density of dry ionomer
EW	Equivalent weight of dry ionomer
ϵ_I	Volume fraction of ionomer inside CLs
η	Local overpotential
η_d	Electro-osmotic drag coefficient

Bibliography

[1] Nima Ahmadi, Sajad Rezazadeh, Abdolrahman Dadvand, Iraj Mirzaee “Study of the Effect of Gas Channels Geometry on the Performance of Polymer Electrolyte Membrane Fuel Cell”. In Periodica Polytechnica Chemical Engineering (2018) pp. 97-105.

[2] Fatemeh Hashemia, Soosan Rowshanzamira, Mashallah Rezakazemia “CFD simulation of PEM fuel cell performance: “Effect of straight and serpentine flow fields”. In Mathematical and Computer Modelling (2012) pp. 1540–1557.

[3] Xuyang Zhang, Andrew Higier, Xu Zhang, Hongtan Liu “Experimental Studies of Effect of Land Width in PEM Fuel Cells with Serpentine Flow Field and Carbon Cloth”. In Energies (2019).

[4] Nguyen Duy Vinh and Hyung-Man Kim “Comparison of Numerical and Experimental Studies for Flow-Field Optimization Based on Under-Rib Convection in Polymer Electrolyte Membrane Fuel Cells”. In Energies (2016).

[5] S. Shimpalee, J.W. Van Zee, “Numerical studies on rib&channel dimension of flow-field on PEMFC performance”. In International Journal of Hydrogen Energy 32 (2007) pp. 842 – 856.

[6] Viorel Ionescu, “Evaluation of sub-rib convection in PEM fuel cell flow fields with different geometrical characteristic” Procedia manufacturing 22 (2018) pp. 642 – 550.

[7] Mohammad Ziauddin Chowdhury, Omer Genc, Serkan Toros, “Numerical optimization of channel to land width ratio for PEM fuel cell”. In International journal of hydrogen energy (2018) pp. 1-12.

[8] Chao Wang, Qinglei Zhang, Shuiyun Shen, Xiaohui Yan, Fengjuan Zhu, Xiaojing Cheng & Junliang Zhang, “The respective effect of under-rib convection and pressure drop of flow fields on the performance of PEM fuel cells”. In Scientific Reports (2017).

[9] Dong Hyup Jeon, “Effect of channel-rib width on water transport behavior in gas diffusion layer of polymer electrolyte membrane fuel cells”. In Journal of Power Sources 423 (2019) pp. 280–289.

[10] Zhuqian Zhang, Li Jia, Xia Wang, Liming Ba, “Effects of inlet humidification on PEM fuel cell dynamic behaviors”. In International journal of energy research (2011) pp. 376–388.

[11] Woo-Joo Yang, Hong-Yang Wang and Young-Bae Kim, “Effects of the humidity and the land ratio of channel and rib in the serpentine three-dimensional PEMFC model”. In International journal of energy research (2012).

[12] Nima Ahmadi, Sajad Rezazadeh, Mirkazem Yekani, Alireza Fakouri, Iraj Mirzaee, “Numerical investigation of the effect of inlet gases humidity on polymer exchange fuel cell (PEMFC) performance”. In Transactions of the Canadian Society for Mechanical Engineering (2013).

[13] Y. B. Kim, “Study on the effect of humidity and stoichiometry on the water saturation of PEM fuel cells”. In In International journal of energy research (2012) pp. 509-522.

[14] Elif Eker Kahveci and Imdat Taymaz, “Effect of Humidification of the Reactant Gases in the Proton Exchange Membrane Fuel Cell”. In Journal of Clean Energy Technologies, Vol. 3, No. 5, September 2015.

[15] Balogun O. Emmanuel, Paul Barendse, Jessica Chamier, “Effect of Anode and Cathode Relative Humidity variance and Pressure Gradient on Single Cell PEMFC Performance”. In IEEE Energy Conversion Congress and Exposition (2018).

[16] Hang Guo, Hao Chen, Fang Ye, Chong Fang Ma, “Baffle shape effects on mass transfer and power loss of proton exchange membrane fuel cells with different baffled flow channels”. In In International journal of energy research (2019) pp. 1–19.

[17] H. Pourrahmani, M. Moghimi, M. Siavashi, M. Shirbani, “Sensitivity analysis and performance evaluation of the PEMFC using wave-like porous ribs”. In Applied Thermal Engineering (2019).

[18] Ikechukwu S. Anyanwu, Yuze Hou, Fuqiang Xi, Xiaoyang Wang, Yan Yin, Qing Du, Kui Jiao, “Comparative analysis of two-phase flow in sinusoidal channel of different geometric configurations with application to PEMFC”. In

[19] Mohammad Ziauddin Chowdhury, Yahya Erkan Akansu, “Novel convergent-divergent serpentine flow fields effect on PEM fuel cell performance” International Journal of Hydrogen Energy (2017), pp. 25686-25694.

[20] ANSYS®Fluent User’s Guide. release 19.1“. In *ANSYS®Fluent* (2019).

[21] Adam Z Weber, Rodney L Borup, Robert M Darling, “A critical review of modeling transport phenomena in polymer-electrolyte fuel cells”. In: Journal of The Electrochemical Society 161.12 (2014), F1254–F1299.

[22] AA Kulikovsky, “Quasi-3D modeling of water transport in polymer electrolyte fuel cells”. In Journal of the Electrochemical Society 150.11 (2003), A1432–A1439.

[23] Adam Z Weber and John Newman, “Transport in polymer-electrolyte membranes I. Physical model”. In Journal of the Electrochemical Society 150.7 (2003) A1008–A1015.

[24] MoC Leverett et al. “Capillary behavior in porous solids”. In: Transactions of the AIME 142.01 (1941), pp. 152–169.

[25] Arthur Thomas Corey. Mechanics of immiscible fluids in porous media. Water Resources Publication, 1994.

[26] Thomas E Springer, TA Zawodzinski, and Shimshon Gottesfeld, “Polymer electrolyte fuel cell model” In Journal of the electrochemical society 138.8 (1991), pp. 2334–2342.

[27] Hannes Scholz, “Modellierung und Untersuchung des Wärme- und Stofftransports und von Flutungsphänomenen in Niedertemperatur-PEM-Brennstoffzellen”. In (2015).

[28] Thomas E Springer, TA Zawodzinski, and Shimshon Gottesfeld. “Polymer electrolyte fuel cell model”. In: Journal of the electrochemical society 138.8 (1991), pp. 2334–2342.

[29] Peter Berg, Keith Promislow, Jean St Pierre, Jürgen Stumper, and Brian Wetton. “Water management in PEM fuel cells”. In: Journal of the Electrochemical Society 151.3 (2004), A341–A353.

[30] Hsieh, S.-S., Chu, K.-M. “Channel and rib geometric scale effects of flowfield plates on the performance and transient thermal behavior of a micro-PEM fuel cell”. Journal of Power Sources (2007), 222–232.

List of figures

Figure1 -a). Polarization curve with different flow field. RHc=30%, δGDL=150 µm.
- b). Polarization curve of R/C=1, δGDL=150µm……...
Figure2 -a) -b). Polarization curve comparison before and after the introduction of coefficients……..
Figure2 -c) -d). Water content before and after the introduction of coefficient……

Figure 2.1 Schematic representation of fundamental PEM fuel cell components. From "Fuel cell. What is it and how does it work?". In Renewable Energy (2017)….……5

Figure 2.2 3D domain in the case of straight channel geometry…….8

Figure 4.1 Profile of solution variables as function of number of elements in y-direction Ny: a) ΔP anode b) ΔP cathode c) Velocity anode outlet d) Velocity cathode outlet e) Current density d) Oxygen mole fraction at cathode outlet……...36

Figure 4.2 Detail of mesh to show a) tridimensional development b) in x-y plane to show symmetry plane position in the middle of the channel and region of MEA under the rib of current collector…… 37

Figure 4.3. Schematic representation of domain and boundary conditions. From Fluent User's Guide release 19.1……..39

Figure 5.1 Contribution of major losses on the trend of the polarization curve...…….47

Figure 5.2. Summary of simulations…….....49

Figure 5.3 Three different configuration...…….50

Figure 5.4 Polarization curve with different flow field. a) RHc=30%, δGDL=150µm.
b) RHc=80%, δGDL=150µm, varying Rib/Channel ratio……52

Figure 5.5 Polarization curves: a) RH=30% GDL=225 µm, b) RH=80% GDL=225 µm, c) RH=30% GDL=300 µm, d) RH=80% GDL=300 µm……...53

Figure 5.6 Liquid water saturation contour plot on a section placed at 50 % of channel length, varying R/C ratio-ΔV=0.30V………..55

Figure 5.7 Water vapour contour plot on a section placed at 50 % of channel length, varying R/C ratio-ΔV=0.30V……56

Figure 5.8 Oxygen mole fraction contour plots on a section placed at 50 % of channel length, varying R/C ratio-ΔV=0.30V……56

Figure 5.9 Contour plots of evaporative volumetric rate on a section placed at 50% of channel length-ΔV=0.30V……..57

Figure 5.10 Local profiles of water content, exported from lines oriented parallel to y-directions through ACL-Mem-CCL placed on a section at 50% of channel lenght in correspondence of the center of the channel, the center of the rib and the interface rib-channel, for three different case, changing R/C ratio-ΔV=0.30V. Starting from the left R/C=1/3, R/C=1, R/C=3……57

Figure 5.11 Local profiles of current density magnitude and normalized current density, exported from a line oriented parallel to x-direction in the middle of membrane region placed on a section at 50 % of channel length-ΔV=0.30V……58

Figure 5.12. Polarization curves a) R/C=1/3 RH=30%, b) R/C=1/3 RH=80%, c) R/C=1 RH=30%, d) R/C=1 RH=80%, e) R/C=3 RH=30%, f) R/C=3 RH=80%.....59

Figure 5.13 Case R/C=1/3. Water vapour mole fraction contour plots on a section placed at 50 % of channel length-ΔV=0.30V……60

Figure 5.14 Case R/C=1/3. Contour plots of evaporative volumetric rate on a section placed at 50% of channel length-ΔV=0.30V……..60

Figure 5.15 Case R/C=3. Oxygen mole fraction contour plots on a section placed at 50 % of channel length-ΔV=0.30V……..62

Figure 5.16 Case R/C=3. Water vapour fraction contour plots on a section placed at 50 % of channel length-ΔV=0.30V……62

Figure 5.17 Case R/C=3. Contour plots of evaporative volumetric rate on a section placed at 50% of channel length-ΔV=0.30V……63

Figure 5.18. a) R/C=1/3 GDL=150μm, b) R/C=1/3 GDL=225μm, c) R/C=1/3 GDL=300μm, d) R/C=1 GDL=150μm, e) R/C=1 GDL=225μm, f) R/C=1 GDL=300μm, g) R/C=3 GDL=150μm, h) R/C=3 GDL=225μm, i) R/C=3 GDL=300μm……..65

Figure 5.19 Water content through the membrane exported from a line oriented parallel to y-direction from ACL-membrane to membrane-CCL interfaces placed on a section at 50 % of channel length……...66

Figure 5.20 ΔV=0.80V. Current density contour plots on a section parallel to membrane placed in the middle of it……67

Figure 5.21 ΔV=0.80V. Water vapour mole fraction contour plots on a section placed at 50 % of channel length……...67

Figure 5.22 ΔV=0.30V. Oxygen mole fraction contour plots on a section placed at 50 % of channel length……68

Figure 5.23 ΔV=0.30V. Water content contour plots on a section parallel to membrane placed in the middle of it……68

Figure 5.24 Case R/C=3, GDL=150-ΔV=0.80V. Current density contour plots on a section parallel to membrane placed in the middle of it……68

Figure 5.25 Case R/C=1/3, GDL=300-ΔV=0.30V. Current density contour plots on a section parallel to membrane placed in the middle of it……70

Figure 5.26 Oxygen mole fraction contour plots on a section placed at 50 % of channel length……71

Figure 5.27 Water vapour mole fraction contour plots on a section placed at 50 % of channel length……71

Figure 5.28 Contour plots of evaporative volumetric rate on a section placed at 50% of channel length-ΔV=0.30V……..71

Figure 5.29 Water content contour plots on a section parallel to membrane placed in the middle of it. ΔV=0.30V……...71

Figure 5.30 Current density (left) and water content (right) contour plots on a section parallel to membrane placed in the middle of it. ΔV=0.30V…….73

Figure 5.31 Oxygen mole fraction (left) and water mole fraction (right) contour plots on a section parallel to membrane placed in the middle of it. ΔV=0.30……74

Figure. 5.32: Water content profiles through electrodes and membrane placed in the middle of channel region, in the middle of rib region and between them, considering $p_{O2,dry}^{in}$ *= 10 %*.....75

Figure 6.1. Case R/C=0.33 GDL=300 µm RH=30%. Local profile of water content and liquid saturation in the middle of CCL and oxygen mole fraction in the middle of GDL, comparing different R/C ratio on first line, and different GDL thickness on second line.82

Figure 6.2. Detail of reference Mesh in z-direction with indication of line (50%) used for comparison purposes…….83

Figure 6.3 Case R/C=1/3, GDL=300, RH=80%. Local profiles of solution variables at 0.9 V across-through plane direction in 1D and 3D, without presence of liquid phase, under operating conditions described in Table 3.3……...84

Figure 6.4 Case R/C=1/3, GDL=300, RH=30%. Local profiles of solution variables at 0.9 V across-through plane direction in 1D and 3D, without presence of liquid phase, under operating conditions described in Table 3.3……...84

Figure 6.5 Case R/C=1/3, GDL=300, RH=30%. Local profiles of solution variables at 0.3 V across-through plane direction in 1D and 3D, with the presence of liquid phase, under operating conditions described in Table 3.3……...85

Figure 6.6 Case R/C=1/3, GDL=300, RH=80%. Local profiles of solution variables at 0.3 V across-through plane direction in 1D and 3D, with the presence of liquid phase, under operating conditions described in Table 3.3……...86

Figure 6.7 a) Case R/C=1/3, GDL=300, RH=30%. b) Case R/C=1/3, GDL=300, RH=80%. Polarization curves……...88

Figure 6.8 Influence of kads,g on local profiles of selected variables simulated with 1D model under operating condition described in Table (5.1). a) Polarization curves b) Water content c) Liquid saturation……90

Figure 6.9 Influence of $k_{ads,l}$ on local profiles of selected variables simulated with 1D model under operating condition described in Table (5.1). a) Polarization curves b) Water content c) Liquid saturation……92

Figure 6.10 Influence of δ_{GDL} on local profiles of selected variables simulated with 1D model under operating condition described in Table (5.1). a) Polarization curves b) Water content c) Liquid saturation……...94

Figure 6.11. Case R/C=1/3, GDL=300, RH=80%. Local profiles of solution variables at 0.3 V across-through plane direction in 1D and 3D, under operating conditions described in Table 5.1……96

Figure 6.12. Case R/C=1/3, GDL=300, RH=30%. Local profiles of solution variables at 0.3 V across-through plane direction in 1D and 3D, under operating conditions described in Table 5.1……97

Figure 6.13. Case R/C=3, GDL=150, RH=80%. Local profiles of solution variables at 0.3 V across-through plane direction in 1D and 3D……98

Figure 6.14. a) Relation between R/C ratio and δ_{GDL} thanks to analysis performed on polarization curves. b) Relation between GDL thickness and δ_{GDL} thanks to analysis performed on polarization curves……99

Figure 6.15. Case R/C=2, GDL=300, RH=30%. Local profiles of solution variables at 0.3 V across-through plane direction in 1D and 3D……100

Figure 6.16. Case R/C=0.33, GDL=300, RH=30%. Local profiles of solution variables at 0.3V across-through plane direction in 1D and 3D…….102

List of Tabels

Table. 4.1. Results of GCI for cathode and anode pressure inlet……..37

Table. 4.2. Simulated PEM fuel cell geometry and parameters……38

Table. 5.1 Operating conditions used in the study……51

Table. 6.1 Operating conditions used in the base case study……80

Table. 6.2.Calibration parameters values…….96